Revealing plasmotype variability affecting photosystem II efficiency and growth parameters in *Arabidopsis thaliana*

MSc thesis (36 ECTs)

Federico Fornaguera Espinosa

WAGENINGEN UNIVERSITY
WAGENINGEN UR

Revealing plasmotype variability affecting photosystem II efficiency and growth parameters in *Arabidopsis thaliana*

Name: Federico Fornaguera Espinosa

Registration number: 1034426

Study program: M.Sc. Plant Science, Plant Breeding and Genetic Resources

Supervisors: Tom Theeuwen, M.Sc. and prof. dr Mark Aarts.

Chair group: Laboratory of Genetics.

June 2022

Contents

Summary.

The plant cell has three genomes located among separate compartments: nuclei, mitochondria, and chloroplasts. Organellar genomes (collectively called the plasmotype) are much smaller and more conserved than the nuclear genome (nucleotype). Most remnant genes in the plastids encode for photosynthesis and housekeeping proteins, enabling some independence from the nucleus. The interactions between cytonuclear genomes represent a classic co-adaptation example, where multiple additive and cytonuclear epistatic effects work together to maximise an organism's fitness in a given environment. Light is hardly ever stable under natural conditions, and plants, as sessile organisms, need to adjust photosynthesis when exposed to light fluctuations to ensure efficient photochemistry while avoiding photodamage. Non-photochemical quenching is the most efficient strategy by which plants dissipate excesses absorbed light energy as heat and nuclear and plastid-encoded genes orchestrate its control. Nonetheless, plasmotype-derived phenotypic diversity affecting NPQ responses is hard to study as nucleotype-plasmotype interactions and specific environmental conditions severely influence its expression. Here we show that plasmotypic variation affecting photosystem II efficiency and growth responses is present in cybrid panels of *A. thaliana* grown under controlled and field-like conditions. Our results ratify that additive plasmotypic variation affecting NPQ responses is rare among a species-wide representative cybrid panel of *A. Thaliana* and identified *NDHG* as the causal gene behind the Bur-0 plasmotype's additive effect in the recovery of PSII efficiency. Moreover, It is shown that the Bur-0 *NDHG* allele impacts shoot biomass accumulation in *A. thaliana* cybrids differentially according to the nucleotype background, degree of light fluctuation and temperature in which plants grow. The findings of this study reaffirm the importance of plasmotype diversity in understanding plant adaptations to different environments and how this knowledge can be applied in plant breeding efforts.

Introduction.

Plants are sessile organisms constantly challenged by changing environments where multiple (a)biotic stressors limit their growth and development during their life cycles. By modulating the expression of genes spread among three separate compartments (the nuclei, mitochondria, and chloroplasts), plants adjust their physiology to cope with environmental stress. The nuclear genome houses the most considerable amount of the cell's genetic material and variability. In contrast, organellar genomes (collectively referred to as the plasmotype) are smaller and highly conserved. For instance, *Arabidopsis thaliana* nuclear genome is ~125Mb spanning five chromosomes and containing more than 26,000 protein-coding genes. In contrast, mitochondrial and chloroplast genomes are ~367 kb and ~154kb, each coding for 58 and 79 protein-coding genes, respectively (The Arabidopsis Genome Initiative, 2000). Most phenotypes conferring plant adaptative traits have been linked to nuclear genetic variation in the past. Nonetheless, the plasmotype is emerging as a promising source of genetic variability responsible for (a)biotic stress responses in plants (Budar & Roux, 2011; Roux *et al*., 2016; Zhang *et al*., 2020).

Organellar genomes in plant cells are the genetic remnants of two free-living ancestral prokaryotes acquired through separate endosymbiotic events more than a billion years ago (Timmis *et al.*, 2004; Archibald, 2015). The primitive relative of mitochondrion was probably an α-proteobacteria (likely an Asgard Archea), which through a symbiotic relationship, allowed its host the capability of performing the aerobic respiration (Spang *et al*., 2019). Separately, chloroplasts originated from a cyanobacterium engulfed by an ancient eukaryotic cell, which enabled its host to perform oxygenic photosynthesis (Green, 2011). In this context, these ancestral prokaryotes partially sacrificed their autonomy to become specialized energy-producing organelles in exchange for a protective environment. Nonetheless, their encoded genetic variation still partly governs plant metabolism, cellular homeostasis, and environmental sensing (Chan *et al.*, 2016).

Most of the organelle's original genome was lost or physically translocated to the nucleus during evolution, an event known as endosymbiotic gene transfer (EGT). By sharing their genetic load with the nucleus, the prokaryotic ancestors of the plasmotype enabled the host cell the authority to regulate and coordinate their functions (Choubey & Rajam, 2015). It has been estimated that 18% of nuclear-encoded genes (~4500) in *A. thaliana* can be assigned a cyanobacterial origin (Martin *et al.,* 2002), and just 1-2% of the organellar proteome is translated within these organelles (Christensen, 2020). Thereby, mitochondria and chloroplasts heavily depend on nuclear-imported proteins to maintain their biochemical function, as well as maintaining and expressing some of their original genes (Smith & Keeling, 2015; Millar *et al.*, 2005; Soll *et al*., 2004). However, even after losing and relocating a large extent of their genomes, present-day organellar genomes keep certain genetic autonomy by retaining a core set of protein-coding genes essential for energy-related functions (Kleine *et al*., 2009; Green, 2011). Therefore, even after EGT, the plasmotype and nucleotype keep an intricate relationship in forming several multicomplex enzymes and sophisticated crosstalk mechanisms essential to

adjust the plant's physiology when facing environmental stress (Dowling *et al*., 2008; Dobler *et al*., 2014).

Mitochondrial genome (mtDNA) gene content is higher and less variable in chloroplasts. Typically chloroplastic genomes (cpDNA) contain between 120 and 130 genes, while plant mtDNA contains about 50 to 100 genes depending on the plant species (Daniell *et al.*, 2016; Morley *et al*., 2017). Most remnant genes in the plastids encode for the photosystem and electron transport chain subunits. At the same time, those in the mitochondrion encode essential subunits of the respiratory chain. Additionally, both organelles code sets of the specific membrane, replication machinery, and housekeeping proteins, enabling some independence from the nucleus (The Arabidopsis Genome Initiative, 2000).

Nonsynonymous mutations in essential respiration and photosynthetic genes coded in the plasmotype can result in severe fitness consequences or lethality, implying that strong purifying selection is likely in action (Green, 2011; Lane & Martin, 2010; Budar & Roux, 2011; Greiner & Bock, 2013). Tight mechanisms that restrict variability in the organellar genomes are in place to limit the spread of mutations (Bock *et al*., 2014; Burger *et al*., 2003; Christensen, 2013; Gualberto *et al*., 2014; Palmer *et al*., 2000; Sloan *et al*., 2012). The uniparental inheritance of the plasmotype is one most evident factors contributing to the limitation in plasmotype variability. In plants, organellar genomes are mainly adquired from the maternal parent. Since meiosis is absent in the plasmotype, nonsynonymous mutations are continuously selected as they will be unavoidably present in the offspring. As a result, high conservation in organellar genes is observed across plant species (Budar & Roux, 2011). Even if genetic diversity evolves slower in the plant's plasmotype, its adaptation role is still considerable. Moreover, variability can be affected via introgression (e.g. horizontal gene transfer), and novel nuclear-plasmotype interactions can confer adaptative phenotypes (Birky, 2001; Bock *et al*., 2014; Hertle *et al*., 2021).

When exposed to stressful conditions, organellar signals reach the nuclei and profoundly impact nuclear gene expression, RNA turnover, and splicing to adjust cellular homeostasis. As sessile organisms, plants have developed multiple short and long-term responses to acclimate to environmental conditions (Chan *et al.*, 2016; Chi *et al*., 2013; Y. Zhang *et al*., 2020, Morales and Kaiser, 2020). These responses are coordinated by retrograde (organelle to the nucleus) and anterograde (nucleus to organelle) signalling (Chan *et al*., 2016). This communication can be divided into biogenic signalling (which mediates the formation of new plastids within the cell) and operational signalling, which alters plastid homeostasis in response to environmental cues. The interactions between cytonuclear genomes represent a classic co-adaptation example, where multiple additives and cytonuclear epistatic effects work together through complex signalling cascades to maximise an organism's fitness in a given environment (Dobler *et al*., 2014; Joseph *et al*., 2013; Roux *et al*., 2016; Zhang *et al*., 2020).

The question of why the whole organellar genomes were not lost or wholly exported to the nucleus remains partially unsolved. Although various theories have been proposed, more questions than answers remain. For instance, it has been suggested that plastid genes code for proteins with hydrophobic properties that (if expressed in the nucleus) would limit them from being efficiently targeted to the organelles (Daley & Whelan, 2005). Nonetheless, highly

hydrophobic proteins have been found to be coded in the nucleus and can still be targeted to plastids (Kleine *et al*., 2009; de Vries & Archibald, 2018). Moreover, Allen (2015) has hypothesised that the conservation of remaining protein-coding genes and gene expression machinery allows the organelles a fast response to repair or avoid damage in their electron transport chains when exposed to redox imbalances resulting from environmental stress (Allen, 2015; Kleine *et al*., 2009; Choubey & Rajam, 2015). An example is the *psbA* protein, part of the D1 reaction centre of PSII, in which translation is upregulated in response to high light and cold stress acclimation (Gao *et al.,* 2022). Nonetheless, many proteins in the plasmotype are not directly linked to the electron transport chains and/or redox balance; thereby, a final answer to why some genes were retained in the plasmotype remains a matter of debate.

Oxidative damage resulting from the light reactions of photosynthesis is common in plants subjected to environmental stress. Photosynthetic electron transport and proton gradients in the thylakoid membrane of chloroplasts need to be regulated to drive an efficient conversion of photons to chemical energy in the form of ATP and NADPH (Ma *et al*., 2021). Positive selection has acted towards maximizing light absorption at low intensities. By modifying the light-harvesting complex spatial and spectral properties, plants have developed mechanisms that optimize light abortion under low light (Ruban *et al.,* 2012; Ruban, 2017). Nonetheless, as light intensity varies according to temporal and spatial gradients, plants also need to adapt to excess light energy (Rumeau *et al*., 2007; Ruban *et al.,* 2012). In field conditions, where light is often fluctuating between high and low intensities, the amount of photons absorbed by the PSII supercomplex often exceeds the ability to use energy for $C0_2$ fixation (Shikanai, 2016). Under these conditions, the capacity of the electron transport chain is saturated, leading to P680 triplet formation and, ultimately, the formation of reactive oxygen species (ROS), which will bleach P680 leading to photoinhibition and reduction of active PSII and PSI units (Rodriguez-Heredia *et al.,* 2022). The electron transport chain can also become saturated in response to other environmental conditions, such as drought and cold stress, under which carbon fixation capacity is exceeded. Therefore, plants need to modulate photosynthesis under particular environments using a complex, multi-level network of light-harvesting and photoprotective mechanisms to increase biomass production whilst avoiding photoinhibition (Ruban *et al*., 2012; Kromdijk & Walter, 2022).

To avoid oxidative damage, plants must strategically control the efficiency of light energy utilization in light reactions (Shikanai, 2016). The plant's responses to high and fluctuating light stress can be classified into long-term (acclimatization) and short-term regulatory mechanisms. Moreover, responses range from the whole organism level to the subcellular level (Ruban *et al*., 2014). For instance, morphological adaptations such as leaf deposits or trichome formation to limit light absorption are long-term responses. In the short term, gas diffusion adjustment and Calvin cycle regulation, chloroplast number regulation, and chloroplast movement happen at the cellular level (Koller., 1990; Tanaka *et al.,* 2019: Kromdijk & Woese, 2022). The most efficient response occurs in the thylakoid membrane by the quick element of nonphotochemical quenching (NPQ), qE. Here, excess energy is effectively dissipated through the light-harvesting complex II (LHCII) associated with the PSII core as heat (Shikanai, 2016; Strand & Kramer, 2014; Ruban, 2016). To determine excess light energy, the chloroplasts monitor the acidification of the thylakoid lumen via *PSBs*, which is triggered when electron

transport dependant H^+ uptake by the thylakoid lumen exceeds H^+ release through the ATP synthase (Shikanai, 2016). NPQ mechanisms operate at higher speeds ranging from seconds to minutes in qE or minutes to hours in those related to xanthophyll cycle regulation (qZ). These photoprotective strategies are a rich source of genetic diversity, split between nuclear and organellar genomes with the potential to maximise photosynthesis in cultivated plants. Nonetheless, artificial selection in cultivated plants has focused on yield index, quality and biotic resistance while ignoring NPQ mechanisms that are difficult to observe and quantify (Ruban, 2016).

The study of phenotypic variation resulting from the plasmotype is complicated as phenotypes are often the result of complex interactions between organellar and nuclear genes, causing additive and epistatic effects (Dobler *et al*., 2014). As the nucleotype is inherited biparentally, often resulting in a heterozygous genome, this genetic variability can mask the effects of the plasmotype through cytonuclear epistasis. To accurately assess the effect of the plasmotype on plant phenotypes, the effects resulting from plasmotype-derived genes must be untangled from those generated by nucleotype variability. This can be achieved by producing plants with a shared nuclear background and contrasting plasmotypes. By doing this, it is possible to separate the phenotypic contribution from the nucleotype. Moreover, it is possible to identify plasmotype additive and nucleotype-plasmotype epistatic effects generating determined phenotypes.

A rough, time-consuming method to achieve such assessment consists of backcrossing a maternal plasmotype donor with a paternal nucleotype donor. After multiple rounds of backcrossing the resulting nuclear background will be nearly homogenous, and the resulting plants can be addressed as "cybrids" (from cytoplasmatic hybrids) (Roux *et al*., 2016)). For instance, Miclaus *et al.,* (2016) found that 96 nuclear genes responsible for crucial metabolic and morphological traits were controlled by retrograde signalling in maize cybrids generated through nine generations of backcrossing. In *A. thaliana*, several authors have used backcrossing approaches to identify the effect of plasmotypic variation on morphology, phenology, seed physiology and nitrate starvation in relatively small cybrid panels of *A. thaliana* (Moison *et al.*, 2010; Boussardon *et al*., 2019; Chardon *et al*., 2020; Roux *et al*., 2016).

There are various limitations to cybrid generation through backcrossing. First, backcrossing is time-consuming as multiple generations are required to create a homozygous nuclear background. Second, this method is heavily reliant on using markers to check the plant for heterozygosity, and residual heterozygosity or new mutations are often hard to detect. Last, local adaptation to rearing conditions and maternal effects that mask the results of the plasmotype are more prone to occur during various generations. (Roux *et al*., 2016; Christensen, 2020; Flood *et al.*, 2020). For example, Roux *et al.* (2016) used three rounds of backcrossing and marker-assisted selection to explore the effect of plasmotype on germination, phenology, fecundity, morphology, and resource acquisition. These crosses resulted in a nuclear background that was approximately 93,75% homogeneous. Although three generations should be relatively low for mutation rates and adaptation effects, this percentage leaves a 6.25% of genes generating possible interfering cytonuclear epistatic effects.

To address this problem, Flood *et al.* (2020) used Ravi & Chan, (2010) method to generate a haploid inducer (HI) line in *A. thaliana* that allows a precise evaluation of plasmotypic phenotypes produced from a single generation. The method uses *A. thaliana* transgenic plants carrying modified centromeric histone (CENTROMERIC HISTONE3 (CENH3)-tailswap). When crossed with wild-type (WT) plants, the chromosomes from the CENH3-tailswap mutants are lost during meiosis, producing a fertile haploid plant that can become a doubled haploid. The resulting plant displays a paternally inherited nucleus and maternally inherited cytoplasm (Flood *et al*., 2020). This method offers greater precision in assessing the effect of plasmotype variation on the phenotype.

Using this method, Flood *et al*., (2020) created a cybrid panel representing a snapshot of *A. thaliana's* natural genetic variation (Figure 1). This panel was then used to explore the role of plasmotype variability in the regulation of φPSII recovery when exposed to fluctuating light conditions. High throughput phenotyping through chlorophyll fluorescence imaging was used to score 1859 photosynthetic phenotypes. Results demonstrated considerable heritability (H^2)from plasmotype and nucleotype-plasmotype interactions, mainly in φPSII recovery, NPQ and cytoplasmatic male sterility (CMS) traits. Moreover, H^2 due to plasmotype and plasmotype-nucleotype interactions of φPSII and NPQ phenotypes were more pronounced under stress-inducing light treatments, and nucleotype-plasmotype interactions were found to have more significant effects than those from additive plasmotype effects. Apart from the strong additive effects caused by the Ely plasmotype, the Bur-0 plasmotype was also found to produce an additive effect that increased the recovery of φPSII and NPQ while reducing qE under fluctuating light conditions. These results show that plasmotypic genetic variation affecting photosynthesis efficiency is present within *A. thaliana* (Flood *et al*., 2020).

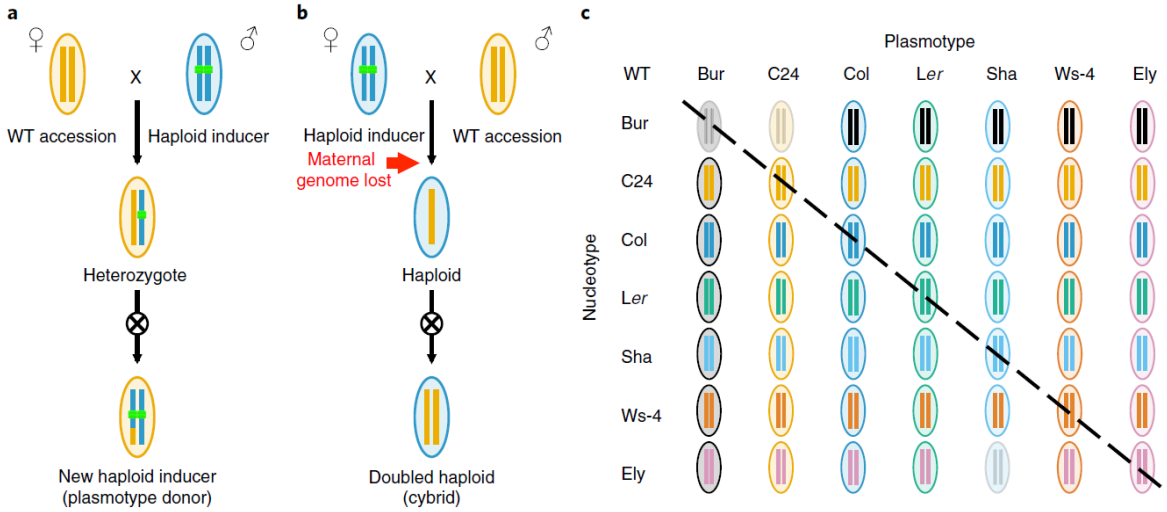

Figure 1. *Generation of cybrids through A. thaliana (CENH3)-tailswap).* ***A.*** *Generation of a double haploid with paternally inherited nuclei and maternally inherited cytoplasm.* ***B.*** *Generation of a new haploid inducer line with a new plasmotype.* ***C.*** *Representation of Full diallel of all plasmotype nucleotype combinations Reproduced from Flood et al., (2020).*

Given the relevance of Flood *et al.* (2020) findings, Theeuwen *et al.* (unpublished) have created a larger cybrid panel which encapsulates a more representative picture of the species-wide genetic variation of *A. thaliana.* Theeuwen *et al*. (unpublished) estimated that Flood *et al.*

(2020) cybrid panel contained only approximately 5% of available organellar genotypic variation in *A. thaliana*. Using the At-CENH3-tailswap method, Theeuwen *et al.* (unpublished) created a cybrid panel consisting of four nucleotype and sixty plasmotype donors, resulting in 240 different nucleotype-plasmotype combinations. This panel gives a much broader representation of the plasmotype variation of the species. Plasmotype donors consist of accessions originating from contrasting geographical locations, many of which diverged during the last glacial era (Durvasula et al., 2017; Fulgione *et al.*, 2018; Theeuwen *et al*., unpublished). Theeuwen *et al.,* (unpublished) chose nucleotype donors (Bur-0, Cvi-0, Col-0 and Tanz-1) due to their contrasting genetic diversity, diverging geographic origin and availability of mutants in the case of Col-0 (Fulgione *et al.,* 2018; Theeuwen *et al*., unpublished). Since 2018, multiple experiments using this cybrid panel at Wageningen University (WUR) and Michigan State University (MSU) have been phenotyped for a wide array of photosynthetic, morphological and fecundity traits. Nonetheless, it is still unclear if the plasmotype diversity present in Theeuwen *et al*. (unpublished) has an observable effect on photosynthesis and plant morphology parameters under field-like conditions simulating where *A. thaliana* naturally occurs.

By phenotyping Theeuwen *et al*. (unpublished) cybrid panel under field-like conditions, this project aimed to answer if there is additional plasmotype genetic variation resulting in photosynthesis efficiency and plant morphology phenotypes in outdoor-grown species-wide representative cybrid panel of *A. thaliana*. Additionally, the amount of variation due to additive plasmotype effects and nucleotype-plasmotype interaction effects will be addressed by estimating H^2. For this, an experiment was set in a gauze tunnel in Unifarm (WUR) during spring 2021, simulating how *A. thaliana* naturally occurs. A high throughput phenotyping platform of the Netherlands Plant Eco-phenotyping Centre (NPEC) in WUR was used to score 63 photosynthesis and plant morphology parameters through chlorophyll fluorescence imaging. A light protocol designed by Theeuwen *et al.* (unpublished) was used in the phenotyping to record φPSII and NPQ parameters during light fluctuation. The $H^2$of the nucleotype, additive plasmotype effects and nucleotype-plasmotype interactions (N/P/N×P) was estimated to quantify the amount of phenotypic variation resulting from genetic effects. Principal component analysis (PCA) was used to identify plasmotypes generating contrasting photosynthesis and growth phenotypes. Once identified, the presence of missense variants in possible candidate genes was explored by exploring polymorphisms previously identified by Theeuwen *et al.* (unpublished).

Based on these results, the additive effect of the Bur-0 plasmotype stood out. Further experimentation focused on revealing the genetics behind the Bur-0 plasmotype effect on the recovery of φPSII and whether these photosynthetic phenotypes influence plant growth parameters (leaf area and shoot biomass) under fluctuating light and cold temperatures under controlled and field-like conditions. A reciprocal F1 crosses approach was used to map the causal gene behind the Bur-0 additive effect on φPSII recovery. *A. thaliana* accessions that share or lack SNP's in previously identified candidate genes of the Bur-0 plasmotype (*MATK, NDHG, YCF1*) were used to produce the F1 plants. An experiment was set under a growth chamber with fluctuating light conditions at Klima (WUR). Plants were phenotyped at the

NPEC facilities using Theeuwen *et al*. (unpublished) light protocol to reveal the causal gene through statistical analysis of the F1 crosses.

In addition, experiments with cybrids with either Col-0 or Bur-0 plasmotypes were performed under controlled and field-like conditions to determine if the Bur-0 additive plasmotype effects on φPSII recovery have an impact on shoot biomass production. Two experiments were performed. First, an experiment took place under field-like conditions at Unifarm (WUR) using a reduced replicate Flood *et al.,* (2020) cybrid panel to test the response of the plasmotype under semi-natural conditions. Additionally, an even more reduced version of Flood *et al.* (2020) cybrid panel, including Col knockouts of *NDHM* and *NDHO* subunits used as controls, was set in growth chamber conditions under diverging fluctuating light treatments (Constant, moderate, high). Both experiments were phenotyped photosynthesis and plant morphology parameters using the NPEC facilities, and their shoot biomass was measured. Statistical analysis using R studio (version 4.1.2) was performed to determine if the Bur-0 plasmotype was affecting shoot biomass responses and what percentage of H^2 changes under the different light treatments and field-like conditions.

Materials and methods

Plant material.

All plant material used in these experiments belongs to the species *A. thaliana.* Except for Col-*ndhm* and Col-*ndho* knockouts (KOs) acquired from the NASC stock centre (https://arabidopsis.info), all plant material used in the experiments was created and provided by Theeuwen *et al.* (unpublished). A detailed view of the plasmotype-nucleotype combinations used in each experiment is available in the appendix (Appendix table 1). Additionally, in the experiment on the genetics behind Bur-0 φPSII recovery, wild-type plants of natural accessions and their respective F1 crosses were produced with the help of Theeuwen *et al*. (unpublished). For this experiment, KASP™ primers for *NDHG* and *MATK* were used to verify the genotype of accession ID471 (Appendix Table 2). The parentals of F1 plants for this experiment were grown under the same environmental conditions. Nonetheless, some of the seeds in cybrids experiments came from different generations.

Seeds were pre-sowed in Petri dishes containing a sheet of filter paper soaked in purified water. Petri dishes were staked inside a plastic box fitted with a wet paper towel in the bottom to maintain proper humidity and prevent drying the seeds. To break seed dormancy, seeds were stored for four days in a conditioned darkroom at 4°C. Subsequently, the box was placed for 24 hours in a growth chamber at 22 °C and 16 hours light/ 8 hours dark photoperiod before sowing the different experiments.

Nomenclature.

Cybrids are labelled as nucleotype^{plasmotype}, meaning Col^{Bur} is a cybrid with Columbia nucleotype and Burren plasmotype. When F1 crosses were used, the nomenclature is Female parent x Male parent. Thereby an F1 cross of Burren x Columbia will be referred to as Bur-Col, which has a Heterozygous nucleotype with the plasmotype of the female parent (Bur-0).

Phenotyping.

All phenotyping platforms used are part of the NPEC joint initiative between WUR and Utrecht University. The Plant screen System^{TM} located in Unifarm greenhouses WUR and supplied by Photon System Instruments was used for the phenotyping of all experiments. This high throughput phenotyping platform can screen up to 20 *A. Thaliana* plants simultaneously through fluorescence and RGB imaging for photosynthesis and morphological parameters, including leaf area (mm). A 6-minute protocol developed by Theeuwen *et al*. (unpublished) was used to screen every set of 20 plants (Figure 2). During the light protocol, 43 photosynthetic parameters were measured from chlorophyll fluorescence during a light fluctuation treatment. This protocol allows the measurement of photosynthesis efficiency parameters under fluctuating light conditions like those occurring in nature.

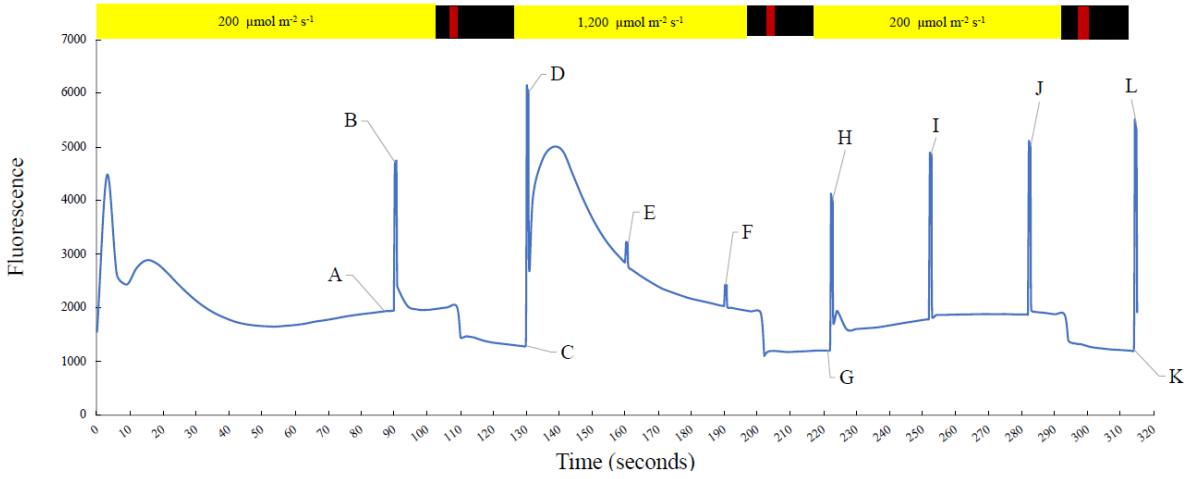

Figure 2. *An example of Theeuwen et al. (unpublished) 6-minute imaging protocol for a specific plant phenotyped by Lawson et al. (2020) using the Plant Screen System^{TM} with time point measurement annotations. Yellow bars on top represent the light input. Blan and red bars indicate periods of fark and infra-red, respectively. A-B: Actinic FqFm (φPSII), CD: Actinic NPQ, φNPQ, φNO, qL, qI, and qE. E: High FqFm 1 (φPSII). F High fqFM 2(φPSII), G-H: High NPQ, φNPQ, φNO, qL, qI, and qE. I: Low FqFm2 (φPSII), J: Low FqFm 2 (φPSII), K-L: NPQ, φNPQ, φNO, qL, qI, and qE. Reproduced from Lawson (2020).*

Data Analysis.

Theeuwen (unpublished) provided an R script used to translate raw fluorescence data obtained from the Plant Screen System™ into 43 photosynthetic parameters per plant used in the analysis. An additional twenty parameters related to plant morphology also recorded by The Plant screen System™ were added to the csv-files obtained. Further analysis was based on this file containing 63 phenotypes for all experiments. Outliers were excluded using an R script provided by Theeuwen (unpublished). Depending on the observed variance in each experiment, the script was set to exclude plants that present leaf area (based on the number of pixels recorded by The Plant screen System™), which present sizes between 1.25 to 1.5 standard deviations (SD) from the mean size. A lower SD was used in experiments where high variation in leaf was suspected to be due to the use of different seed batches or in which plants needed to be resown several days after the initial sowing. These plants were excluded from all subsequent analyses by changing their values to NA.

Experiment 1: Species-wide representative cybrid panel of *A. thaliana* grown under field-like conditions.

An outdoor experiment was set up under gauze tunnels at Unifarm, WUR. The floor of the tunnels was covered in black landscape material. Tunnels measure 8m × 5m and are entirely enclosed by gauze material that allows rainwater, sunlight, and wind to penetrate, thereby simulating field conditions without the interference of herbivores and preventing GM material from being spread to the environment. Watering was performed through a hose according to rain patterns and the observed environmental conditions. Additionally, sampling of the growing substrate was performed daily to ensure plants had enough water. Rain gauges were placed inside the tunnels to estimate precipitation and irrigation requirements.

Plant pots, trays, and growing substrate.

The growing protocol was adapted from a previous experiment by Lawson (2020). Black plastic pots of 7cm × 7cm with 18 cm depth were used for individual plant growth. 40 cm × 60 cm × 20 cm grey trays were used to house 40 pots each and allow transport of the plants to the phenotyping platform. A seedling tray was placed at the bottom of the trays, allowing the pots to be above the edge of the trays. The trays were organized into six rows of 12 trays (Figure 3). Pots were filled with a substrate of sand-peat in a 1:1 proportion. The peat substrate was obtained from Lensli® substrates which includes powdered nutrients YARA PG-MIX™ containing 15-10-20+3 of N, P_2O_5, K_2O and MgO. The electrical conductivity and pH of the substrate were monitored. To avoid algal growth, a blue rubber matt of 7cm × 7cm was placed on top of each pot, with a hole for plants to grow and small holes to allow water penetration.

Sowing design and randomization.

The experiment was sown outdoors during 17-19 of March 2021. An R script provided by Theeuwen (unpublished) was used to create an unbalanced, incomplete block design to randomize the cybrids among pots resulting in every block contained in 6 trays (2 x 3 arrangement), which included all 240 cybrids (Figure 3; Appendix Table 1 contains information on all the nucleotype-plasmotype combinations of the cybrid panel). Plastic labels were used in each pot, having the corresponding location of each pot within the tray and tunnel. The number of replicates was 12 for the cybrid genotypes and 60-80 for the four-wild types. A fine paintbrush was used to select approximately 4-5 pregerminated seeds and place them on top of the substrate in each pot. After 24 days of growth, the most vigorous plants were selected, and the remaining seedlings were removed and discarded. Plants that presented any shading limitation were helped to be exposed to full light.

Maintenance and growing conditions.

The gauze tunnel provided a reliable barrier for herbivores, and this was assessed weekly through the inspection of the tunnel and plant damage. Photosynthetically active radiation (PAR), temperature, CO_2 concentration, soil water content, relative humidity and dewpoint point were monitored during the whole of the experiment through remote sensors placed in the tunnel (Appendix Figure 1-4).

Figure 3: *Left: Arrangement of the experiment within the gauze tunnel. Blue boxes correspond to trays containing 40 pots each (5x8). Blocks consisted of 6 trays (2x3) which housed all 240 cybrids. Additionally, one block with WT plants was used per Row. Overall, three rows, each housing four blocks, were used. Right: Picture of the gauze tunnel at Unifarm (WUR).*

Data Analysis.

Raw chlorophyll fluorescence was processed as described in the general section on data analysis for all experiments described above. Outliers were excluded using an R script provided by Theeuwen (unpublished) based on their genotype. Given that some cybrids came

from different seed batches, causing considerable variation in the mean leaf, the R script for outlier removal was set to exclude plants with a standard deviation of more than ±1.25 from the mean size. These plants were excluded from all subsequent analyses by changing their values to NA. Following Theeuwen (unpublished) approach, the lme4 package in R studio was used for fitting a linear mixed model to perform ANOVA analysis using the Kenward-Roger approach and calculate Best Linear Unbiased Estimators (BLUEs) (Bates *et al*., 2015) (Equation1). Pairwise differences were calculated using the Benjamini & Hochberg test. Cybrids that failed to germinate or only germinated under certain nucleotype backgrounds (Agl-0, Agl-5, Kolyv-6 & IP-Con) were removed from the data set to conserve a balanced design. Additionally, the Ely plasmotype was removed from the final data to avoid overestimating plasmotypic contributions to H^2. In total, 55 plasmotypes (220 cybrids) were taken into account final data analysis.

To calculate the H^2 contributions of the nucleotype, plasmotype and epistatic effects derived from nucleotype-plasmotype interactions, the VarCorr function from the Bates package was used (Bates *et al*., 2015). Additionally, blocks, rows, columns and tunnel rows within the experiment were tested for their contribution to the explained variance as random factors. As the influence in the observed variance from blocks and tunnel rows was considerable, they were included in the model as random factors.

$$Y=\text{Nucleotype} + \text{Plasmotype} + (\text{Nucleotype}\times\text{Plamotype}) + \underline{\text{Block}} + \underline{\text{Tunnel Row}} + \underline{\varepsilon}$$

Equation 1: *Linear Model used for the initial ANOVA and Kenward Roger adjustment. Underlined variables are random terms, and epsilon denotes the residual.*

$$Y= \text{Plasmotype} + \underline{\text{Block}} + \underline{\text{Tunnel Row}} + \underline{\varepsilon}$$

Equation 2. *Linear model used for the initial ANOVA and Kenward Roger adjustment to analyse cybrids of a specific nucleotype. Underlined variables are random terms, and epsilon denotes the residual*

$$Y=\underline{\text{Nucleotype}} + \underline{\text{Plasmotype}} + (\underline{\text{Nucleotype}\times\text{Plamotype}}) + \underline{\text{Block}} + \underline{\text{Tunnel Row}} + \underline{\varepsilon}$$

Equation 3: *Linear Model used for estimation of variance. Underlined variables are random terms, and epsilon denotes the residual.*

Principal component analysis (PCA) was used to visualize the variation between plasmotypes using R Studio based on the BLUE's for the plasmotypes. Phenotypes for the PCA were chosen as they were observed to present high H^2 for the plasmotype or nucleotype-plasmotype interaction. Plasmotypes that could potentially act as outliers were removed from the data set to avoid confounding effects. Based on the PCA's results, plasmotypes with high variability in the phenotypes used for PCA were chosen for further analysis. The native plasmotypes of each nucleotype were selected in this list (Bur-0, Col-0, Cvi-0 & Tanz-1 in addition to twelve contrasting plasmotypes.

Given the short time frame of this project, an extensive analysis of missense variants in cpDNA of these accessions was not feasible. Based on Flood *et al*. (2020) suggestion that the *NDHG* missense variant found in Bur-0 is the strongest candidate gene for its photosynthetic phenotypes, further analysis for missense variants in *NDH* genes was performed. The analysis focused on finding missense variants in the less conserved genes of the NDH complex in *A.*

thaliana suggested by Sato *et al*. (1999) (*NDHF, NDHG, NDHA and NDHK).* By searching in the chloroplast genomes previously genotyped and analysed for polymorphisms by Theeuwen *et al*. (unpublished), missense variants in the selected plasmotypes were identified.

Experiment 2: Genetic cause behind Bur-0 additive effect on the recovery of φPSII

For this experiment, a complete diallel design with seven parents was sown in a growth chamber in Klima, WUR. The seven parentals used were A. *thaliana* accessions: Tanz-1, Reuv, Bur-0, NL1467, NL2373, NL332, and ID471. The accessions were chosen as they share or lack SNPs with the candidate genes previously identified in the Bur-0 plastid genome, suspected to be responsible for its photosynthetic phenotypes. Accession NL1467 was chosen as it shares four SNPs, two in *MATK*, one in*YCF1* and one in *NDHG*; accession NL332 and NL2373 have two identical SNPs in *MATK* and *YCF1*; accession ID-471 share a single distinct SNP in *MATK*. Accessions Tanz-1 and Reuv did not contain any of Bur-0 distinct plastid SNPs and were chosen as controls (Table 2). KASP genotyping with two primers for chloroplast SNP's (*MATK* and *NDHG*) was conducted on accession ID471, as this accession was recently acquired and required reconfirmation (Appendix Table 2 contains the primers used).

		# SNP	♂ Male parent						
			BUR	NL-1467	NL-332	NL-2373	ID-471	Reuv	Tanz
♀ Female parent	BUR	4							
	NL-1467	4							
	NL-2373	2							
	NL-332	2							
	ID-471	1							
	Reuv	0							
	Tanz	0							

Table 1*: Complete diallel design including A. thaliana accessions used. Grey diagonal indicates Wild-types, which were excluded from the analysis. The white block shows the ID-471-Reuv cross, which failed to germinate and was excluded from the experiment.*

Sowing and randomization.

An R script was used to create an unbalanced, complete block design to randomize the genotypes among twelve blocks (Figure 4). As the Plant Screen System^{TM} can only phenotype twenty plants at a time, each block contained 60 plants to include the 49 genotypes. Therefore, one block of plants was measured over three different Plant Screen System^{TM} trays. A total of 720 plants were sown. Each genotype was sown at twelve (n=12) for 588 plants (12x49=588). To fill the remaining 132 plants needed for complete blocks (720-588=132), Col-WT and Col-*ndho* were sown to complete the remaining ones. Since the cross of ID471-Reuv produced seeds of poor quality that failed to germinate, this genotype was replaced by another filler

genotype(Col-*ndhm*). Additionally, some crosses failed to germinate. As there were no extra seeds, they were replaced and resown with a filler genotype (Col-WT) to maintain complete blocks.

Plants were sown in rockwool cubes of 4cm x 4 cm x 4 cm previously soaked in Hyponex nutrient solution (provided by Unifarm, WUR). A grey rubber square slightly larger than the blocks was placed on top of the cubes and pinned with a translucent pipet tip to prevent algal growth. Plastic labels were used in every block to map the experiment. Sowing was conducted using a single seed and resown three days after if they failed to germinate. The experiment was sown in a growth chamber with a single hydroponic basin and organized into blocks, as displayed in figure 4.

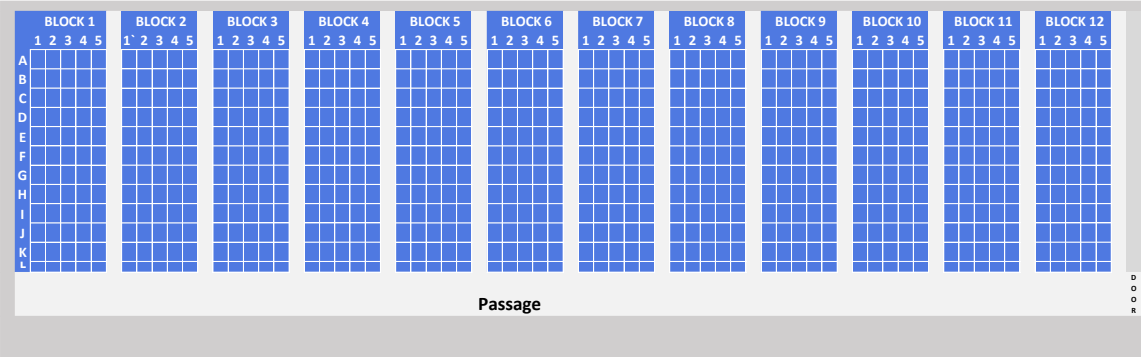

Figure 4: *Arrangement of the experiment in a growth chamber at Klima (WUR). Half a growth camber was used in which a single hydroponic basin was present. Squares correspond to experimental units sown in rockwool cubes. Blocks consisted of 60 plants containing all crosses and filler genotypes.*

The experiment was grown in a climate chamber with a constant light intensity of 250 (µmol $m^{-2}s^{-1}$) 10H Light/ 14H dark. The temperature was set at 20º C during the day and 18º C during the night, with constant relative humidity at 70%. Seventeen days after sowing the experiment, fluctuating light conditions were started every 20 minutes between 100 µmol m^{-2} $s^{-1}$and 400 µmol m^{-2} s^{-1} (Figure 5). A handheld light meter was sampled to confirm the uniformity of light intensity in the growth chamber. After 23 days of growth, the plants were taken into Unifarm greenhouses in two batches and phenotyped using the Plant Screen System™ with the above-described light protocol provided by Theeuwen *et al*. (unpublished).

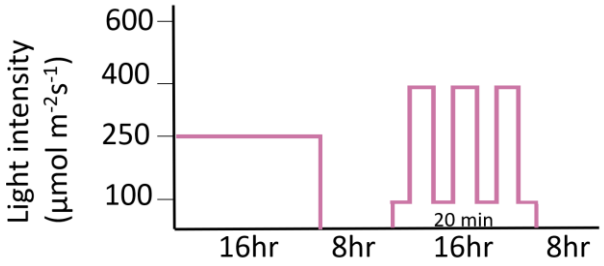

Figure 5: *Graphical representation used to visualize the daily light treatments of the plants in the growth chamber at Klima (WUR). Constant light was provided during the first 17 days of growth at 16H light/8 dark photoperiod. Using the same photoperiod, on the 18th day of growth, fluctuating light conditions were started every 20 minutes till day 23 of growth.*

Data Analysis.

Raw chlorophyll fluorescence was processed as described in the general phenotyping section above. Filler genotypes Col-WT, Col-*ndho*, and Col-*ndhm,* were removed from the analysis, as were the WT accessions. After doing so, outliers were excluded using an R script provided by Theeuwen (unpublished) based on their genotype. The script excluded plants that present leaf area more than ±1. 5 standard deviations from the mean size. These plants were excluded from all subsequent analyses by changing their values to NA. The data analysis was initially performed on the "low_FqFMp_induction" phenotype, as it measures the efficiency of photosystem II after high light conditions, mimicking fluctuating light in nature. Additionally, this parameter has been repeatedly observed by Theeuwen *et al*. (unpublished) as a reliable and replicable photosynthetic parameter where the Bur-0 plasmotype additive effect can be observed. To check whether the results were also observable under NPQ phenotypes, parameters low_NPQt and low_qEt were also analysed.

Since *A. thaliana* inherits the plasmotype maternally, results were divided according to the maternal and paternal donors to a particular genotype for data analysis. For example, the crossing between Bur-0 x ID471 was classified in both Bur-0 and ID471 groups. Thereby the genetic source of variation in this cross was denoted as "50% nucleotype and plasmotype" (donated by the maternal parent) and "50% nucleotype" (donated by the paternal parent). Accordingly, plants were classified based on the source of their plasmotype or strictly nucleotype donor. For instance, the Bur-0 x ID471 cross would be classified as having a "plasmotype" in the Bur-0 group and (50%) "nucleotype" in the ID471 group. A linear mixed model was used to fit the data where blocks were fixed. The interaction between the nucleotype x plasmotype was not considered due to the heterogeneous nature of the nucleotypes (Equation 1). Moreover, WT accessions were removed as they cannot be contained in both groups at once. An R script was used to perform an ANOVA of the produced data (Theeuwen unpublished).

$$Y = Group1 + Group2 + \underline{Block} + \underline{\varepsilon}$$

Equation 4. *Linear model used for the ANOVA and Kenward-Roger adjustment of the data. Underlined variables are random terms, and epsilon denotes the residual*

Experiment 3: Impact of the Bur-0 plasmotype additive effects on shoot biomass.

These experiments took place under growth chamber and field-like conditions to assess the impacts on shoot biomass in cybrids with either a Bur-0 or Col-0 plasmotype.

3.1. Impact of the Bur-0 plasmotype additive effects on shoot biomass under growth chamber conditions with fluctuating light treatments.

A growth chamber at Klima, WUR, was used for these experiments. The growth chamber was split into three separate spaces, each housing an independent light treatment. It was divided by a reflective plastic sheet that ensured the light treatments were properly isolated to avoid light escaping to the adjacent space. Every space consisted of two hydroponic basins able to house

120 plants (for 240 plants in total per light treatment), as portrayed in (Figure 6). Hydroponic basins were used as a blocking factor.

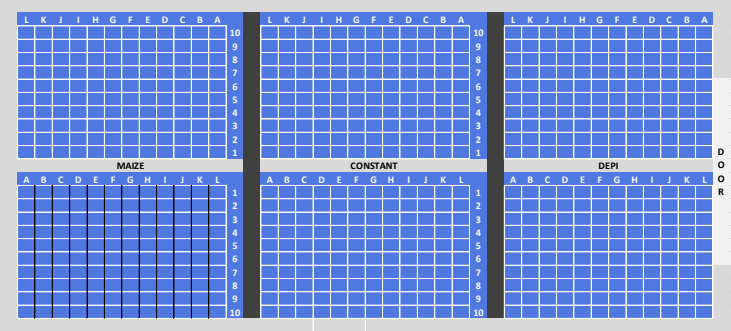

Figure 6. *Arrangement of the Biomass experiments in a growth chamber at Klima (WUR). A growth chamber was split into three separate spaces with reflective material. 2 hydroponic basins were used per light treatment. Each hydroponic basin was used as a block and contained 120 plants (12 replicates of each cybrid and Col-ndhm and Col ndho KOs).*

The three-light treatments were executed through a program that controlled LED lights in the growth chambers. Cumulative daily light exposure was the same for all light treatments (418 µmol m^{-2} s^{-1}). The first light treatment consisted of constant light at the intensity mentioned above. The moderate light fluctuation is an adapted protocol from MSU Dynamic Environmental Photosynthesis Imager (DEPI) in which are exposed to a sinusoidal light intensity pattern, similar to that plants are exposed throughout the day in natural conditions. The light intensity starts initially low in the morning and gradually increases to reach a maximum of 1000 µmol m-^{2} $s^{-1,}$ from which it decreases back to zero. Moreover, this light treatment presents minor fluctuations every 10 and 20 minutes, simulating the reflection of sunlight by clouds which reduces the maximum light at noon to 500 (Cruz *et al*., 2016). The second light fluctuation treatment (high light fluctuation, created by Theeuwen *et al.* (unpublished), is denoted as "Maize" and simulates the incoming light that reaches a small plant under the canopy of a fully developed maize crop. Light intensity also follows a sinusoidal pattern but is generally low with sporadic bursts of very high-intensity light up to 1500 µmol m^{-2} s^{-1}) that simulate sun coming through the maize canopy. Figure 7 shows a representation of the light treatments. All treatments were subjected to a 12h light / 12h dark photoperiod. The temperature was set at 20º C during the day and 18º C during the night, with constant relative humidity at 70%.

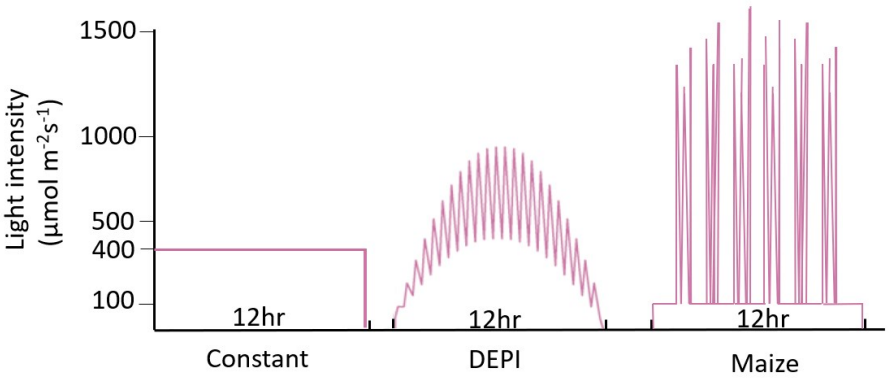

Figure 7*: Graphical representation of light treatments used to assess the impacts of the recovery of φ PSII on shoot biomass under a growth chamber at Klima (WUR). Left: Constant light. Centre: Moderate light fluctuation (DEPI). Right: High light fluctuation (Maize). Photoperiod was set at 12H light/12 dark. Note: The cumulative daily light exposure is the same for all light treatments (418 µmol m^{-2} s^{-1}).*

Sowing and randomization.

An R function was used to randomize each genotype within the hydroponic basin that acted as blocks within the different treatments. The cybrid panel consisted of 8 cybrids derived from 4 nucleotypes backgrounds under Col-0 and Bur-0 plasmotypes. Additionally, two knockouts of nuclear-encoded *NDHO & NDHM* genes with a Columbia wild-type background (Col-*ndhm* & Col-*ndho*) were used as controls (Table 2). Plants were sown in rockwool cubes with the protocol described in the diallel experiment. Sowing was conducted using a single seed and resown 3-6 days after if they failed to germinate.

Description	Plasmotype	Nucleotype	Genotype	Growth Chamber	Tunnel
Cybrid	Col	Bur	Bur^{Col}	✓	✓
		C24	$C24^{Col}$	✓	✓
		Tanz	$Tanz^{Col}$	×	✓
		Cvi	Cvi^{Col}	×	✓
		Ws-4	$Ws\text{-}4^{Col}$	×	✓
		Ler	Ler^{Col}	✓	✓
		Shah	$Shah^{Col}$	×	✓
		Ely	Ely^{Col}	×	✓
Self-Cybrid		Col	Col^{Col}	✓	✓
Wildtype	Col	Col	Col^{Col}	×	✓
Knock out	Col	Col-*ndhm*	Col-*ndhm*	✓	×
Knock out	Col	Col-*ndho*	Col-*ndho*	✓	×
Cybrid	Bur	Col	Col^{Bur}	✓	✓
		C24	$C24^{Bur}$	✓	✓
		Tanz	$Tanz^{Bur}$	×	✓
		Cvi	Cvi^{Bur}	×	✓
		Ws-4	$Ws\text{-}4^{Bur}$	×	✓
		Ler	Ler^{Bur}	✓	✓
		Shah	$Shah^{Bur}$	×	✓
		Ely	Ely^{Bur}	×	✓
Self-cybrid		Bur	Bur^{Bur}	✓	✓
Wildtype		Bur	Bur^{Bur}	×	✓
Knock out		none		×	×
Knock out				×	×
Used=✓					
Not Used=×					

Table 2: Overview of genotypes of the plants for screening the reduced cybrid panel to assess the Bur-0 photosynthetic phenotypes under field-like conditions.

Phenotyping.

Twenty-four days after sowing, plants were phenotyped for photosynthesis and morphology parameters using The Plant Screen System^{TM} using the same light protocol designed by Theeuwen *et al*. (unpublished) described above for experiment 1 (Figure 2). Twenty-six days after sowing, when the first plants showed signs of flowering, the shoots were harvested and dried on a stove for over 48 hours at 60 °C. Immediately after drying, their dry weight was measured.

Data Analysis.

Raw chlorophyll fluorescence was processed as described in the general phenotyping section above. The data was then divided according to the light treatment. Consequently, two separate groups were created for each light treatment: Cybrids (excluding Col-*ndhm* and Col-*ndmo*) and Col-0 self-cybrids (Col^{Col}) and Col-*ndhm and Col-ndh0* (excluding all other cybrids). After doing so, outliers were excluded using an R script provided by Theeuwen (unpublished) based on their genotype. As high variability in leaf area was found among hydroponic basins and some cybrids that had to be resown after five days, the script excluded plants that presented leaf area more than ±1.25 standard deviations from the mean size. These plants were excluded from all subsequent analyses by changing their values to NA. To determine plasmotype-nucleotype interaction, the Kenward-Roger approach was used in a linear model (Equation2). The variance explained by blocks, rows and columns within the experiment was tested. As Blocks (hydroponic basins) were found to be explaining a considerable amount of the variance observed in growth parameters, they were included in the model as random factors. Following Theeuwen (unpublished) approach, the lme4 package in R studio was used for fitting a linear mixed-effects model to perform ANOVA analysis and calculate Best Linear Unbiased Estimators (BLUEs) (Bates *et al*., 2015)

$$Y = \text{Nucleotype} + \text{Plasmotype} + (\text{Nucleotype} \times \text{Plasmotype}) + \underline{\text{Block}} + \underline{\varepsilon}$$

Equation 5: *Linear model used for the ANOVA and Kenward-Roger adjustment of the data of cybrids. Underlined variables are random terms, and epsilon denotes the residual.*

$$Y = \text{Genotype} + \underline{\text{Block}} + \underline{\varepsilon}$$

Equation 6: *Linear model used for the ANOVA and Kenward-Roger adjustment of the data involving Col-0 self-cybrids and Col-ndhm and ndho KOs. Underlined variables are random terms, and epsilon denotes the residual.*

$$Y = \underline{\text{Nucleotype}} + \underline{\text{Plasmotype}} + (\underline{\text{Nucleotype} \times \text{Plasmotype}}) + \underline{\text{Block}} + \varepsilon$$

Equation 7: *Model used to estimate the variance of data from data of cybrids. Underlined variables are random terms, and epsilon denotes the residual.*

$$Y = \underline{Genotype} + \underline{Block} + \underline{Tunnel\ Row} + \underline{\varepsilon}$$

Equation 8: *Model used to estimate the variance of data from Col-0 self-cybrids and Col-ndho and ndhm KO's. Underlined variables are random terms, and epsilon denotes the residual.*

3.2. Impact of the Bur-0 plasmotype additive effects on shoot biomass under field-like conditions.

An additional outdoor experiment was set up under the adjacent gauze tunnel at Unifarm (WUR). Growing conditions and plant maintenance were performed as described above.

Sowing and randomization.

Sowing took place between 25th and 26th March 2021. A fine paintbrush was used to select approximately 4-5 pregerminated seeds and place them on the substrate in each pot. After 24 days of growth, the most vigorous plants were selected, and the remaining seedlings were removed and discarded. Plants that present any shading limitation were helped to be exposed to full light. An Excel function provided by Theeuwen (unpublished) was used to randomize the trays of the experiment. Eighteen cybrids derived from 9 nucleotypes and two plasmotypes combinations and their corresponding (two) WT were sown for 20 genotypes (table 2). Two rows, each with nine trays with 40 plants (each tray represents a block with two replicates of each genotype), were organized across the gauze tunnel. Every plasmotype-nucleotype combination had 40 replicates for a total of 720 cybrids. Plastic labels were used in every pot map of the experiment.

Phenotyping.

Forty days after sowing, plants were phenotyped for photosynthesis and morphology parameters using The Plant Screen System^{TM} using the same light protocol provided by Theeuwen (unpublished). Forty-three days after sowing, when the first plants showed signs of flowering, the shoots were harvested and dried on a stove for over 48 hours at 60 °C. Immediately after drying, their dry weight was measured.

Data Analysis.

Raw chlorophyll fluorescence was processed as described in the general phenotyping section above. After doing so, outliers were excluded using an R script provided by Theeuwen (unpublished). Depending on the observed variance, the script excluded plants that present leaf area (based on the number of pixels recorded by The Plant Screen System^{TM}) more than ±1.5 standard deviations from the mean size. These plants were excluded from all subsequent analyses by changing their values to NA. To determine plasmotype-nucleotype interaction, the Kenward-Roger approach was used in a linear model (Equation1). The block number, rows and columns within the experiment were tested for significance as random factors. Only blocks explained a considerable amount of the variance observed in growth parameters, and they were included in the model as random factors. Following Theeuwen et al. (unpublished) approach,

the lme4 package in R studio was used for fitting a linear mixed model to perform ANOVA analysis (Bates *et al*., 2015)

$$Y=\text{Nucleotype} + \text{Plasmotype} + (\text{Nucleotype}\times\text{Plamotype}) + \underline{\text{Block}} + \underline{\varepsilon}$$

Equation 9: *Linear model used for the ANOVA and Kenward-Roger data adjustment. Underlined variables are random terms, and epsilon denotes the residual.*

$$Y= \text{Genotype} + \underline{\text{Block}} + \underline{\varepsilon}$$

Equation 10: *Linear model used for the ANOVA and Kenward-Roger adjustment of the data when comparing Col-0 cybrids (Col^{Bur} and Col^{Col}) and Col-0 wild-type. Underlined variables are random terms, and epsilon denotes the residual.*

$$Y= \underline{Nucleotype} + \underline{Plasmotype} + \underline{(Nucleotype\times Plamotype)} + \underline{Block} + \underline{\varepsilon}$$

Equation 11: *Model used to estimate the variance of data from data of cybrids. Underlined variables are random terms, and epsilon denotes the residual.*

Results.

Experiment 1: Species-wide representative cybrid panel of *A. thaliana* grown under field-like conditions.

Previous research has identified significant plasmotype variability affecting photosynthesis efficiency phenotypes in the model plant *A. thaliana,* and the effect of such variability is more pronounced under fluctuating light conditions (Flood *et al.,* 2020). Nonetheless, previous research has focused on a narrow cybrid panel that was wholly phenotyped under controlled (growth chamber) environmental conditions (Flood *et al.,* 2020). Moreover, the effects of plasmotype variability on photosynthetic efficiency under multiple abiotic stresses that influence photosynthesis have not yet been addressed. This experiment aims to determine whether plasmotype genetic variation results in photosynthesis efficiency and plant morphology phenotypes in an outdoor grown species-wide representative cybrid panel of *A. thaliana.* To achieve this, a cybrid panel created by Theeuwen *et al*., (unpublished) was grown under field-like conditions similar to that *A. thaliana* naturally occurs and phenotyped using NPEC high throughput phenotyping platform at Unifarm (WUR). H^2 of N/P/N×P was calculated, and phenotypes recording high H^2 for the plasmotype were analysed.

Photosynthesis parameters at low light conditions in the Plant Screen System™ were analysed (Low_FqFmp 2, Low_NPQt and Low_qEt) and compared to leaf area phenotypes. These photosynthetic parameters measure the recovery of φPSII, NPQ and its fast element qEt at low light after being exposed to a high light pulse, simulating light fluctuation in nature. Before calculating the H^2 and variance components for the experiment, cybrids carrying the Ely plasmotype were removed from the dataset. The reason behind this is the large-scale effect mutation found on the Ely plasmotype that would lead to an overestimation of plasmotypic contributions to H^2 if Ely is left on the dataset.

Variance components were calculated for selected phenotypes (Table 3). On average, among the 43 photosynthesis phenotypes evaluated, H^2 due to N/P/N×P was 17,28%, 0,43% and 2,74%, respectively. A considerable effect of additive and nucleotype-plasmotype interactions was found among some φPSII and NPQ parameters. For example, when summed up, H^2 due to additive plasmotype and plasmotype-nucleotype interactions of low_NPQt was 17.26 % (1.16%+16.10%) and for Low_FqFmp_2 8.18% (1.3% +6.88%).When inspecting the variance components, the row within the tunnel explained a considerable amount of the variation in multiple phenotypes and was used as a random factor in the fitted linear model. The average variation explained by blocks, the tunnel row and error across photosynthesis phenotypes was 21.49%, 19.9% and 38.17%, respectively. Accordingly, of 10 morphology phenotypes analysed, H^2 due to N/P/N×P was on average 25.51%, 0.51% and 2.93%, respectively. Variance explained by blocks, tunnel rows, and uncontrolled factors for these phenotypes was 4.13%, 4.83 and 66.08%, respectively. Finally, in the eight colour parameters evaluated, the average H^2 due to N/P/P×N was 33,85%, 1.49% and 1.33%, respectively. The variance explained by blocking, tunnel row and uncontrolled factors in these phenotypes was 4.16%, 3.36% and 57.49%.

Phenotype	Nucleotype	Nucleotype:Plasmotype	Plasmotype	Block	Tunnel_Row	Residual
low_FqFmp_2	0,5054	0,0688	0,0130	0,1398	0,0180	0,2550
low_NPQt	0,1930	0,1610	0,0116	0,1158	0,2311	0,2874
low_qEt	0,2065	0,0543	0,0130	0,0844	0,1025	0,5391
RGB2,Morpho,AREA_MM	0,3330	0,0545	0,0056	0,1067	0,1459	0,3543

Table 3: *Variance components for selected phenotypes of a species-wide representative cybrid panel of A. thaliana grown in a gauze tunnel simulating field-like conditions at Unifarm (WUR)*

Photosynthesis parameters measured at low light after a high pulse light in the Plant Screen System™ were particularly affected by the plasmotype. For example, the parameter Low_FqFMp_2 confirmed the already known additive effect on the Bur-0 plasmotype for the recovery of φPSII (Figure 8). Moreover, another interesting observation for this parameter was a slightly higher φPSII for plasmotype Melni-2, which was significantly higher than 7 out of 55 plasmotypes evaluated. Additionally, the plasmotypes Shah and Sus-1 produced significantly lower recovery of φPSII than all other plasmotypes. More graphs showing additive plasmotype effects on selected photosynthesis phenotypes that explain the Bur-0 plasmotype impact on fast recovery of φPSII (NPQ and qEt) are presented in the appendix (Appendix figures 5 & 6)

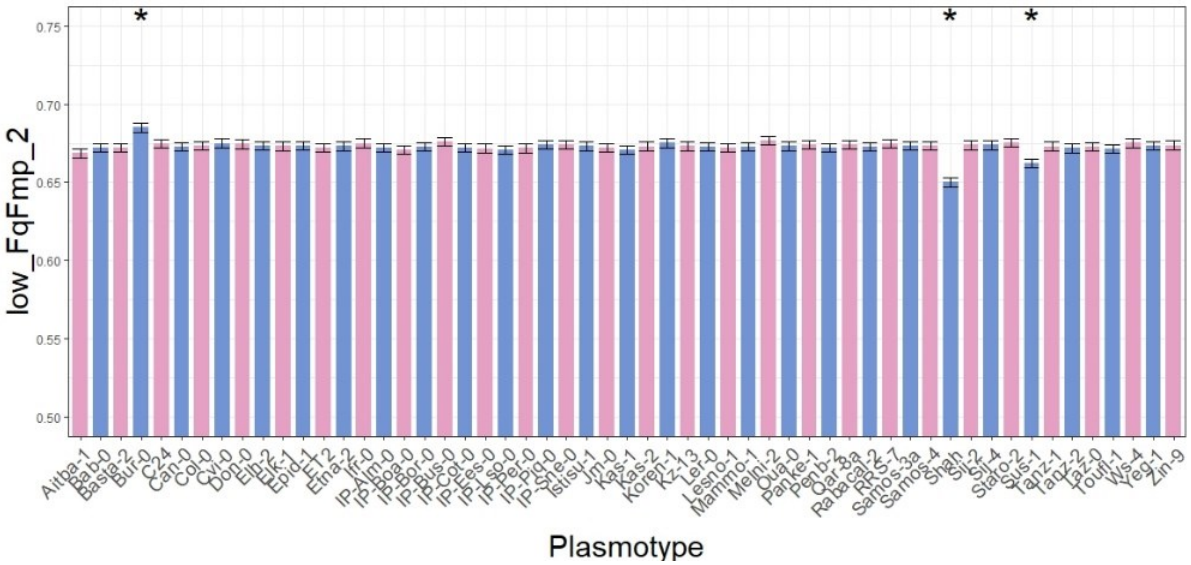

Figure 8: *Additive plasmotype effects on the recovery of φPSII (Low_FqFMp_2) measured at low light after a high light pulse in the Plant Screen System™. Asterisks show significant differences from all other plasmotypes. Multiple comparisons were made using Benjamini & Hochberg test (α=0.05).*

It was possible to observe nucleotype-plasmotype epistatic effects on photosynthesis phenotypes by analysing the specific nucleotype-plasmotype combinations within the cybrid panel (Figure 9; Appendix Figures 7 & 8). For instance, in the Bur-0 plasmotype, the recovery of φPSII (Low_FqFmp_2) was consistently higher among all nucleotypes. However, the Bur-0 plasmotype recovery of φPSII was not significant (α=0.05) under the Cvi-0 or Tanz-1 nucleotype background, yet more pronounced under the Col-0 nucleotype background. By analysing nucleotype-plasmotype combinations, the additive effects found for the Shah and Sus-1 plasmotypes were driven by a significant scale effect under the Cvi-0 nucleotype, but not other nucleotypes (Figure 9; Appendix Figures 7 & 8).

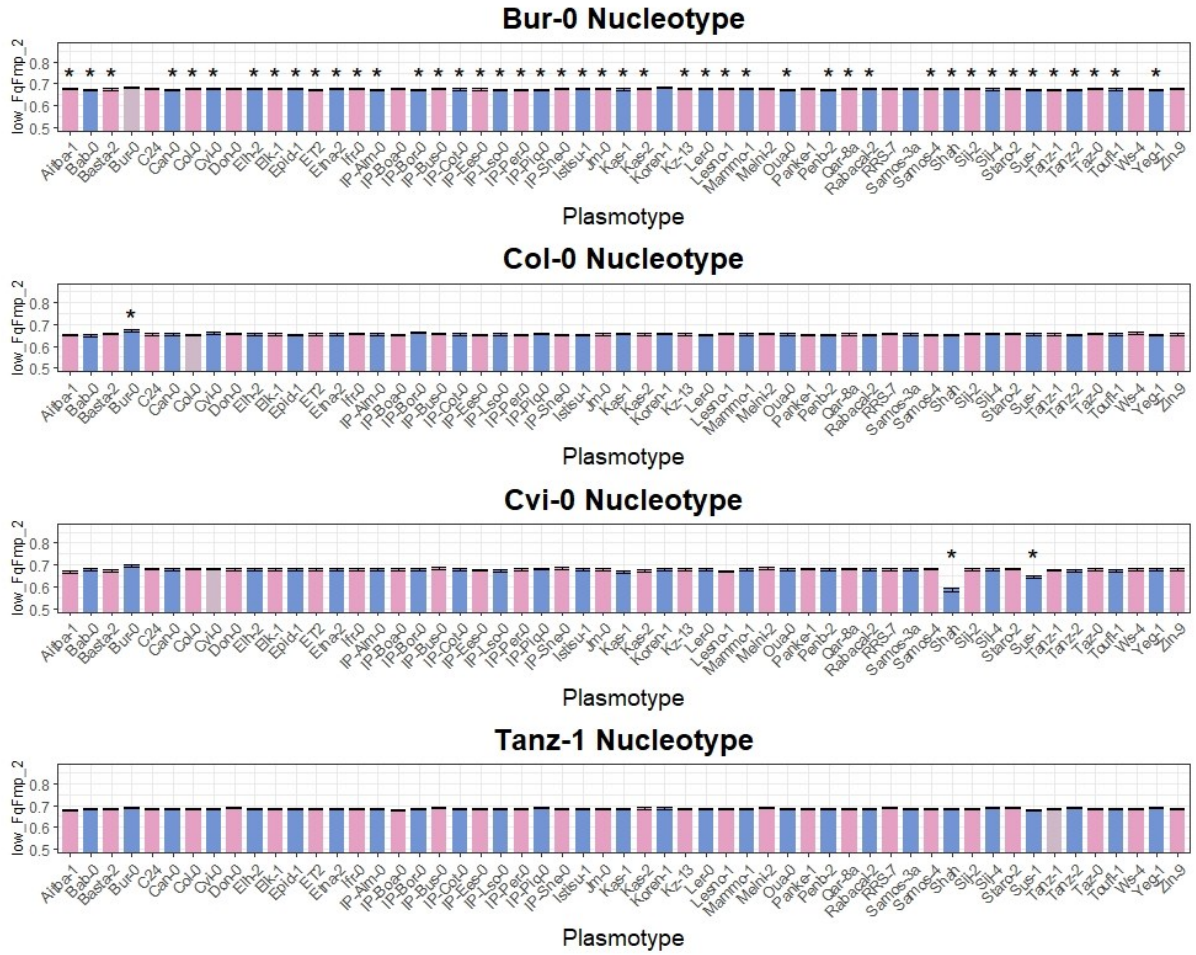

Figure 9: *Effect of Nucleotype-plasmotype combinations on the recovery of φPSII (Low_FqFMp_2) measured at low light after a high light pulse in the Plant Screen System™. Asterisks show significant differences as compared to the native plasmotype. Native plasmotypes are shown in brown. Multiple comparisons were made using Benjamini & Hochberg test (α=0.05).*

NPQ values were lower under all nuclear backgrounds with a Bur plasmotype, but these differences were not significant under the Cvi-0 nucleotype (Appendix Figure 7). Moreover, Bur^{Bur} cybrids were not significantly different to Bur^{Melni} or Bur^{Panke}. Additionally, as observed with Bur-0, the IP-Bor-0 plasmotype presented significantly lower NPQ values under the Col-0 nucleotype (Appendix Figure 7). A similar pattern was found for qE values. The Bur-0 plasmotype presented lower qE values under all nucleotypes, but the differences were only significant under the Bur-0 and Col-0 nucleotypes. Moreover, no plasmotype produced significant differences in qEt when phenotyped under low light conditions under the Tanz-1 nucleotype (Appendix Figure 8).

As a proxy to quantify plant growth parameters, the leaf area of all cybrids was measured using the Plant Screen System™ (Figure 10). Estimated H^2 for this trait was 31.1% due to nucleotype, 0.63% for plasmotype effects and 5.3 % for nucleotype-plasmotype interactions. Cybrids carrying the Col-0 Nucleotype were the largest, with an average of 1162mm, followed by the Bur-0 Nucleotype (average 1077mm), Cvi-0 nucleotype (average 852mm and Tanz-1 Nucleotype (average 747mm). Overall nucleotype backgrounds, the Kas-1, and to a lesser

extent, the Staro-1 plasmotype recorded substantially larger plants than most but not all plasmotypes. On the contrary, cybrids with either a Shah or Sus-1 plasmotype produced significantly smaller leaf areas than most, but not all, plasmotypes. However, when inspecting nucleotype-plasmotype interactions (Appendix Figure 9), these effects were only found under the Cvi-0 nucleotype, and sample sizes for Cvi^{Shah} and $Cvi^{Sus\text{-}1}$ cybrids revealed that only a few plants were taken into account in the statistical analysis after outlier removal (4/12 and 5/12 plants taken into account from all seeds sowed, respectively). The large effect of the nucleotype is an expected result as leaf area is a complex quantitative trait. Nucleotypes of African origin (Cvi-0 and Tanz-1) had the lowest leaf areas, probably affected by the spring conditions in the gauze tunnels. Moreover, additive plasmotype effects were not found. Instead, nucleotype-plasmotype interactions appear to have a strong effect.

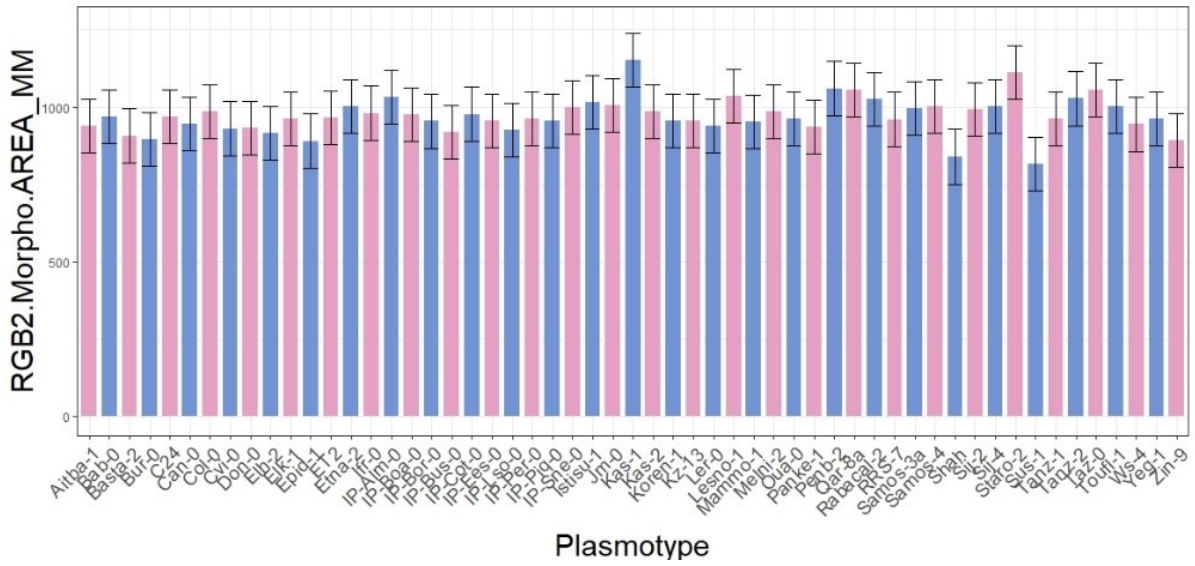

Figure 10. *Additive effect of the plasmotype on Leaf Area (mm) recorded in the Plant Screen System™. Asterisks show significant differences from all other plasmotypes. Multiple comparisons were made using Benjamini & Hochberg test (α=0.05).*

To visualize the variation between plasmotypes, a principal component analysis (PCA) was performed based on the BLUE's for the plasmotypes (Figure 11). Phenotypes for the PCA were chosen as high H^2 for the plasmotype or nucleotype-plasmotype interaction was observed. Plasmotypes that could potentially act as outliers were removed from the data set to avoid confounding effects. This was the case for Shah and Sus-1 since their large-scale effects under the Cvi-0 nucleotype were masking the small-scale effects of other plasmotypes. Based on the PCA's results, plasmotypes with high variability in the phenotypes used for PCA were chosen for further analysis.

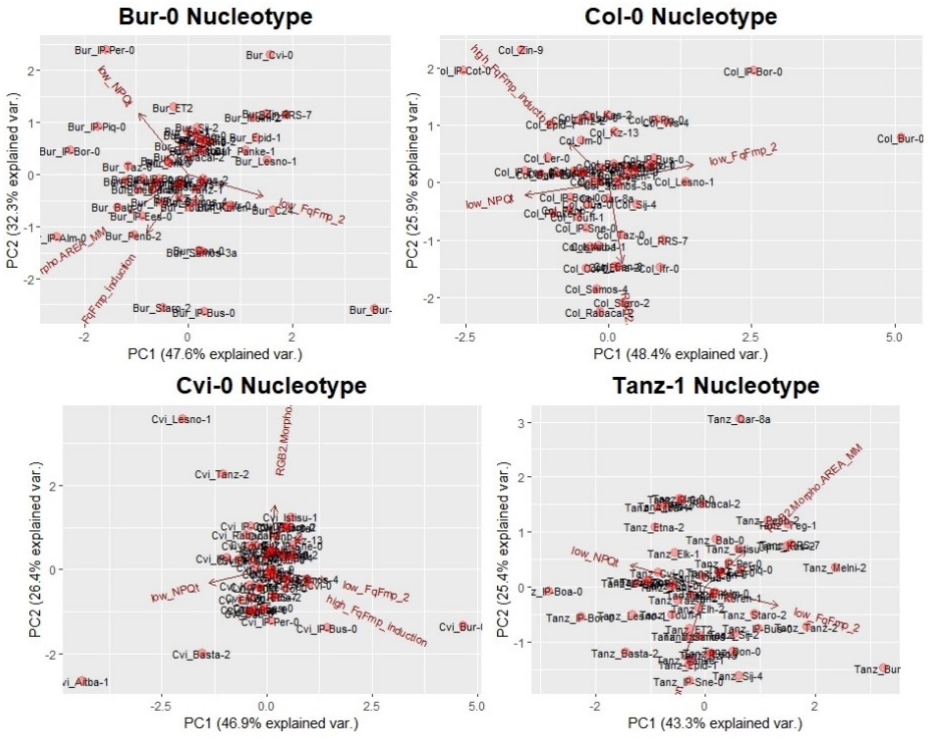

Figure 11. *Principal component analysis (PCA) of the different nucleotype-plasmotype combinations. Four phenotypes in which the plasmotype generated high H^2 were used for the analysis (Low_NPQt, High_FqFmp_induction, Low_FqFMp and leaf area)***.**

A clear effect of various plasmotypes was observed among the phenotypes analysed. Most notable was the large effect of the Bur-0 plasmotype, which was consistently observed at the edges of the PCA plots indicating this plasmotype generates large-scale effects, particularly on photosynthesis phenotypes. Apart from Bur-0, no plasmotype generated a large-scale additive impact on any phenotypes (Figure 12; Appendix Figure 10). Nonetheless, the IP-Alm-0, Ip-Per-0 and Staro-2 plasmotypes produced slightly larger plants across some nucleotypes (Figure 11). A nucleotype-plasmotype interaction was observed for $Bur^{IP\text{-}Alm}$ cybrids, which presented higher than average φPSII when phenotyped under high light conditions (Appendix Figure 11) under the Bur plasmotype.

The highest variability in phenotypic responses due to plasmotype effects was observed in the Cvi-0 nucleotype. Unlike most cybrids with a Cvi-0 nucleotype, $Cvi^{Kas\text{-}1}$ presented the largest plants in the whole cybrid panel (Figure 12). However, this was not the case with Kas-2, which showed an average leaf area under the Cvi-0 nucleotype, but a significantly lower leaf area under a Col-0 nucleotype. $Cvi^{Kas\text{-}1}$ and Cvi^{Lesno} also recorded significantly lower recovery of φPSII (Appendix figure 11). Other plasmotypes causing significant differences in phenotypes analysed were the $Cvi^{Aitba\text{-}1}$ cybrids which registered significantly lower recovery of φPSII, higher NPQ values and lower leaf area under the Cvi-0 nucleotype (Figure 12; Appendix Figure 11).

Further analysis to find any underlying missense variations in these plasmotypes was undertaken. Given the significant scale effects of the Bur-0 plasmotype and that the *NDHG* missense variant found in Bur-0 is the strongest candidate for these photosynthetic phenotypes

(Flood *et al*., 2020), the analysis focused on NDH genes. By searching in the chloroplast genomes previously genotyped and analysed by Theeuwen *et al*. (unpublished), missense variants were found for Cvi-1 (1 SNP *NDHA*), Kas-2 & Kas-1 (1 SNP in *NDHF) and* Staro-2 (1 SNP *NDHA and* 1 SNP in *NDHK*).

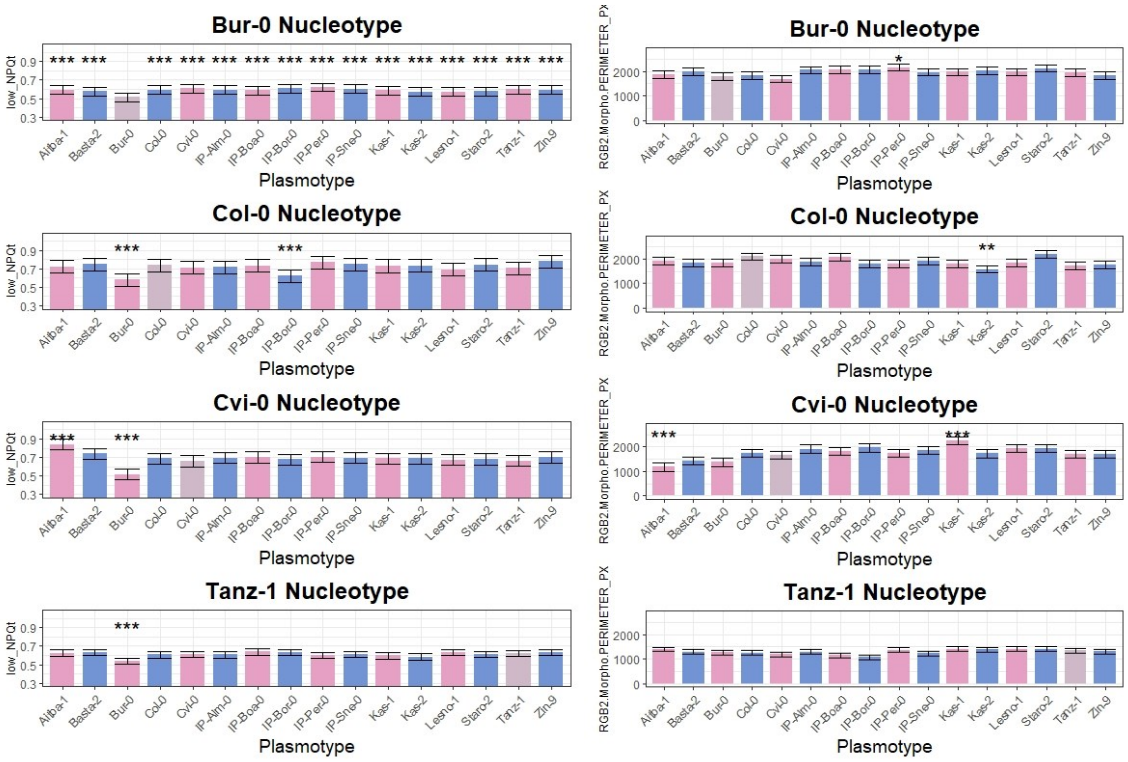

Figure 12. *Effects of PCA-selected plasmotypes on NPQ and Leaf area (mm). Asterisks show significant differences as compared to the native plasmotype. Native plasmotypes are shown in brown. Multiple comparisons were made using Benjamini & Hochberg test (***α=0.01, ** α=0.05, * α=0.1).*

Experiment 2: Genetic cause behind Bur-0 additive effect on the recovery of φPSII.

This experiment used natural accessions that share all or some of the same SNP's found in the Bur-0 plastid genome candidate genes to discard those that do not explain the genetic cause behind Bur-0 φPSII recovery. A complete diallel design was constructed by making crosses of 7 parentals (including reciprocal crosses). As a complete diallel was used, it was possible to create two groups: one with 50 % the same nucleotype and random plasmotypes (common male genotype donor) and one with 50% the same nucleotype and the same plasmotype (common female genotype donor). Phenotypes of WT plants were removed from the data set for analysis, as WTs would be contained in both groups at once. Comparing these two groups

independently through Anova and Tukey's multiple comparison tests made it possible to determine if a specific plasmotype was the genetic origin of φPSII recovery.

An additive plasmotype effect was found to cause significantly higher φPSII recovery (α=0.05) in the group of F1 accessions in which Bur-0 or NL146 was the maternal genotype donor (Figure 13). Moreover, these groups also presented higher φPSII recovery values than any other group, including those where Bur-0 and NL1467 acted as paternal genotype donors (50% nucleotype with random plasmotypes). The groups of F1 accessions in which NL2373 or NL332 acted as a maternal genotype donor scored significantly lower φPSII recovery values after the highlight exposure than groups where Bur-0 or NL146 was the maternal genotype donor. These lower φPSII recovery values compared to groups where Bur-0 or NL146 was the maternal genotype donor were also confirmed for controls, Reuv and Tanz-1. Finally, the group of F1 accessions where ID471 acted as a maternal genotype donor presented significantly lower φPSII recovery values than groups where Bur-0 or NL146 was the maternal genotype donor. These results align with previous reports by Tijink (2021).

Nonetheless, accession ID471 had not been identified when Tijink (2021) used reciprocal crosses to narrow the candidate genes explaining the Bur plasmotype effect on φPSII recovery. Thereby, Tijink (2021) discarded one *MATK* and one *YCF1* SNPs present in accessions in NL2373 or NL332 and suggested the causal gene was either *NDHG* or *MATK* (as there was a remaining SNP that could not be excluded). Given accession, ID471 carries the additional SNP in *MATK* that could not be discarded, and the group of F1 accessions in which ID471 is the maternal genotype donor does not display the additive effect on φPSII recovery found in the Bur-0 plasmotype, it is possible to discard *MATK* as being the causal gene behind this phenotype. Therefore, as no other SNPs remain to be discarded, *NDHG* is the most likely causal gene.

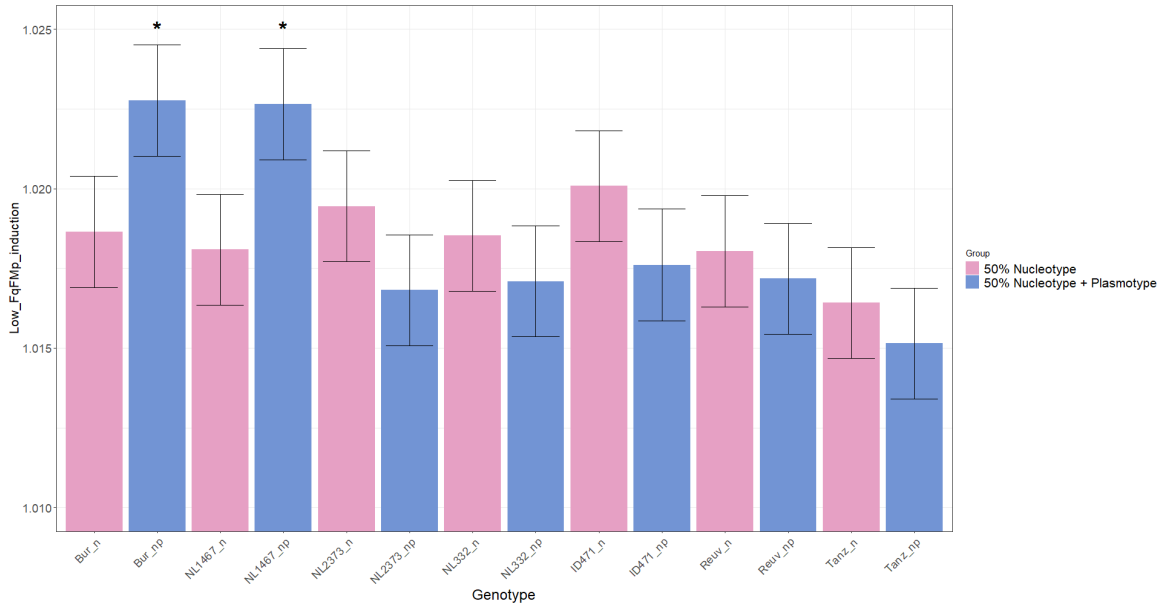

Figure 13: *Effects on "Low_FqFmp_induction" parameter reflecting the recovery of φ PSII in groups with 50% Nucleotype or 50% Nucleotype + Plasmotype used to map the genetic origin of the Bur-0 plasmotype additive effect on the recovery of φPSII. Pink bars represent the average phenotype for groups of crosses with 50% Nucleotype. Blue bars represent the average phenotype of the group with 50% Nucleotype + Plasmotype.*

Asterisks show significant differences. Multiple comparisons were made using the Tukey test for the group with 50% Nucleotype + Plasmotype (α=0.05).

Experiment 3: Impact of the Bur-0 plasmotype additive effects on shoot biomass.

Building on previous evidence that plants that carry the Bur-0 plasmotype show increased recovery φPSII and faster relaxation of NPQ after high light exposure, these experiments under controlled and field-like conditions were designed to assess if these additive effects translate to responses in shoot biomass. Three light treatments were used in a growth chamber in Klima (WUR): Constant, DEPI (moderate light fluctuation) and Maize (High light fluctuation). As the mutation on chloroplast *NDHG* is the most likely candidate gene responsible for the Bur-0 plasmotype additive effect on the recovery of PSII, Col-0 knockouts with nuclear mutations on *NDHM* and *NDHO* have been added to the growth chamber experiments. By doing so, it was possible to compare Col^{Col} self-cybrids with those plants carrying non-functional subunits of the NAD(P)H complex. Furthermore, phenotyping Col-*ndhm* and Col-*ndho* provided valuable insights supporting *NDHG* as the genetic cause of Bur-0 plasmotype effects on the recovery of φPSII.

Additionally, to assess shoot biomass under conditions that simulate those in which *A. thaliana* naturally grows, a separate experiment was set in a gauze tunnel outdoors at Unifarm (WUR) during the spring of 2021. Both experiments were phenotyped for a set of 63 photosynthesis and morphological parameters using the plant screen system.

3.1. Impact of the Bur-0 plasmotype additive effects on shoot biomass under growth chamber conditions with fluctuating light treatments.

Variance componence was estimated for the selected phenotypes under all light treatments and cybrids and Col-0 self-cybrids vs Col-*ndhm &* Col-*ndho*. A considerable effect of blocks (hydroponic basin) on Leaf Area (MM) and shoot biomass was observed in the moderate light fluctuation and constant light treatments. Thereby, blocks were included as a random factor to adjust the fitted linear model. Although this was mostly the case in the moderate light fluctuation and constant light treatments, blocks were used as a random factor to fit the linear model for all light treatments. In general, calculated H^2 for plasmotype and nucleotype-plasmotype interactions were higher for photosynthetic parameters. The estimated H^2 of plasmotype and nucleotype-plasmotype interactions was close to 0% and 1.18%, respectively, for shoot biomass under constant light treatment but increased under fluctuating light (0% and 9,3% for moderate light fluctuation & 8.7% and 3,6% for high light fluctuation, respectively). H^2 was higher in all light treatments for Col^{Col} cybrids vs Col-*ndh*-KOs, especially when plants were grown under high light fluctuation; the genotype explained 78,4% of differences in shoot biomass. A full table with variance components of the selected phenotypes can be found in Appendix Tables 6 & 7.

Photosynthesis parameters were analysed to confirm the additive effect of cybrids with the Bur plasmotype and compare if these phenotypes explain shoot biomass results. The analysis of photosynthesis phenotypes focused on "low" parameters, which measure the recovery of φ PSII and NPQ after a high light pulse in the light protocol used in The Plant Screen System™. The average Bur-0 plasmotype effect on the recovery φ PSII was significantly higher (α=0.05) under constant and moderate fluctuating light treatments (DEPI)(Figure 14). However, under highly fluctuating light conditions (Maize), the additive effect of the Bur-0 plasmotype on the recovery φPSII displayed lower values than cybrids with a Col-0 plasmotype. Zooming in to the different nucleotype-plasmotype combinations confirmed the additive effect of the Bur-0 plasmotype, as all cybrids with a Bur-0 plasmotype presented a significantly different phenotype (Appendix Figure 13). However, the reduction in the recovery of φPSII under highly fluctuating light conditions was even more significant (α=0.01) on cybrids on C24, Col-0 and Ler-0 nuclear backgrounds (Appendix figure 13). Col-*ndhm* and Col-*ndho* KOs presented significant differences compared to Col^{Col} cybrids. Interestingly, Col-n*dhm* and Col-*ndho* recorded a severe decrease in recovery φPSII when plants were grown under highly fluctuating light conditions (Figure 14). Moreover, a comparison with Col^{Bur} cybrids revealed that their phenotypes were quite similar under constant and moderate fluctuating light treatments, but when plants were grown under highly fluctuating light conditions, the recovery of φ PSII was markedly lower (Appendix Figure 13)

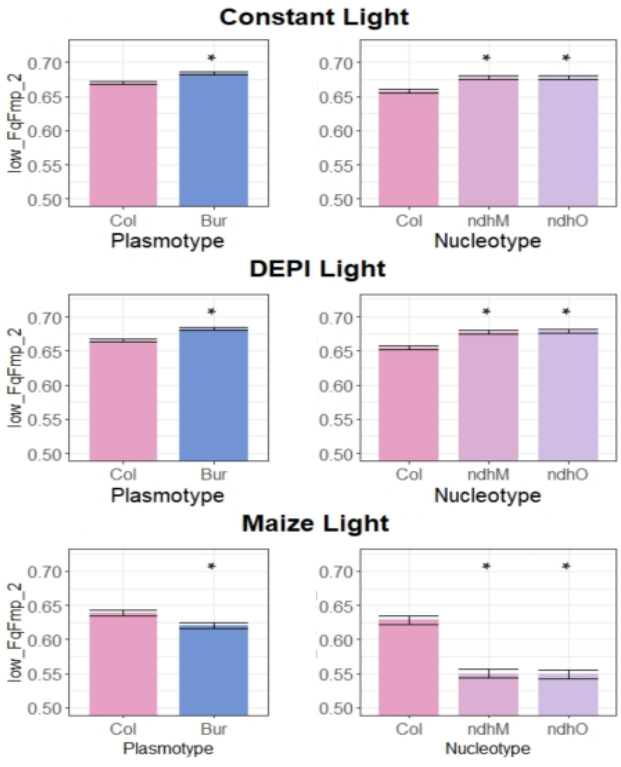

Figure 14: *Effects on "low FqFmp_2" parameter reflecting the recovery of φ PSII after exposure to a high light pulse in the Plant Screen System™. Left: additive effects of Col-0 and Bur-0 plasmotypes. Right: Col^{Col} vs. Col-ndhm & Col-ndho. Asterisks show significant differences. Multiple comparisons were made using Benjamini & Hochberg test (α=0.05).*

Non-photochemical quenching and its fast element (qE) were also measured at low light conditions in the Plant Screen System^{TM}. NPQ and qE are essential for the recovery of φPSII as the speed at which they relax determines the restoration of φPSII. A similar pattern to the recovery of φPSII occurred in NPQ (Figure 15). On average, cybrids carrying the Bur-0 plasmotype presented significantly lower NPQ values under Constant and moderate fluctuating light treatments. Nucleotype-Plasmotype combinations revealed this was the case under most nuclear backgrounds (Excluding C24 at constant light) (Appendix Figure 14). However, as observed for the recovery of PSII efficiency at low light conditions, NPQ at low light conditions was significantly higher under highly fluctuating light conditions for the average plasmotype effect.

Nonetheless, when inspecting the specific Nucleotype-Plasmotype combinations, cybrids with Bur-0 plasmotype under Bur-0 nucleotype only produced insignificantly elevated NPQ values at low light conditions under this light treatment (Appendix Figure 15). Col-*ndhm* and *Col-ndho* presented significant differences as compared to Col^{Col}. Moreover, they followed a similar pattern to the additive Bur-0 plasmotype effect, but values were considerably higher under Maize light treatment. The Bur-0 plasmotype presented significantly lower qE values than the average for the Col-0 plasmotype under constant and moderate fluctuating light treatments (Figure 15). However, these differences were considerably more pronounced under moderate fluctuating light treatment. Yet again, the average Bur-0 presented an inverted phenotype under highly fluctuating light conditions, with significantly higher qE values than the average Col-0 plasmotype. Specific nucleotype-plasmotype combinations showed that qE values were significantly different for cybrids with a Bur-0 plasmotype (Appendix figure 15). Also, the C24 and Col-0 nucleotypes presented higher qE values, especially when plants were grown under high fluctuating light. Finally, Col-*ndhm* and Col-*ndho* KO's presented extreme phenotypes, with significantly lower (negative)values compared to Col^{Col} cybrids when grown under constant and moderate light fluctuation conditions and significantly higher values under highly fluctuating light conditions. Furthermore, compared to Col^{Bur} cybrids, these values were also considerably more pronounced.

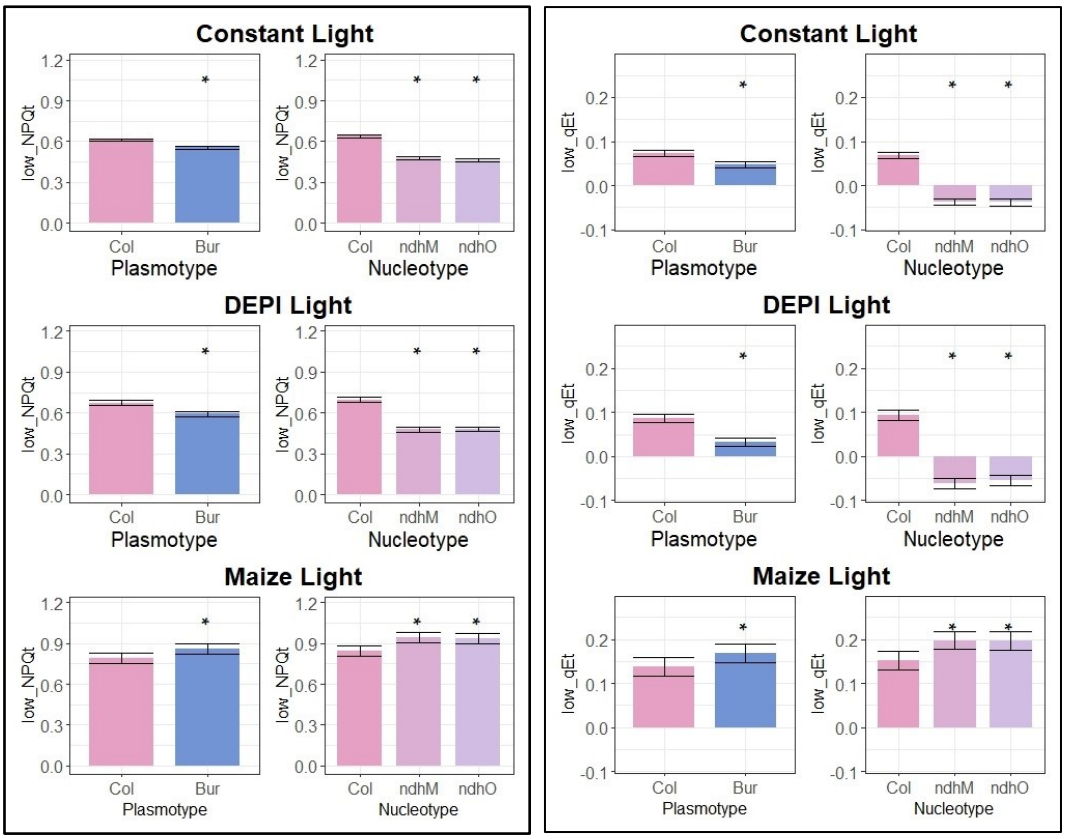

Figure 15: *Effects on "low_NPQt" and "Low_qEt" parameters, reflecting non-photochemical quenching and its fast element qE after exposure to a high light pulse in the Plant Screen System™. Left additive effects of Col-0 and Bur-0 plasmotypes. Right Col^{Col} vs. Col-ndhm & Col-ndho. Asterisks show significant differences. Multiple comparisons were made using Benjamini & Hochberg test (α=0.05).*

Even if cumulative daily light exposure was the same for all light treatments (418 µmol m^2 s^{-1}), the light treatments in the growth chamber experiments considerably impacted the shoot biomass of plants (Figure 16), plants grown under constant light produced an increased shoot biomass accumulation (average= 0.1175g), followed by the moderate light fluctuation treatment (0.0964g or -17,96 %) and finally the high light fluctuation treatment, which produced the plants with on average lower shoot biomass (0.0549g or -53.28 %).

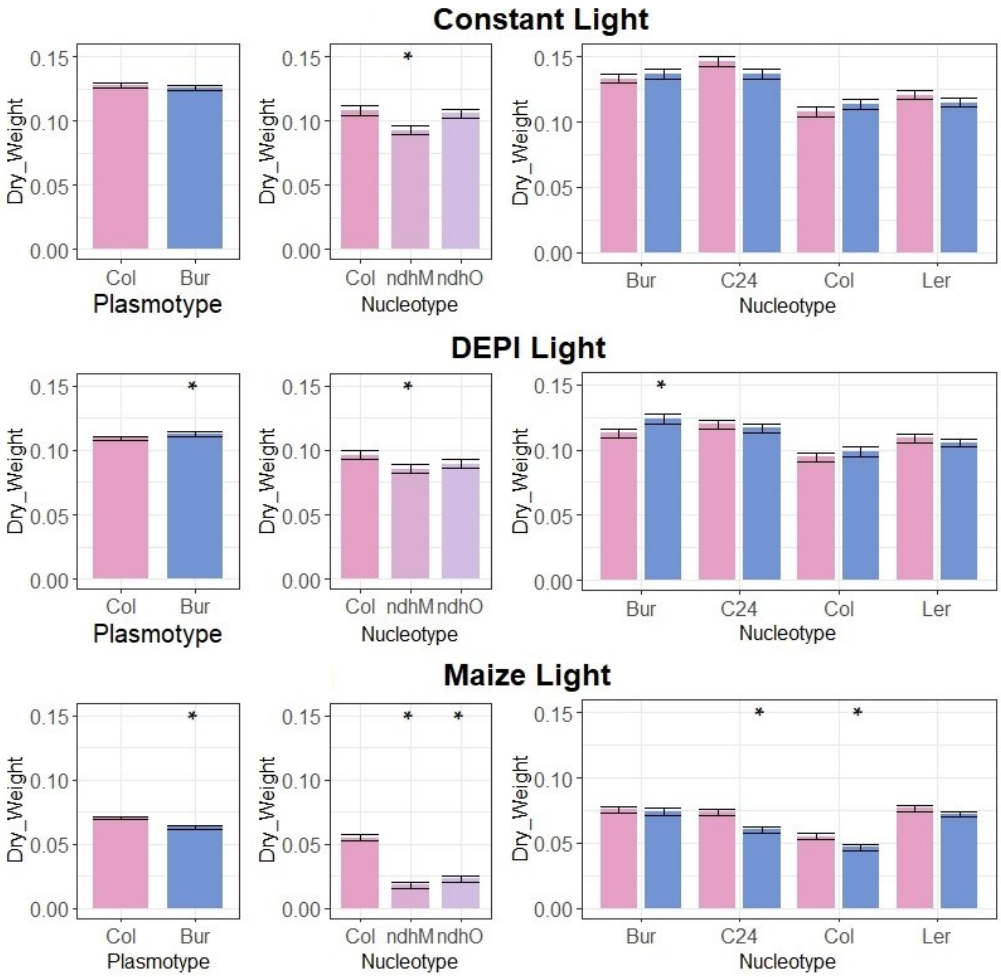

Figure 16: *Effects on shoot biomass after twenty-six days of growth under different light treatments. Left additive effects of Col-0 and Bur-0 plasmotypes. Centre: Col^{Col} vs. Col-ndhm & Col-ndho. Right: Interaction effects of different Nucleotype-Plasmotype combinations. Asterisks show significant differences. Multiple comparisons were made using Benjamini & Hochberg test (α=0.05).*

The Bur-0 plasmotype generated significant differences in shoot biomass. However, these depended on the light treatment and nucleotype plasmotype combinations (Figure 16). Under constant light treatment, no significant differences for shoot biomass between plasmotypes were found. On the contrary, moderate and high light fluctuation significantly affected shoot biomass on cybrids with a Bur-0 plasmotype, with opposite behaviours. When plants were grown under moderate light fluctuation, cybrids with a Bur-0 plasmotype generated an additive effect producing considerably higher shoot biomass (+3.28%). Conversely, under high light fluctuation treatment, cybrids carrying the Bur-0 plasmotype had an additive effect with a negative impact on shoot biomass (-11.15%).

Under moderate light fluctuation conditions, analysis of nucleotype-plasmotype interactions showed that the additive effect was driven by Bur^{Bur} cybrids, which produced significantly higher shoot biomass (+14.32%) than Bur^{Col}. The other cybrids generated small increments in shoot biomass, except for Ler^{Bur} cybrids, where a slight decrease was observed. Under high

light fluctuation conditions, $C24^{Bur}$ and Col^{Bur} cybrids produced plants with significantly lower shoot biomass (-18,55% and -13,89%, respectively). Although shoot biomass was also lower under this light treatment in Bur^{Bur} and Ler^{Bur} cybrids (-6.21% and -5.95%, respectively), differences were insignificant. Col-*ndhm* and Col-*ndho* plants recorded a decrease in shoot biomass under all light treatments. However, these effects were only significant for Col-*ndho* plants grown under high fluctuating light conditions, whereas they were significant for Col-*ndhm* knockouts under all light treatments.

These experiments reveal intriguing data supporting the importance of the plasmotype in photosynthetic responses to light fluctuation. On one side, the findings of these experiments add to the evidence provided by Flood *et al*. (2020) that the Bur-0 plasmotype generates an additive effect that increases the recovery of φPSII and NPQ while reducing qE under constant and moderate light fluctuation. However, an opposite response was observed on plants grown under high light fluctuation, confirming that the environment has a decisive role in determining the response. Moreover, the Bur plasmotype seems to impact shoot biomass considerably, specifically under high light fluctuation. In addition, nucleotype-plasmotype interactions play a significant role in modulating these responses, as observed in Bur^{Bur} cybrids under moderate light fluctuation and Bur^{Bur} and Bur^{Ler} cybrids under high light fluctuation treatments.

3.2. Impact of the Bur-0 plasmotype additive effects on shoot biomass under field-like conditions.

Environmental conditions in nature are rarely stable, and shifts in light and temperature happen at multiple time scales. Plants need to be prepared to adjust their physiology when being challenged by multiple abiotic stress throughout their growing season. Given φPSII and NPQ are determining factors for plants to adapt to fluctuating light conditions and cold stress, this experiment aimed to answer if the known additive effect of the Bur-0 plasmotype on the recovery of φPSII also impacts shoot biomass under dynamic environmental conditions similar to those where *A. thaliana* naturally occurs. The experiment was set under a gauze tunnel in Unifarm, WUR. Relatively cold and dry conditions characterized the spring of 2021, the time during which the experiment took place

Variance componence was estimated to establish the contribution of genetic and experimental factors to the phenotypes (Table 4). Blocking (the tray containing all genotypes) explained a considerable amount of shoot biomass variation (9.95%). Therefore, it was included as a random factor in the fitted linear model to correct for this variation. H^2 due to plasmotype and nucleotype-plasmotype interactions were considerable for the photosynthetic parameters analysed but not for shoot biomass. H^2 for this phenotype was explained in 0.1% by the plasmotype, whilst nucleotype-plasmotype interactions explained 0.8% of the variability. Shoot Biomass was mainly explained by nucleotype H^2 (51.7%) and environmental and non-controlled experimental conditions (residual= 37.5%), showing that shoot biomass is a complex quantitative trait influenced mainly by the environment.

Cybrids under field-like conditions					
Phenotype	**Nucleotype**	**Plasmotype**	**Nucleotype: Plasmotype**	**Tray**	**Residual**
low_FqFmp_2	0,311	0,176	0,011	0,030	0,473
low_NPQt	0,251	0,109	0,004	0,001	0,636
low_qEt	0,135	0,242	0,020	0,033	0,571
Dry_Weight	0,517	0,001	0,008	0,099	0,375

Table 4: *Variance components for selected phenotypes of reduced cybrid panel of A. thaliana grown in a gauze tunnel simulating field-like conditions at Unifarm (WUR)*

Photosynthesis parameters were analysed to confirm the additive effect of cybrids with the Bur plasmotype and compare if these phenotypes explain shoot biomass results. The Bur-0 plasmotype produced a strong additive response on photosynthetic phenotypes. The recovery φPSII was consistently higher for cybrids carrying the Bur-0 plasmotype. Furthermore, this effect was significant (α=0.05) in almost all nuclear backgrounds (Figure 17). Cybrids with a Bur-0 plasmotype registered decreased NPQ values overall nuclear backgrounds (Appendix Figure 15). Nonetheless, these effects were only significant under the C24, Col-0, Ely and Ler-0 nuclear backgrounds. Cvi-0 Cybrids presented the highest NPQ values. Moreover, cybrids with a Bur-0 plasmotype recorded consistently significant lower values of qE(Low_qEt) under most nuclear backgrounds excluding Bur-0 (Appendix Figure 16).

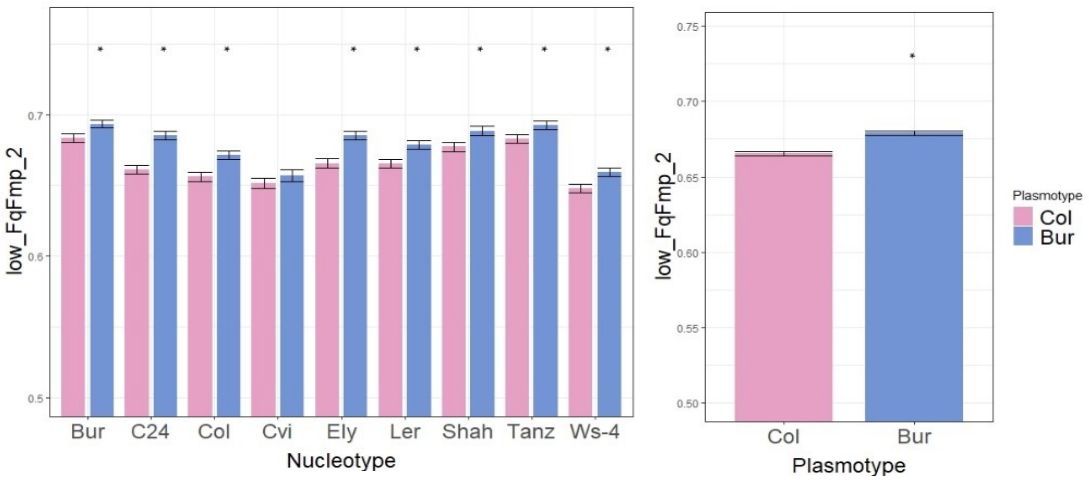

Figure 17. *Effects on "low FqFmp_2" parameter reflecting the recovery of φ PSII after exposure to a high light pulse in the Plant Screen System™. Left Interaction effects of different Nucleotype-Plasmotype combinations. Right: Additive plasmotype effects. Asterisks show significant differences. Multiple comparisons were made using Benjamini & Hochberg test (α=0.05).*

The effect of the plasmotype on shoot biomass was less evident under field-like conditions than in growth chamber conditions (Figure 18). On average, cybrids carrying the Bur-0 presented higher shoot biomass (+3.06%). However, the difference was not significant. Inspecting the nucleotype-plasmotype combinations, six out of nine nucleotypes registered higher shoot biomass under a Bur-0 plasmotype. However, under nucleotypes Ely and Ler-0, these differences were marginal and significant differences were only observed under nucleotypes Col-0 (+24.58%; α=0.05) and C24 (+12.46%; α=0.1). Overall, shoot biomass was explained mainly by nuclear-encoded variation. The accessions of an African origin (Cvi-0 and

Tanz-1) had the lowest growth responses under the spring conditions in the gauze tunnels. Again, these results show the importance of nucleotype-plasmotype interactions for a plant to have the most efficient biomass production under determined environmental conditions.

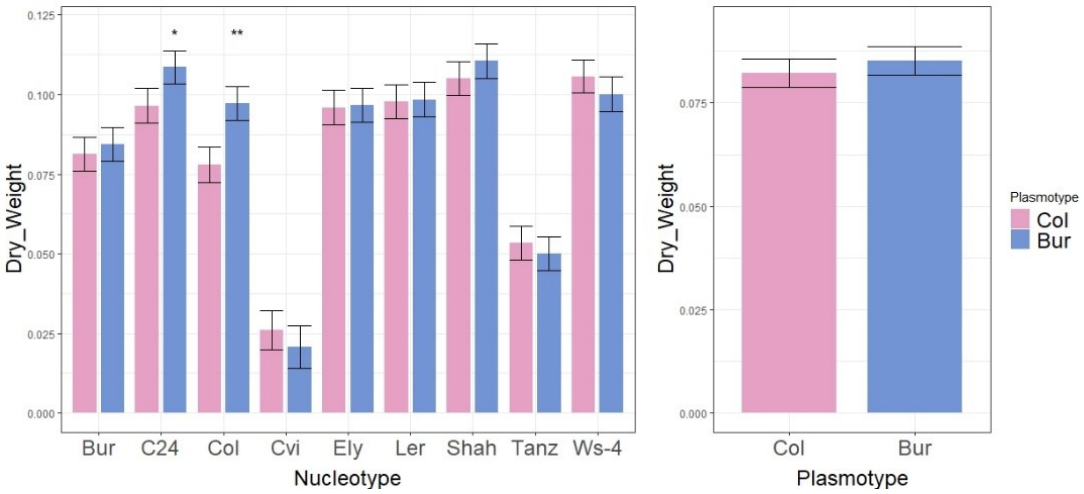

Figure 18. Effects on shoot biomass after forty-two days of growth under a gauze tunnel simulating field-like conditions at Unifarm (WUR). *Left Interaction effects of different Nucleotype-Plasmotype combinations*. *Right: additive effects of Col-0 and Bur-0 plasmotypes. Asterisks show significant differences from all other plasmotypes. Multiple comparisons were made using Benjamini & Hochberg test (**α=0.05, *α=0.1)

Discussion.

Light is the primary input for photosynthesis, and the ability to efficiently use this resource largely determines plant adaptation to different environmental conditions. As light is hardly ever stable under natural conditions, plants need to adjust photosynthesis when exposed to light fluctuations. Chloroplasts are the organelles in which the photosynthetic reactions happen. Their encoded genetic variability is emerging as an important source of genetic variation, partly explaining photoprotective responses that ensure optimal photosynthesis. Using cybrids, previous research has identified meaningful plasmotype variability affecting fast photoprotective responses that restore photosynthesis efficiency under fluctuating light conditions in the model plant *A. thaliana* (Flood *et al.,* 2020). Moreover, H^2 for these phenotypes seems to increase under stressful environmental conditions. Nonetheless, previous research has focused on a narrow cybrid panel that was wholly phenotyped under controlled (growth chamber) environmental conditions.

Ongoing research by Theeuwen *et al.* (unpublished) and the MSc thesis by Lawson (2020) and Tijink (2021) have attempted to find further plasmotype diversity affecting photosynthetic efficiency. In addition, experimentation has focused on assessing whether photoprotective mechanisms found in certain plasmotypes and nucleotype plasmotype combinations lead to effects on plant growth parameters (leaf area and shoot biomass). The whole cybrid panel and

reduced selected versions have been grown under controlled (growth chamber) and field-like conditions during spring 2020 and Autumn-winter 2020/21 at Klima and Unifarm (WUR). Promising yet inconclusive results have been found regarding whether the Bur-0 plasmotype effects on photosystem II recovery lead to differences in growth parameters.

So far, results indicate multiple cytonuclear epistatic effects could be in play, where the Bur-0 plasmotype seems to confer increased growth parameters under certain nuclear backgrounds and specific environmental conditions. Nonetheless, as growth is a complex quantitative trait, Lawson (2020) and Tijink (2021) suggest that further experimentation is needed to determine whether the observed shoot growth parameters originate from the plasmotype rather than environmental and experimental intervening factors

By phenotyping a species-wide representative cybrid panel of *A. thaliana* under field-like conditions, this project aimed to determine whether plasmotype variation affects photosynthesis efficiency and plant morphology phenotypes. Additionally, the amount of variation due to additive plasmotype effects and nucleotype- plasmotype interaction effects was addressed by estimating H^2. Building on the results obtained, an additive effect found in the Bur-0 plasmotype leading to increased recovery of φ PSII stood out and was used as a case study to find the precise genetic variant causal for these photosynthetic phenotypes and whether these photosynthetic phenotypes caused by the plasmotype were impacting growth parameters.

Experiment 1: Species-wide representative cybrid panel of A. thaliana grown under field-like conditions.

This experiment contributed to ratifying the additive effect of the Bur-0 plasmotype initially reported by Flood *et al*. (2020) and verified Lawson's (2020) observations that effects are still present under field-like conditions. H^2 due to N/P/N×P observed in this study (17,28%, 0,43% and 2,74%,) was considerably lower than the observed by Flood *et al*., (2020) under controlled conditions (91.9%, 2.9% and 5.2%). Nonetheless, the results align with Lawson (2020), where H^2 due to N/P/N×P was 32.1%, 0.2%, and 1.8%, respectively. The decrease in H^2 observed in field-grown *A. thaliana* shows the deep impact of the environment on plant phenotypes. As multiple abiotic stresses happen simultaneously under field-like conditions, the effect of plasmotype-derived effects could be overshadowed by nuclear epistatic effects. Nonetheless, the small increase in H^2 from plasmotype-derived effects observed in this study compared to Lawson (2020) is proof that small adjustments in experimental settings have a strong impact in observing precisely the contribution of the plasmotype on observed phenotypes.

Apart from Bur-0, no other plasmotype produced a large-scale additive effect for the phenotypes analysed. Significant differences were found regarding the Bur-0 plasmotype additive effect on the recovery of φPSII and NPQ phenotypes. Nonetheless, the scale of the effect(s) observed in the Bur plasmotype was not uniquely significant under any nucleotype, proving that additional plasmotype diversity is also present in the cybrid panel and can be observed under specific nucleotype-plasmotype combinations. Interestingly, significant differences in the recovery of φPSII were not observed under the Tanz-1 nucleotype, and only

NPQ was significantly different (α=0.05). This observation is intriguing, as although the Bur plasmotype did generate higher recovery of φPSII and lower qE values, differences were not significant.

Moreover, cybrids with a Tanz-1 (or Cvi-0) nucleotype scored lower leaf area than cybrids with a Bur nucleotype, known for their small shoot size (Vlad *et al.,* 2010), possibly pointing at the effects of cold stress. Tanz-1 originates from Tanzania, is a relict in *A. thaliana* (1001 Genomes Consortium) and is highly divergent from Moroccan and Eurasian clades of this species (Durvasula *et al*., 2017). Therefore, possibly nuclear diversity acquired from its distant origins is masking significant plasmotype effects on the phenotype.

Multiple phenotypes were influenced by the plasmotypic diversity found in Theeuwen *et al*. (unpublished) cybrid panel. In line with previous reports, nucleotype-plasmotype interactions produced highly variable phenotypes (Lawson, 2020). Most remarkable effects were found in Cvi^{Shah} cybrids and, to a lesser extent, in Cvi^{Sus} cybrids which recorded significantly low recovery of φPSII and high NPQ values when measured at low light conditions. Cvi^{Kas-1} cybrids recorded a significant effect in leaf area, producing the largest plants in the cybrid panel. This observation is in line with previous studies by Lawson (2020). Moreover, various plasmotypes also generated significant small-scale effects of potential interest. These punctual examples confirm Flood *et al.* (2020) observation that nucleotype-plasmotype interactions create more significant phenotypic effects in general.

This experiment was able to ratify previous observations of the effect of certain plasmotypes on the phenotype. However, to verify if plasmotype variation is behind the phenotypes, it is essential to distinguish if the phenotypic variability found in the cybrid panel has a true genetic source rather than an environmental or maternal origin. Apart from slight environmental gradients, the tunnel provided overall even growing conditions. More of the observed variation is likely to come from nuclear-plasmotype interactions. The high variability of phenotypes observed among cybrid with a Cvi-0 nuclear background strongly suggests that nucleotype-plasmotype interactions could explain these phenotypes and represents a good case study. Cvi-0 is adapted to drier, hotter and high irradiance conditions of the Cape Verde Islands and displays a slower growth and pronounced leaf thickness (Coneva & Chitwood 2018).

Moreover, RIL populations of Cvi-0 and European accessions have produced high phenotypic plasticity in traits, including leaf area (Alonso-Blanco *et al*., 1998). Therefore, it makes sense to assume that some but not all nucleotype-plasmotype interactions result in phenotypic effects, especially if the donor accessions come from contrasting genetic and geographical origins, as in this experiment, where Cvi-0 was the nucleotype donor. However, cybrids with a Cvi-0 nucleotype recorded the smallest sample sizes in the experiment. Therefore, a problem in the methodology used to analyse the results in this experiment was to use such a stringent SD for outlier removal (1.25) as some cybrids were left with extremely low sample sizes leading to the low statistical power of the results (Appendix Table 1).

The phenotypes observed on the Cvi-0 cybrids include examples of large- and small-scale effects. For instance, the Shah plasmotype has been reported to cause cytoplasmatic male sterility (CMS) under some nuclear combinations (Roux *et al*., 2016; Flood *et al*., 2020).

Therefore, Cvi^{Shah} might have resulted in poor quality seeds producing weak plants that were not considered in the analysis after removing outliers. Although a maternal effect might be in action, the cause is also related to plasmotype variability. A similar case affecting seed quality could explain the results for Cvi^{Sus}. However, no reports CMS are known for this accession. Nonetheless, only one plant was considered for these two cybrids after outlier removal. Thereby repeating a small-scale experiment with higher replicates for these two cybrids would be advisable to confirm the obtained results. The scope and timeframe of this project did not allow for checking any missense variants in the Sus-1 plasmotype that could be behind these phenotypes. Thereby, determining if maternal effects or genetic causes are behind these results would be recommendable, as CMS is a valuable breeding resource.

On the other hand, given that Cvi^{Kas-2} presented no large-scale effect on leaf area, the repeated observation of Cvi^{Kas-1} having an extreme impact on leaf area is another puzzling result. Besides producing the largest plants on the cybrid panel, Cvi^{Kas-1} cybrids recorded significantly lower than average φPSII values than other plasmotypes under a Cvi-0 nucleotype (Appendix Figure 11). Moreover, Kas-2 scored significantly lower leaf area than many plasmotypes under a Col nucleotype (Figure 12). Given that the two accessions were collected in Kashmir (India) and that Cvi^{Kas-1} plants came from a different seed batch than Cvi^{Kas-2}, it is tentative to speculate that a maternal effect could be responsible for the phenotypes observed. Additionally, the methodology used for outlier removal (1.25) also complicates this analysis as Cvi^{Kas-1} presented a relatively small sample size compared to Cvi^{Kas-2} (Appendix Table 1).

Interestingly, $Cvi^{Lesno-1}$ also recorded significantly lower recovery of φPSII values than the PCA-selected plasmotypes under a Cvi-0 nucleotype and produced slightly larger plants (a result also reported by Lawson (2020)). Potentially, the repeated observation of larger leaf areas and lower recovery of φPSII values could be an interesting adaptation to fluctuating light and cold conditions. Nonetheless, given the significant scale impact of the results and phenotypic plasticity present in the Cvi-0 nucleotype, it would be advisable to genotype both cybrids and realize seed batch assays to compare if phenotypes are still present in plants from the same generation. Additionally, looking for additional missense variants in the Kas-1 and Lesno-1 plasmotypes is also advisable. Multiple low-scale plasmotype effects on various phenotypes were also recorded among nucleotypes. Examples are the Iberian Peninsula plasmotypes and Atiba-1, Lesno-1, Staro-2 and Zin-9 (Figure 12 and Appendix Figure 10). *NDHG* was suggested as the most likely causal gene for the Bur plasmotype additive effect on the recovery of φPSII by Flood *et al*. (2020). *NDHG* codes for a subunit of NAD(P)H dehydrogenase-like complex (NDH complex), which acts as a proton pump in cyclic electron flow (CEF) around photosystem and chlororespiration (Shikanai, 2014). Following this lead, missense variants were found in the plasmotype of Cvi-1 (1 SNP *NDHA*), Kas-2 and Kas-1 (1 SNP in *NDHF)* and Staro-2 (2 SNP *NDHA, 1 SNP NDHK*). Interestingly, cybrids with Kas-1 and Kas-2 plasmotypes presented significant differences in the recovery of φPSII as compared to other PCA-selected plasmotypes (Appendix Figure 11). Moreover, Kas-2 & Kas-1 and Staro-2 presented considerable variation in leaf area. However, neither Cvi-0 nor Staro-1 presented significantly different photosynthetic phenotypes from the PCA-selected plasmotypes analysed. This points out that mutations on different subunits of the NDH complex affect photosynthesis differentially. Finally, this example shows that high throughput phenotyping

and PCA analysis are powerful tools for identifying candidate genes implied in photosynthetic regulation and growth responses.

The analysis produced on this cybrid panel revealed intriguing plasmotypic diversity acting mainly through nucleotype-plasmotype interactions. Nonetheless, the information analysed only scratched the surface of possible plasmotype variation affecting phenotypes, as less than 10% (5/63) of the phenotypes provided by The Plant Screen System™ were used. For instance, the analysis of colour information was not used in this project. Anthocyanin production is a clear indicator of plant stress. Further analysis is advised to search for phenotypes that could help reveal meaningful plasmotype diversity and compare them with other experiments to verify their replicability. Finally, identifying plasmotypes that generate the most diverging phenotypes under particular nucleotypes and linking this information to additional missense variants might help shed light on valuable nucleotype-plasmotype interactions.

Experiment 2: Genetic cause behind Bur-0 additive effect in the recovery of φPSII.

The additive effect of the Bur-0 plasmotype is characterized by an increase in the efficiency of photosystem II and a decrease in non-photochemical quenching (NPQ) (Flood *et al*., 2020; Lawson, 2020, Tijink, 2021). In the past, four likely candidates explaining Bur-0-photosynthetic phenotypes have been identified in the Bur-0 plasmotype: two unique missense variants in MATURASE K (*MATK*), one in NAD(P)H-QUINONE OXIDOREDUCTASE SUBUNIT G (*NDHG*) and one in Chloroplast open reading frame 1 (*YCF1*) (Flood *et al*., 2020). This list has been refined to two candidates (MATK and *NDHG)* by Tijink(2021). Since *NDHG* codes a subunit of the *NDH* complex directly involved in regulating photoprotective mechanisms, it has been repeatedly suggested as the most likely causal gene (Flood *et al.*, 2020; Tijink, 2021). Theeuwen *et al.* (unpublished) recently identified accession ID471, which only shares the *MATK* allele with Bur-0 that Tijink (2020) could not discard. Using this key accession and a reciprocal crosses approach, this experiment was undertaken to further characterize the role of the Bur-0 *MATK* allele in the recovery of φPSII and solve the genetic cause behind the Bur plasmotype additive effect recovery of φPSII.

The use of the reciprocal crosses showed to be a rough yet effective method of understanding the role of the Bur-0 *MATK* allele in the recovery of φPSII. As groups of F1 accessions that carry the Bur-0 *MATK* allele without the Bur-0 *NDHG* allele do not display increased recovery of φPSII, it was possible to discard *MATK* as the causal gene behind this phenotype (Figure 13). This confirms Flood *et al.* (2020) and Tijink (2021) suggestion that the Bur-0 *NDHG* allele is the causal gene for its phenotype in the recovery of φPSII.

However, the reciprocal crossing approach proved to be time-consuming as 42 crosses had to be produced and evaluating the results in the F1 generated various limitations. For example, failure to retrieve viable (or limited) seeds from some crosses decreased the statistical power of the analysis. A further limitation of the use of reciprocal crosses is the statistical analysis of the results. Having two groups (maternal and paternal genotype donors) complicates the

statistical analysis because it is impossible to compare both groups at once with the statistical methods used in this project. Thereby, a separate analysis had to be made for each, and the impact of nucleotype plasmotype interactions was not possible to analyse. For instance, the group in which ID471 acts as a paternal genotype donor presents a slightly higher recovery of φPSII. These elevated values can be explained by the fact that Bur-0 and ID1467 plasmotypes are also considered in the general average of this group.

Lastly, the reciprocal crosses approach also complicates finding causal genes in the plasmotype as the potential effects of nucleotype-plasmotype interactions can interfere. In this experiment, F1 plants were used; therefore, the nucleotype was heterogeneous due to recombination, and no nuclear markers were used. Thereby, 50% of genes could potentially generate unknown nucleotype-plasmotype interactions that can influence the results. For instance, for the recovery of the φPSII phenotype, a clear pattern can be observed for the groups of F1 accessions which carry the Bur-0 *NDHG* allele. Nonetheless, the pattern was not as clear for the NPQ parameters analysed, which nucleotype-plasmotype interactions could explain (Appendix Figure 12).

NPQ is a complex trait in which various mechanisms are in action. Genes that contribute to NPQ functioning are also present in the nucleotype, for example, PSII subunit S (PsbS) or enzymes controlling the xanthophyll cycle kinetics as violaxanthin de-epoxidase *(VDE*) and Zeaxanthin epoxidase (ZEP).NPQ values recorded in this experiment displayed an inconsistent response with no apparent pattern within genotypes sharing a common cytoplasm. Moreover, the response was similar to those who shared 50% of their nucleotype but not the plasmotype. To a less extent, this was also true for qEt. However, a more precise pattern can be observed for qEt, although significance was not observed for the group of F1 accessions with NL1467 as cytoplasm. Therefore, the results on NPQ could be explained by potential interactions with nuclear genes that also control this trait. These genes could have been identified if nuclear markers were used, but this was out of this project's scope. Thereby, repeating this experiment using cybrids (e.g., Col^{ID471} vs $ID471^{Col}$) instead of F1 crosses might give more specific phenotypes avoiding effects from undetected nuclear introgression and simplifying the statistical analysis of these results.

Based on the results of this experiment, it is possible to discard that this *MATK* allele is solely responsible for the recovery of φPSII observed in plants with a Bur-0 plasmotype. As all other candidate genes have been discarded, *NDHG* is the most likely causal gene. Literature review supports Bur-0 *NDHG* allele can be responsible for the recovery of φPSII. NDH acts as a proton pump which creates a pH gradient in the lumen that triggers non-photochemical quenching (Strand *et al*., 2017; Laughlin *et al*., 2019). The NDH complex is formed by 35 subunits, from which 11 subunits (*NDH A-K*) are encoded in the chloroplast (Laughlin *et al.,* 2020). Moreover, NDH acts as a proton pump acidifying the lumen, triggering NPQ, supplying extra ATP for photosynthesis and partly mediates cyclic electron flow (Shikanai and Yamamoto, 2017; Ma *et al*., 2021).

Even though this experiment is a strong proof suggesting *NDHG* as the genetic origin behind the recovery of φPSII observed in cybrids with the Bur-0 plasmotype, further experimentation will provide definitive evidence. *NDHG's* role can be confirmed by phenotyping accession that uniquely carries the Bur-*NDHG* allele. However, this phenotype has only been observed in

Bur-0 and NL1467, with SNPs in *YCF1* and *MATK*. Therefore, although undoubtedly *NDHG* is causing the phenotype, a question remains if these other genes contribute to the expression of the phenotype. Therefore, it is suggested to keep screening *A. thaliana* accessions to find plants that exclusively present the Bur-0 *NDHG* allele for definitive proof. An alternative route will be to edit the plasmotype genome to generate the Bur-0 *NDHG* allele. Although chloroplast transformation has proved to be particularly difficult in *A thaliana*, new methods have been reported that allow to precisely edit point mutations in the chloroplast (Ruf *et al*., 2019; Kang *et al*., 2021).

Experiment 3: Impact of the Bur-0 plasmotype additive effects on shoot biomass.

Abiotic factors such as fluctuating light and cold stress are known to limit the efficiency of photosynthesis. When light intensity varies from low to high, plants need to adapt to excess light energy to avoid saturating the capacity of the electron transport chain and keep an adequate balance of ATP/NADPH production. Moreover, when temperatures decline, electron transport might exceed carbon fixation capacity leading to oxidative stress, and further disruption of ATP/NADPH ratios NPQ processes are fundamental for dissipating excess energy under these conditions, avoiding photodamage and restoring efficient photosynthesis (Rumeau *et al*., 2007; Tikkamen *et al*., 2012, Strand & Kramer, 2014). Environmental factors, such as fluctuating light stress, are known to influence the scale of the additive effect of Bur-0 plasmotype on the recovery of photosystem II efficiency (Flood *et al*., 2020; Theeuwen *et al*., (unpublished). Given that the most likely cause for the recovery of φ PSII in Bur-0 plasmotype is its *NDHG* allele and the NDH complex regulates fast NPQ responses and ATP/NADPH ratios, these experiments were designed to test whether the Bur plasmotype impacts shoot biomass accumulation.

Here, the effect on shoot biomass in Bur-0 plasmotype cybrids under controlled conditions was assessed under different light treatments (Constant, moderate and high light fluctuation). Additionally, a replicate with a higher sample size of past efforts to characterize the Bur-0 plasmotype effect in biomass accumulation under field-like conditions took place during spring 2021.

3.1. Impact of the Bur-0 plasmotype additive effects on shoot biomass under growth chamber conditions with fluctuating light treatments.

To precisely assess the impact of fluctuating light and plasmotype variability affecting photosynthesis efficiency and biomass production, this experiment took place under growth chamber conditions with three light treatments in Klima, WUR. Plants were phenotyped for photosynthesis parameters and harvested, dried, and immediately weighted after 26 days of growth.

The light treatments used on growth chambers caused marked photosynthesis phenotypes. In particular, more variance was found as the intensity of light fluctuation increased (Appendix

Tables 5 & 6). Overall, the recovery of φPSII was low in the high light fluctuation treatment, suggesting photoinhibition in all cybrids. In addition, light fluctuation also affected shoot biomass, producing significantly lower biomass accumulation for all genotypes, particularly when plants were grown under high light fluctuation. These observations were expected and confirmed light stress's outcome on shoot biomass. Plants have adapted to maximise light use efficiency under low light conditions by optimizing photon absorption. When light intensity suddenly increases, excess absorption of photons saturates the electron transport chain, and NPQ is upregulated to avoid photodamage. Inversely, when light is high and switches to low, NPQ needs to be relaxed. In both cases, the photosynthetic machinery has to recover for up to several minutes to restore optimal CO_2 assimilation rates (Pearcy, 1990; Tanaka *et al*., 2019: Kramer *et al.,* 2022). In this experiment, the high light fluctuation treatment designed by Theeuwen *et al*. (unpublished) resembles the light under a fully developed maize canopy. Thereby, plants grew adapted to a base low light conditions and were exposed to brief bursts of very high light. Therefore, the results of this experiment suggest that shoot biomass is more affected when extreme transitioning from low to high light happens.

To understand if biomass responses were linked to the Bur plasmotype additive effect, the ability to rapidly restore the efficiency of PSII after high light in the Bur-0 plasmotype was verified. The Bur-0 plasmotype additive effect showed significant differences for all parameters analysed (recovery of φPSII, NPQ and qEt). Interestingly, under high light fluctuation, the recovery φPSII was lower for cybrids with a Bur-0 plasmotype. These results indicate a greater degree of photoinhibition. As the high light pulses in this treatment were fast and intense, the Bur-0 plasmotype probably contributes to relaxing NPQ too quickly. When high light strikes again, it is not prepared, leading to damage to the photosystems. Zooming in to the nucleotype-plasmotype interactions, significantly lower values were recorded under a C24 or Col-0 nuclear background but not on the Bur-0 or Ler-0 nuclear backgrounds. These results suggest a cytonuclear epistatic effect in these cybrids, where the Bur-0 and Ler-0 nuclear backgrounds might have mechanisms to avoid a higher degree of photoinhibition. The non-photochemical quenching phenotypes for cybrids with a Bur plasmotype grown under high light fluctuation also produced interesting phenotypes. For this light treatment, the NPQ pattern switched from low to significantly higher for plants with a Bur-0 plasmotype under all nucleotypes apart from Bur-0, where values were slightly higher than Bur^{Col} cybrids.

The fast element of NPQ, qE, also presented the inverted phenotype for plants grown under high light fluctuation. Instead of the lower values observed under constant and moderate light fluctuation, cybrids with a bur plasmotype presented higher values, but significance was only observed for the C24 nucleotype. Additionally, as with NPQ, Bur^{Bur} cybrids presented very similar values to Bur^{Col} cybrids. Again, these phenotypes suggest that cytonuclear epistatic effects affect the effect sizes caused by the bur plasmotype. As *NDHG* has been identified as the causal gene behind Bur plasmotype effect, these results support the role of the NDH complex in affecting qE responses (Ma *et al.,* 2021) and contribute a phenotype for this particular subunit in *A. thaliana*. Nonetheless, the question of how mutations in other NDH subunits contribute to a differential response to multiple degrees of fluctuating light stress remains.

The Bur-0 plasmotype impact on shoot biomass depended on the light treatment. Under constant light, no significant differences were found in cybrids carrying the Bur-0 plasmotype. On the contrary, the Bur-0 plasmotype affected shoot biomass grown under moderate and high light fluctuation with contrasting behaviour depending on the light treatment. Under moderate light fluctuation, the additive effect on shoot biomass (+3.28%) was driven by Bur^{Bur} cybrids, presenting +14.32% biomass compared to Bur^{Col} cybrids. Additionally, Col^{Bur} cybrids presented +3.71% biomass compared to Col^{Col} cybrids, but the differences were insignificant. Interestingly, these results correlate with the effects sizes in the recovery of φPSII of cybrids with either a Col-0 or Bur-0 nucleotypes. When the Bur-0 plasmotype was present, considerably higher recovery of φPSII was recorded. Therefore, its likely cytonuclear epistatic effects are in action, where coevolution of the Bur plasmotype and nucleotype have stimulated shoot biomass production.

Conversely, an additive effect on shoot biomass was observed in cybrids with a Bur-0 plasmotype grown under high light fluctuation resulting in a decrease in shoot biomass (-11.15%). Although all cybrids recorded lower biomass under a Bur-0 plasmotype, significant differences were only recorded in $C24^{Bur}$ and Col^{Bur} (-18,55% & -13,89%, respectively). Bur^{Bur} & Ler^{Bur} cybrids were not as severely affected by high fluctuating light conditions (-6,21% and -5,95%, respectively). Again, under these nucleotypes (Bur-0 & Ler-0), the recovery of φPSII was not as affected. Therefore, these observations point to nucleotype-plasmotype interactions involving *NDHG* regulating photosynthesis and growth responses depending on light fluctuation intensity.

As *NDHG* appears to be behind the additive effects in the Bur plasmotype, the addition of Col-*ndhm* and Col-*ndho* provided valuable data on the effect of mutations in the NDH complex on the phenotypes envaulted. Rumeau *et al*. (2005) reported that *NDHM* and *NDHO* are essential subunits of the NDH complex needed for a correct assembly. Col-*ndhm* and Col-*ndho* were significantly different from Col^{Col} for all photosynthetic phenotypes analysed. Furthermore, they presented certain similarities in photosynthetic phenotypes of cybrids with a Bur-0 plasmotype. Nonetheless, Col-*ndhm* and Col-*ndho* plants that grew under high light fluctuation conditions showed much more pronounced phenotypes than Col^{Bur} cybrids. The observation that qE was negative for Col-*ndhm* and Col-*ndho* plants grown under constant and moderate light fluctuation indicates that plants lacking a functional NDH complex fail to regulate qE efficiently. Additionally, plants grown under high light fluctuation recorded increased qE, evidencing an alternative mechanism triggered to avoid further damage to photosynthetic machinery once a certain threshold is reached.

Col-*ndhm* and Col-*ndho* plants generally registered a decrease in shoot biomass production. Under constant light, shoot biomass was significantly reduced in Col-*ndhm* knockout (but not in Col-*ndho*) compared to Col^{Col} cybrids. However, when Col-*ndh* knockouts were grown under fluctuating light treatments, the adverse effects on shoot biomass were more evident. Moreover, when comparing Col-*ndh* KOs to Col^{Bur} cybrids, the decrease in biomass on the knockouts was more evident. Results obtained from Col-NDH mutants are in line with literature reports. Soursa *et al.* (2012) found that *A. thaliana* plants lacking *NDHO* showed no differences in growth compared to WT plants under low constant and mild fluctuating light

treatments. Moreover, tobacco (*Nicotiana tabacum*) and A. *thaliana* plants defective for the *ndhB* subunit have also been reported to present average growth similar to wild-type plants under mild environmental conditions (greenhouse) and low constant light, respectively (Shikanai *et al.,* 1998). These results imply that NDH is essential to maintain efficient photochemistry under stressful light fluctuation conditions.

Most importantly, similarities in phenotypes of Col-*ndhm* and Col-*ndho* corroborate that the causal gene behind the Bur plasmotype recovery of φPSII is its *NDHG* allele, as none of the other candidate genes has been observed to create these phenotypes. Moreover, it appears that the Bur *NDHG* allele still produces a functional NDH complex as neither photosynthesis nor biomass phenotypes are as affected as in Col-*ndhm* and Col-*ndho*. Nonetheless, the specific role of the Bur *NDHG* allele in sustaining photoprotection and boosting biomass or sustaining efficient photochemistry for shoot biomass production under certain nucleotypes and light fluctuation conditions is worth further research. A possibility to address this would be using proteomics to characterize the NDH complex in Bur-0 plants grown under fluctuating light conditions.

The observation of higher biomass for cybrids with a Bur-0 plasmotype grown under moderate light fluctuation is a controversial result and worth further research. Although it is tentative to speculate that genetics are indeed contributing to more efficient photoprotective mechanisms that lead to higher biomass, some Bur^{Bur} cybrids had germination problems that led to small sample size (Constant n=15/24, DEPI n=12/24, Maize n=10/24) (Appendix table 5) could have a substantial effect on the observed results. The remaining plants in the analysis might have been the result of maternal effects, for example, if they originated from bigger or more vigorous seeds. As discarding a possible true nucleotype-plasmotype epistatic effect could lead to significant findings, it is suggested to repeat this experiment with a higher replicate number paying specific attention to factors generating maternal effects that determine seed uniformity.

3.2. Impact of the Bur-0 plasmotype additive effects on shoot biomass under field-like conditions.

Compared to plants grown in the growth chambers, plants under field-like conditions took sixteen additional days to develop. Moreover, although a higher replicate number was used, higher variability was observed due to less uniform experimental conditions (Light, shading, temperature, humidity, sand-peat proportions, nutrient availability, irrigation uniformity, substrate pH). H^2 for shoot biomass was low for plasmotype derived effects (Plasmotype=0.1%, Nucleotype-Plasmotype: 0.8%). These H^2 are comparable to those observed under the moderate light fluctuating light treatment in the growth chambers. Still, the additive effect of the plasmotype is more appreciable under field-like conditions. Therefore, when cybrids with this plasmotype are exposed to fluctuating light in nature and cold conditions simultaneously, the effect on shoot biomass seems to be more pronounced.

The additive effect of the Bur plasmotype on the recovery of photosystem II and NPQ was confirmed using The Plant Screen System™. Overall, the recorded photosynthetic parameters

were similar to those observed in cybrids for Constant and moderate light fluctuation treatments under growth chamber conditions. Contrary to the observations recorded in the species-wide representative cybrid panel, Bur^{Tanz} cybrids recorded significant differences in the recovery of φ PSII and qE. A possible reason behind this is the higher replicate number used on this experiment and the shorter time needed to phenotype the experiment, generating a clearer phenotype. Interestingly, as observed for *Col-ndhm* and *Col-ndho,* under field-like conditions, some cybrids with a Bur plasmotype (C24, Col, Ely, Ler, Shah) recorded negative qE values. Moreover, the highest increases in the recovery of φ PSII were also observed in cybrids with a Bur plasmotype and the C-24, Col-0, and Ely nuclear backgrounds.

Overall, shoot biomass was explained mainly by nuclear-encoded variation, where the accessions with an African origin had the lowest growth responses under the spring conditions in the gauze tunnels. Moreover, nucleotypes of African origin did not increase their shoot biomass production under a Bur plasmotype. No additive plasmotype effects were observed on shoot biomass, but cybrids with a Bur-0 plasmotype, on average, scored higher on shoot biomass (+3.06%). Additionally, the observation of higher shoot biomass in Bur^{Bur} cybrids grown under moderate light fluctuation in the growth chambers was not repeated in this experiment. The increase in shoot biomass for cybrids with a Bur-0 plasmotype was mainly driven by nucleotype-plasmotype interactions in Bur^{Col} (+24.58%; α=0.05) and Bur^{C24} (+12.46%; α=0.1). Notably, these shoot biomass observations in Bur^{Col} and Bur^{C24} correlate with their higher recovery of φ PSII and negative qE values. However, checking previous reports by Tijink (2021), these particular cybrids did not register increased shoot biomass in past experiments. Nonetheless, Tijink (2021) experiment took place under fall-winter conditions, and plants took almost twice as much to be harvested. Therefore, the specific environmental conditions likely explain these differences.

Due to the low H^2 observed from plasmotype-derived effects, the possibility of epistatic effects stemming from the Bur plasmotype was further analysed. Here it was observed that Col^{Col} cybrids had a smaller sample size. Due to lack of germination and poor development, just 25 out of 40 plants were considered in the statistical analysis after outlier removal. As wild-types for Col-0 were included for this experiment, an analysis was made taking genotype as an explaining factor between Col^{Col} Col^{Bur} and Col WT plants (Appendix Figure 16). From this analysis, it was possible to observe that the Col^{Col} cybrids recorded significantly lower biomass than Col-WT. Therefore, the observed differences could likely result from the seed batch used or a haploidization event that occurred while generating these cybrids. However, the (less significant) effects within the C24 nucleotype could not be confirmed to be caused by experimental factors as WTs for this accession were not included in the experiment. As this is still a considerable effect (12.46%) and there is a correlation between higher recovery of φ PSII and increased shoot biomass, further investigation into these nucleotype-plasmotype combinations could provide valuable insights into the Bur plasmotype additive effect on shoot biomass.

Given that cold stress further impacts photosynthesis efficiency, various stresses are in action in this experiment, adding multiple layers of complexity to the analysis. There is a high probability that nucleotype-plasmotype interactions are due to other nuclear genes or

chloroplast genes coding for other important proteins that help alleviate cold stress in the photosynthetic machinery or the Calvin-Benson cycle (Gao et al., 2022). Furthermore, eliminating further confounding environmental factors to provide higher uniformity of experimental conditions could be essential to precisely assess the impact of natural light fluctuation under cold and natural conditions. For instance, water stress and phosphorous also limit photosynthesis efficiency (Rumeau *et al.,* 2007). Since this experiment used a sand-peat substrate and hose to irrigate the plants, it is likely that water, pH and nutrient availability are not even across the pots. Therefore, implementing a hydroponic system outdoors to keep such differences minimal is advised if further research is undertaken. Alternatively, using drip irrigation or watering the plants uniformly from below instead of using a hose could limit these confounding effects.

The results observed in these biomass experiments suggest that cytonuclear epistatic effects could be generating shoot biomass responses when plants are exposed to fluctuating light and cold conditions. Nonetheless, the results between past experiments and the present are inconclusive, finding that different nucleotype-plasmotype combinations explain the differences in shoot biomass. A strong influence of environmental conditions is likely, and several trade-offs must be in action to grant an adequate response to multiple abiotic and biotic stresses that confer plant fitness in particular environments (Garcia-Andrade *et al.,* 2013; Zhang *et al.,* 2020). Given that Bur-0 *NDHG* was found to cause photosynthetic phenotypes and NPQ is an important mechanism to adapt to fluctuating light and cold stress, some of the increases in shoot biomass recorded are intriguing. For instance, rice (*Oryza sativa*) plants that lack NDH activity have been reported to decrease biomass production under fluctuating light and low temperatures (Yamori et al., 2011). Thereby, measuring NDH activity could provide further insights into how nucleotype-plasmotype interactions affect biomass production under fluctuating light and cold stress. Another possibility to understand the missing link between the observation of past experiments and those reported in literature reports is the exploration of alternative carbon sinks. For example, in tobacco (*Nicotiana tabacum*), faster relaxation of NPQ through overexpression of xanthophyll cycle proteins (VPZ lines) generated plants that produce increased biomass under fluctuating light. However, biomass increase was particularly evident in roots and stems (Kromdijik *et al.,* 2016). Moreover, Garcia-Molina & Leister (2020) created *A. thaliana* VPZ lines and exposed them to fluctuating light, but no impacts on fresh weight or rosette diameter were found. The authors suggest that sink limitations could explain this in *A thaliana* compared to tobacco. As the Bur-0 *NDHG* allele also produces a faster relaxation of NPQ, exploration of root biomass might overcome the sink limitations Garcia-Molina & Leister (2020) mentioned.

Concluding remarks.

The results of this project contribute to characterising phenotypic variation linked to plasmotype diversity in *A. thaliana*. Results from the species-wide representative cybrid panel demonstrate that plasmotype diversity influences photosynthesis efficiency phenotypes under field-like conditions. The estimated H^2 due to additive plasmotype effects and nucleotype-plasmotype interactions for the 63 photosynthesis and plant morphology parameters measured was 0,43% and 2,74%, respectively, ratifying additive plasmotypic effects are rare within *A. Thaliana.* The Bur plasmotype was a remarkable example of a plasmotype additive effect affecting the recovery of φPSII and NPQ phenotypes. Moreover, several nucleotype-plasmotype effects on photosynthesis and plant morphology phenotypes were identified. Reciprocal crosses of naturally occurring accessions revealed that *NDHG* is the likely causal gene responsible for the recovery of φPSII observed Bur plasmotype, and the molecular role of the NDH complex in NPQ supports this statement. Additionally, this conclusion was possible after observing that F1 crosses of naturally occurring accessions with an SNP in the remaining candidate gene (*MATK)* did not show the recovery of φPSII observed Bur plasmotype. Nonetheless, as plants that exclusively present the Bur-0 *NDHG* allele have not been identified, this study suggests a final proof of concept can be achieved through chloroplast transformation. Furthermore, the Bur plasmotypes additive effect on the recovery of φPSII was found to impact shoot biomass, but responses depend on the nuclear background and specific environmental conditions (light fluctuation, temperature). In general, the H^2 for shoot biomass due to plasmotype and nuclear plasmotype interactions is low under constant light and growth chamber conditions, but as light fluctuation increases, so does H^2 due to plasmotype-derived effects. Based on the findings of these studies, a strong call is made to continue research on genetic diversity in the NDH complex to gain further insight into its functioning and how it contributes to fine-tuning NPQ processes. Ultimately, this knowledge has the potential to be applied in cultivated plants to produce crops adapted to specific environments or eliminate unwanted plasmotype backgrounds that have been inadvertently introgressed.

References.

1. Abarca, D., Roldán, M., Martín, M., & Sabater, B. (2001). Arabidopsis thaliana ecotype Cvi shows an increased tolerance to photo-oxidative stress and contains a new chloroplastic copper/zinc superoxide dismutase isoenzyme. Journal of experimental botany, 52(360), 1417-1425.
2. Allen Elizabeth M., Giudice George J., D. L. A. (1993). ALLEN 1993.pdf (p. 8).Allen, J. F. (2015). Why chloroplasts and mitochondria retain their own genomes and genetic systems: Colocation for redox regulation of gene expression. Proceedings of the National Academy of Sciences of the United States of America, 112(33), 10231–10238. doi: 10.1073/pnas.1500012112
3. 1001 Genomes Consortium. Alonso-Blanco, C., Andrade, J., Becker, C., Bemm, F., Bergelson, J., Borgwardt, K. M., ... & Zhou, X. (2016). 1,135 genomes reveal the global pattern of polymorphism in Arabidopsis thaliana. Cell, 166(2), 481-491.
4. Arabidopsis Genome Initiative. (2000). Analysis of the genome sequence of the flowering plant Arabidopsis thaliana. Nature, 408(6814), 796-815.
5. Archibald, J. M. (2015). Endosymbiosis and eukaryotic cell evolution. Current Biology, 25(19), R911–R921. doi: 10.1016/j.cub.2015.07.055
6. Bates, D., Mächler, M., Bolker, B. M., & Walker, S. C. (2015). Fitting linear mixed-effects models using lme4. Journal of Statistical Software, 67(1). doi: 10.18637/jss.v067.i01
7. Birky, C. W. (2001). T He R Ole of Knox G Enes in. Annual Review of Genetics, 35, 125/148.
8. Björkman, O., & Demmig, B. (1987). Photon yield of O2 evolution and chlorophyll fluorescence characteristics at 77 K among vascular plants of diverse origins. Planta, 170(4), 489-504.
9. Bock, D. G., Andrew, R. L., & Rieseberg, L. H. (2014). On the adaptive value of cytoplasmic genomes in plants. Molecular Ecology, 23(20), 4899–4911. doi: 10.1111/mec.12920
10. Bock, R. (2014). Genetic engineering of the chloroplast: Novel tools and new applications. Current Opinion in Biotechnology, 26, 7–13. doi: 10.1016/j.copbio.2013.06.004
11. Boussardon, C., Martin-Magniette, M. L., Godin, B., Benamar, A., Vittrant, B., Citerne, S., Mary-Huard, T., Macherel, D., Rajjou, L., & Budar, F. (2019). Novel cytonuclear combinations modify Arabidopsis thaliana seed physiology and vigour. Frontiers in Plant Science, 10(February), 1–15. doi: 10.3389/fpls.2019.00032
12. Budar, F., & Roux, F. (2011). The role of organelle genomes in plant adaptation: time to get to work! Plant Signaling & Behavior, 6(5), 635–639. doi: 10.4161/psb.6.5.14524
13. Burger, G., Gray, M. W., & Lang, B. F. (2003). Mitochondrial genomes: anything goes. Trends in genetics, 19(12), 709-716.

14. Chan, K. X., Phua, S. Y., Crisp, P., McQuinn, R., & Pogson, B. J. (2016). Learning the Languages of the Chloroplast: Retrograde Signaling and beyond. Annual Review of Plant Biology, 67, 25–53. doi: 10.1146/annurev-arplant-043015-111854
15. Chardon, F., Cueff, G., Delannoy, E., Aubé, F., Lornac, A., Bedu, M., Gilard, F., Pateyron, S., Rogniaux, H., Gargaros, A., Mireau, H., Rajjou, L., Martin-Magniette, M. L., & Budar, F. (2020). The consequences of a disruption in cyto-nuclear coadaptation on the molecular response to a nitrate starvation in arabidopsis. Plants, 9(5). doi: 10.3390/plants9050573
16. Chi, W., Sun, X., & Zhang, L. (2013). Intracellular signaling from plastid to nucleus. Annual Review of Plant Biology, 64, 559–582. doi: 10.1146/annurev-arplant-050312-120147
17. Choubey, A., & Rajam, M. V. (2015). Organellar genomes of flowering plants. In Plant biology and biotechnology (pp. 179-204). Springer, New Delhi.
18. Christensen, A. C. (2013). Plant mitochondrial genome evolution can be explained by DNA repair mechanisms. Genome biology and evolution, 5(6), 1079-1086.
19. Christensen, A. C. (2020). More than just a powerhouse. Nature Plants, 6(1), 5–6. doi: 10.1038/s41477-019-0576-8
20. Cruz, J. A., Savage, L. J., Zegarac, R., Hall, C. C., Satoh-Cruz, M., Davis, G. A., ... & Kramer, D. M. (2016). Dynamic environmental photosynthetic imaging reveals emergent phenotypes. Cell Systems, 2(6), 365-377.
21. Cutter, A. D., & Payseur, B. A. (2013). Genomic signatures of selection at linked sites: unifying the disparity among species. Nature Reviews Genetics, 14(4), 262-274.
22. Daley, D. O., & Whelan, J. (2005). Why genes persist in organelle genomes. Genome biology, 6(5), 1-6.
23. Daniell, H., Lin, C. S., Yu, M., & Chang, W. J. (2016). Chloroplast genomes: Diversity, evolution, and applications in genetic engineering. Genome Biology, 17(1), 1–29. doi: 10.1186/s13059-016-1004-2
24. de Vries, J., & Archibald, J. M. (2018). Plastid genomes. Current Biology, 28(8), R336–R337. doi: 10.1016/j.cub.2018.01.027
25. Dobler, R., Rogell, B., Budar, F., & Dowling, D. K. (2014). A meta-analysis of the strength and nature of cytoplasmic genetic effects. Journal of Evolutionary Biology, 27(10), 2021–2034. doi: 10.1111/jeb.12468
26. Dowling, D. K., Friberg, U., & Lindell, J. (2008). Evolutionary implications of non-neutral mitochondrial genetic variation. Trends in Ecology and Evolution, 23(10), 546–554. doi: 10.1016/j.tree.2008.05.011
27. Durvasula, A., Fulgione, A., Gutaker, R. M., Alacakaptan, S. I., Flood, P. J., Neto, C., Tsuchimatsu, T., Burbano, H. A., Xavier Pico, F., Alonso-Blanco, C., & Hancock, A. M. (2017). African genomes illuminate the early history and transition to selfing in Arabidopsis thaliana. Proceedings of the National Academy of Sciences of the United States of America, 114(20), 5213–5218. doi: 10.1073/pnas.1616736114
28. El-Lithy, M. E., Rodrigues, G. C., Van Rensen, J. J. S., Snel, J. F. H., Dassen, H. J. H. A., Koornneef, M., Jansen, M. A. K., Aarts, M. G. M., & Vreugdenhil, D. (2005). Altered photosynthetic performance of a natural Arabidopsis accession is associated

with atrazine resistance. Journal of Experimental Botany, 56(416), 1625–1634. doi: 10.1093/jxb/eri157
29. Flood, P. J., Theeuwen, T. P. J. M., Schneeberger, K., Keizer, P., Kruijer, W., Severing, E., Kouklas, E., Hageman, J. A., Wijfjes, R., Calvo-Baltanas, V., Becker, F. F. M., Schnabel, S. K., Willems, L. A. J., Ligterink, W., van Arkel, J., Mumm, R., Gualberto, J. M., Savage, L., Kramer, D. M., … Wijnker, E. (2020). Reciprocal cybrids reveal how organellar genomes affect plant phenotypes. Nature Plants, 6(1), 13–21. doi: 10.1038/s41477-019-0575-9
30. Fulgione, A., Koornneef, M., Roux, F., Hermisson, J., & Hancock, A. M. (2018). Madeiran arabidopsis thaliana reveals ancient long-range and clarifies demography in eurasia. Molecular Biology and Evolution, 35(3), 564–574. doi: 10.1093/molbev/msx300
31. Gao, Y., Thiele, W., Saleh, O., Scossa, F., Arabi, F., Zhang, H., ... & Zoschke, R. (2022). Chloroplast translational regulation uncovers nonessential photosynthesis genes as key players in plant cold acclimation. The Plant Cell, 34(5), 2056-2079.
32. García-Andrade, J., Ramírez, V., Lopez, A., & Vera, P. (2013). Mediated plastid RNA editing in plant immunity. PLoS pathogens, 9(10), e1003713.
33. Garcia-Molina, A., & Leister, D. (2020). Accelerated relaxation of photoprotection impairs biomass accumulation in Arabidopsis. Nature plants, 6(1), 9-12.
34. Gordon, V. S., & Staub, J. E. (2011). Comparative analysis of chilling response in cucumber through plastidic and nuclear genetic effects component analysis. Journal of the American Society for Horticultural Science, 136(4), 256–264. doi: 10.21273/jashs.136.4.256
35. Green, B. R. (2011). Chloroplast genomes of photosynthetic eukaryotes. Plant Journal, 66(1), 34–44. doi: 10.1111/j.1365-313X.2011.04541.x
36. Greiner, S., & Bock, R. (2013). Tuning a ménage à trois: Co-evolution and co-adaptation of nuclear and organellar genomes in plants. BioEssays, 35(4), 354–365. doi: 10.1002/bies.201200137
37. Gualberto, J. M., Mileshina, D., Wallet, C., Niazi, A. K., Weber-Lotfi, F., & Dietrich, A. (2014). The plant mitochondrial genome: dynamics and maintenance. Biochimie, 100, 107-120.
38. Hertle, A. P., Haberl, B., & Bock, R. (2021). Horizontal genome transfer by cell-to-cell travel of whole organelles. Science Advances, 7(1). doi: 10.1126/sciadv.abd8215
39. Hill, G. E. (2015). Mitonuclear ecology. Molecular Biology and Evolution, 32(8), 1917–1927. doi: 10.1093/molbev/msv104
40. Joseph, B., Corwin, J. A., Li, B., Atwell, S., & Kliebenstein, D. J. (2013). Cytoplasmic genetic variation and extensive cytonuclear interactions influence natural variation in the metabolome. ELife, 2, 1–21. doi: 10.7554/elife.00776
41. Kleine, T., Maier, U. G., & Leister, D. (2009). DNA transfer from organelles to the nucleus: The idiosyncratic genetics of endosymbiosis. Annual Review of Plant Biology, 60, 115–138. doi: 10.1146/annurev.arplant.043008.092119
42. Kromdijk, J., & Walter, J. (2022). Relaxing non-photochemical quenching (NPQ) to improve photosynthesis in crops. Burleigh Dodds Science Publishing.

43. Ku, C., Nelson-Sathi, S., Roettger, M., Sousa, F. L., Lockhart, P. J., Bryant, D., Hazkani-Covo, E., McInerney, J. O., Landan, G., & Martin, W. F. (2015). Endosymbiotic origin and differential loss of eukaryotic genes. Nature, 524(7566), 427–432. doi: 10.1038/nature14963
44. Lane, N., & Martin, W. (2010). The energetics of genome complexity. Nature, 467(7318), 929–934. doi: 10.1038/nature09486
45. Lawson, A. Revealing cyto-nuclear interaction through phenotypic variation: a study on cybrids. Wageningen University and Research
46. Ma, M., Liu, Y., Bai, C., & Yong, J. W. H. (2021). The significance of chloroplast NAD (P) H dehydrogenase complex and its dependent cyclic electron transport in photosynthesis. Frontiers in Plant Science, 12, 643.
47. Martin, W., Rujan, T., Richly, E., Hansen, A., Cornelsen, S., Lins, T., & Penny, D. (2002). Evolutionary analysis of Arabidopsis, cyanobacterial, and chloroplast genomes reveals plastid phylogeny and thousands of cyanobacterial genes in the nucleus. Proceedings of the National Academy of Sciences, 99(19), 12246-12251.
48. Miclaus, M., Balacescu, O., Has, I., Balacescu, L., Has, V., Suteu, D., ... & Bruggmann, R. (2016). Maize cytolines unmask key nuclear genes that are under the control of retrograde signaling pathways in plants. Genome biology and evolution, 8(11), 3256-3270.
49. Moison, M., Roux, F., Quadrado, M., Duval, R., Ekovich, M., Lê, D. H., ... & Budar, F. (2010). Cytoplasmic phylogeny and evidence of cyto-nuclear co-adaptation in Arabidopsis thaliana. The Plant Journal, 63(5), 728-738.
50. Millar, A. H., Heazlewood, J. L., Kristensen, B. K., Braun, H. P., & Møller, I. M. (2005). The plant mitochondrial proteome. Trends in Plant Science, 10(1), 36–43. doi: 10.1016/j.tplants.2004.12.002
51. Morales, A., & Kaiser, E. (2020). Photosynthetic acclimation to fluctuating irradiance in plants. Frontiers in Plant Science, 11, 268.
52. Morley, S. A., & Nielsen, B. L. (2017). Plant mitochondrial DNA. Frontiers in Bioscience - Landmark, 22(6), 1023–1132. doi: 10.2741/4531
53. Niu, Y., Lazar, D., Holzwarth, A. R., Kramer, D. M., Matsubara, S., Schrey, S. D., & Nedbal, L. (2022). The dynamics of non-photochemical quenching and cyclic electron transport in A. thaliana exposed to harmonically oscillating light. BioRxiv.
54. Palmer, J. D., Adams, K. L., Cho, Y., Parkinson, C. L., Qiu, Y. L., & Song, K. (2000). Dynamic evolution of plant mitochondrial genomes: mobile genes and introns and highly variable mutation rates. Proceedings of the National Academy of Sciences, 97(13), 6960-6966.
55. Powles, S. B., & Yu, Q. (2010). Evolution in action: Plants resistant to herbicides. In Annual Review of Plant Biology (Vol. 61). doi: 10.1146/annurev-arplant-042809-112119
56. Ravi, M., & Chan, S. W. L. (2010). Haploid plants produced by centromere-mediated genome elimination. Nature, 464(7288), 615–618. doi: 10.1038/nature08842
57. Rodriguez-Heredia, M., Saccon, F., Wilson, S., Finazzi, G., Ruban, A., & Hanke, G. (2022). Protection of photosystem I during sudden light stress depends on ferredoxin: NADP (H) reductase abundance and interactions. Plant Physiology.

58. Roux, F., Mary-Huard, T., Barillot, E., Wenes, E., Botran, L., Durand, S., Villoutreix, R., Martin-Magniette, M. L., Camillerif, C., & Budar, F. (2016). Cytonuclear interactions affect adaptive traits of the annual plant Arabidopsis thaliana in the field. Proceedings of the National Academy of Sciences of the United States of America, 113(13), 3687–3692. doi: 10.1073/pnas.1520687113
59. Ruban, A. V., Johnson, M. P., & Duffy, C. D. (2012). The photoprotective molecular switch in the photosystem II antenna. Biochimica et Biophysica Acta (BBA)-Bioenergetics, 1817(1), 167-181.
60. Ruban, A. V. (2017). Crops on the fast track for light. Nature, 541(7635), 36-37.
61. Rumeau, D., Peltier, G., & Cournac, L. (2007). Chlororespiration and cyclic electron flow around PSI during photosynthesis and plant stress response. Plant, cell & environment, 30(9), 1041-1051.
62. Sato, N. (2021). Are Cyanobacteria an Ancestor of Chloroplasts or Just One of the Gene Donors for Plants and Algae ?
63. Shikanai, T., Endo, T., Hashimoto, T., Yamada, Y., Asada, K., & Yokota, A. (1998). Directed disruption of the tobacco ndhB gene impairs cyclic electron flow around photosystem I. Proceedings of the National Academy of Sciences, 95(16), 9705-9709.
64. Shikanai, T. (2016). Chloroplast NDH: a different enzyme with a structure similar to that of respiratory NADH dehydrogenase. Biochimica et Biophysica Acta (BBA)-Bioenergetics, 1857(7), 1015-1022.
65. Sloan, D. B., Alverson, A. J., Wu, M., Palmer, J. D., & Taylor, D. R. (2012). Recent acceleration of plastid sequence and structural evolution coincides with extreme mitochondrial divergence in the angiosperm genus Silene. Genome biology and evolution, 4(3), 294-306.
66. Smith, D. R., & Keeling, P. J. (2015). Mitochondrial and plastid genome architecture: reoccurring themes, but significant differences at the extremes. Proceedings of the National Academy of Sciences, 112(33), 10177-10184.
67. Soll, J., & Schleiff, E. (2004). Protein import into chloroplasts. Nature Reviews Molecular Cell Biology, 5(3), 198–208. doi: 10.1038/nrm1333
68. Spang, A., Stairs, C. W., Dombrowski, N., Eme, L., Lombard, J., Caceres, E. F., Greening, C., Baker, B. J., & Ettema, T. J. G. (2019). Proposal of the reverse flow model for the origin of the eukaryotic cell based on comparative analyses of Asgard archaeal metabolism. Nature Microbiology, 4(7), 1138–1148. doi: 10.1038/s41564-019-0406-9
69. Strand, D. D., & Kramer, D. M. (2014). Control of non-photochemical exciton quenching by the proton circuit of photosynthesis. In Non-photochemical quenching and energy dissipation in plants, algae and cyanobacteria (pp. 387-408). Springer, Dordrecht.
70. Suorsa, M. (2015). Cyclic electron flow provides acclimatory plasticity for the photosynthetic machinery under various environmental conditions and developmental stages. Frontiers in plant science, 6, 800.
71. Tanaka, Y., Adachi, S., & Yamori, W. (2019). Natural genetic variation of the photosynthetic induction response to fluctuating light environment. Current Opinion in Plant Biology, 49, 52-59.

72. Theeuwen et al., (unpublished
73. Tijinik, D.(2021) Zooming in on plasmotypic variation of *Arabidopsis thaliana*
74. Timmis, J. N., Ayliffe, M. A., Huang, C. Y., & Martin, W. (2004). Endosymbiotic gene transfer: organelle genomes forge eukaryotic chromosomes. Nature reviews genetics, 5(2), 123-135.
75. Vlad, D., Rappaport, F., Simon, M., & Loudet, O. (2010). Gene transposition causing natural variation for growth in Arabidopsis thaliana. PLoS Genetics, 6(5), e1000945.
76. Yamori, W., Sakata, N., Suzuki, Y., Shikanai, T., & Makino, A. (2011). Cyclic electron flow around photosystem I via chloroplast NAD (P) H dehydrogenase (NDH) complex performs a significant physiological role during photosynthesis and plant growth at low temperature in rice. The Plant Journal, 68(6), 966-976.
77. Zhang, G. J., Dong, R., Lan, L. N., Li, S. F., Gao, W. J., & Niu, H. X. (2020). Nuclear integrants of organellar DNA contribute to genome structure and evolution in plants. International Journal of Molecular Sciences, 21(3). doi: 10.3390/ijms21030707
78. Zhang, Y., Zhang, A., Li, X., & Lu, C. (2020). The role of chloroplast gene expression in plant responses to environmental stress. International Journal of Molecular Sciences, 21(17), 1–16. doi: 10.3390/ijms21176082

Appendix.

Experiment 1: Species-wide representative cybrid panel of *A. thaliana* grown under field-like conditions.

Nucleotype: Bur			Nucleotype: Col			Nucleotype: Cvi			Nucleotype: Tanz		
Cybrid	Plasmotipe	Sample size	Cybrid	Plasmotipe	Sample size	Cybrid	Plasmotipe	Sample size	Cybrid	Plasmotipe	Sample size
1_Aitba-1_Bur_1.1	Aitba-1	11	1_Aitba-1_Col_1.1	Aitba-1	8	2_Aitba-1_Cvi_1.1	Aitba-1	5	1_Aitba-1_Tanz_2.1	Aitba-1	12
4_Bab-0_Bur_1.1	Bab-0	8	3_Bab-0_Col_1.1	Bab-0	8	3_Bab-0_Cvi_1.1	Bab-0	8	3_Bab-0_Tanz_1.1	Bab-0	10
1_Basta-2_Bur_1.1	Basta-2	9	1_Basta-2_Col_1.1	Basta-2	10	2_Basta-2_Cvi_1.1	Basta-2	8	2_Basta-2_Tanz_1.1	Basta-2	12
1_Bur-0_Bur_*	Bur-0	8	1_Bur-0_Col_*	Bur-0	8	2_Bur-0_Cvi_3.1	Bur-0	8	1_Bur-0_Tanz_2.1	Bur-0	11
2_C24_Bur_2.1	C24	11	1_C24_Col_*	C24	8	1_C24_Cvi_1.1	C24	11	1_C24_Tanz_1.1	C24	10
1_Can-0_Bur_1.1	Can-0	10	2_Can-0_Col_1.1	Can-0	7	2_Can-0_Cvi_2.1	Can-0	10	2_Can-0_Tanz_1.1	Can-0	10
1_Col-0_Bur_*	Col-0	11	1_Col-0_Col_*	Col-0	6	1_Col_Cvi_2.1	Col	10	1_Col-0-Tanz_1.1	Col-0	10
3_Cvi-0_Bur_1.1	Cvi-0	8	1_Cvi-0_Col_1.1	Cvi-0	8	2_Cvi-0_Cvi_1.1	Cvi-0	11	1_Cvi-0_Tanz_1.1	Cvi-0	12
2_Don-0_Bur_1.1	Don-0	9	2_Don-0_Col_1.1	Don-0	8	2_Don-0_Cvi_1.1	Don-0	8	2_Don-0_Tanz_3.1	Don-0	12
3_Elh-2_Bur_1.3	Elh-2	9	2_Elh-2_Col_1.1	Elh-2	12	2_Elh-2_Cvi_1.2	Elh-2	10	2_Elh-2_Tanz_1.1	Elh-2	11
1_Elk-1_Bur_1.1	Elk-1	8	1_Elk-1_Col_1.1	Elk-1	11	2_Elk-1_Cvi_1.1	Elk-1	8	1_Elk-1_Tanz_1.1	Elk-1	10
1_Epid-1_Bur_1.1	Epid-1	9	1_Epid-1_Col_1.1	Epid-1	9	2_Epid-1_Cvi_1.2	Epid-1	10	2_Epid-1_Tanz_1.1	Epid-1	10
3_ET2_Bur_1.1	ET2	10	1_ET2_Col_1.1	ET2	8	2_ET2_Cvi_1.2	ET2	8	1_ET2_Tanz_1.1	ET2	11
1_Etna-2_Bur_1.1	Etna-2	8	2_Etna-2_Col_1.1	Etna-2	6	2_Etna-2_Cvi_1.1	Etna-2	10	1_Etna-2_Tanz_2.1	Etna-2	12
3_Ifr-0_Bur_1.1	Ifr-0	10	3_Ifr-0_Col_1.1	Ifr-0	10	4_Ifr-0_Cvi_1.1	Ifr-0	12	3_Ifr-0_Tanz_1.1	Ifr-0	9
4_IP-Alm-0_Bur_2.2	IP-Alm-0	8	2_IP-Alm-0_Col_1.1	IP-Alm-0	7	2_IP-Alm-0_Cvi_1.1	IP-Alm-0	8	2_IP-Alm-0_Tanz_1.1	IP-Alm-0	12
3_IP-Boa-0_Bur_1.1	IP-Boa-0	10	1_IP-Boa-0_Col_1.1	IP-Boa-0	8	2_IP-Boa-0_Cvi_2.1	IP-Boa-0	9	1_IP-Boa-0_Tanz_1.1	IP-Boa-0	8
1_IP-Bor-0_Bur_1.1	IP-Bor-0	9	1_IP-Bor-0_Col_1.1	IP-Bor-0	8	2_IP-Bor-0_Cvi_1.1	IP-Bor-0	12	1_IP-Bor-0_Tanz_1.1	IP-Bor-0	5
3_IP-Bus-0_Bur_1.1	IP-Bus-0	8	3_IP-Bus-0_Col_1.1	IP-Bus-0	11	3_IP-Bus-0_Cvi_1.1	IP-Bus-0	11	4_IP-Bus-0_Tanz_1.1	IP-Bus-0	11
3_IP_Cot-0_Bur_1.1	IP-Cot-0	10	2_IP-Cot-0_Col_1.1	IP-Cot-0	7	2_IP-Cot-0_Cvi_2.2	IP-Cot-0	11	3_IP-Cot-0_Tanz_3.1	IP-Cot-0	12
3_IP-Ees-0_Bur_1.1	IP-Ees-0	8	1_IP-Ees-0_Col_1.1	IP-Ees-0	9	2_IP-Ees-0_Cvi_3.1	IP-Ees-0	11	1_IP-Ees-0_Tanz_1.1	IP-Ees-0	12
2_IP-Lso-0_Bur_2.1	IP-Lso-0	11	2_IP-Lso-0_Col_2.1	IP-Lso-0	11	2_IP-Lso-0_Cvi_4.1	IP-Lso-0	9	2_IP-Lso-0_Tanz_2.1	IP-Lso-0	11
2_IP-Per-0_Bur_1.1	IP-Per-0	9	2_IP-Per-0_Col_1.1	IP-Per-0	10	2_IP-Per-0_Cvi_3.1	IP-Per-0	10	2_IP-Per-0_Tanz_1.1	IP-Per-0	11
2_IP-Piq-0_Bur_1.1	IP-Piq-0	10	1_IP-Piq-0_Col_1.1	IP-Piq-0	12	4_IP-Piq-0_Cvi_1.1	IP-Piq-0	11	2_IP-Piq-0_Tanz_1.1	IP-Piq-0	12
2_IP-Sne-0_Bur_1.1	IP-Sne-0	9	2_IP-Sne-0_Col_1.1	IP-Sne-0	10	2_IP-Sne-0_Cvi_1.1	IP-Sne-0	11	2_IP-Sne-0_Tanz_2.1	IP-Sne-0	11
4_Istisu-1_Bur_1.1	Istisu-1	10	1_Istisu-1_Col_1.1	Istisu-1	8	4_Istisu-1_Cvi_1.1	Istisu-1	11	1_Istisu-1_Tanz_3.1	Istisu-1	11
1_Jm-0_Bur_1.1	Jm-0	9	1_Jm-0_Col_1.1	Jm-0	10	2_Jm-0_Cvi_2.1	Jm-0	11	2_Jm-0_Tanz_2.1	Jm-0	11
1_Kas-1_Bur_1.1	Kas-1	9	1_Kas-1_Col_1.1	Kas-1	9	2_Kas-1_Cvi_4.1	Kas-1	6	1_Kas-1_Tanz_1.1	Kas-1	11
2_Kas-2_Bur_1.1	Kas-2	8	2_Kas-2_Col_1.1	Kas-2	10	4_Kas-2_Cvi_1.1	Kas-2	11	2_Kas-2_Tanz_2.1	Kas-2	11
1_Koren-1_Bur_1.1	Koren-1	10	1_Koren-1_Col_1.1	Koren-1	8	3_Koren-1_Cvi_3.1	Koren-1	11	2_Koren-1_Tanz_8.1	Koren-1	11
1_Kz-13_Bur_1.1	Kz-13	10	1_Kz-13_Col_1.1	Kz-13	9	2_Kz-13_Cvi_1.1	Kz-13	12	2_Kz-13_Tanz_1.1	Kz-13	11
1_Ler-0_Bur_*	Ler-0	9	1_Ler-0_Col_*	Ler-0	11	1_Ler-0_Cvi_1.1	Ler-0	12	1_Ler-0_Tanz_1.1	Ler-0	11
1_Lesno-1_Bur_1.1	Lesno-1	9	1_Lesno-1_Col_1.1	Lesno-1	6	2_Lesno-1_Cvi_1.3	Lesno-1	8	1_Lesno-1_Tanz_1.1	Lesno-1	11
1_Mammo-1_Bur_1.1	Mammo-1	9	1_Mammo-1_Col_1.1	Mammo-1	9	2_Mammo-1_Cvi_1.1	Mammo-1	7	1_Mammo-1_Tanz_2.1	Mammo-1	12
2_Melni-2_Bur_1.1	Melni-2	11	2_Melni-2_Col_1.1	Melni-2	9	2_Melni-2_Cvi_4.1	Melni-2	11	2_Melni-2_Tanz_1.1	Melni-2	10
4_Oua-0_Bur_1.1	Oua-0	11	3_Oua-0_Col_1.1	Oua-0	11	3_Oua-0_Cvi_1.1	Oua-0	10	3_Oua-0_Tanz_1.2	Oua-0	12
2_Panke-1_Bur_1.1	Panke-1	11	1_Panke-1_Col_1.1	Panke-1	8	3_Panke-1_Cvi_1.2	Panke-1	11	1_Panke-1_Tanz_1.1	Panke-1	11
2_Penb-2_Bur_2.1	Penb-2	9	2_Penb-2_Col_1.1	Penb-2	9	4_Penb-2_Cvi_1.1	Penb-2	11	4_Penb-2_Tanz_1.1	Penb-2	11
1_Qar-8a_Bur_1.1	Qar-8a	8	1_Qar-8a_Col_1.1	Qar-8a	7	2_Qar-8a_Cvi_2.1	Qar-8a	12	1_Qar-8a_Tanz_1.1	Qar-8a	10
2_Rabacal-2_Bur_1.1	Rabacal-2	7	2_Rabacal-2_Col_1.1	Rabacal-2	7	2_Rabacal-2_Cvi_1.1	Rab-2	11	2_Rabacal-2_Tanz_1.1	Rabacal-2	11
2_RRS-7_Bur_1.1	RRS-7	10	1_RRS-7_Col_1.1	RRS-7	9	2_RRS-7_Cvi_1.1	RRS-7	9	1_RRS-7_Tanz_1.1	RRS-7	11
1_Samos-3a_Bur_1.1	Samos-3a	9	1_Samos-3a_Col_1.1	Samos-3a	10	2_Samos-3a_Cvi_1.1	Samos-3a	12	2_Samos-3a_Tanz_1.1	Samos-3a	11
2_Samos-4_Bur_1.1	Samos-4	9	2_Samos-4_Col_1.1	Samos-4	8	3_Samos-4_Cvi_1.3	Samos-4	10	2_Samos-4_Tanz_1.1	Samos-4	11
1_Shah_Bur_*	Shah	8	1_Shah_Col_*	Shah	9	2_Shah_Cvi_2.1	Shah	1	2_Shah_Tanz_3.1	Shah	12
1_Sij-4_Bur_1.1	Sij-4	10	3_Sij-2_Col_2.1	Sij-2	10	4_Sij-2_Cvi_1.1	Sij-2	12	2_Sij-2_Tanz_2.1	Sij-2	9
4_Staro-2_Bur_1.1	Staro-2	7	1_Sij-4_Col_2.1	Sij-4	8	4_Sij-4_Cvi_1.1	Sij-4	11	2_Sij-4_Tanz_1.1	Sij-4	11
1_Sus-1_Bur_1.1	Sus-1	11	4_Staro-2_Col_1.1	Staro-2	6	4_Staro-2_Cvi_1.2	Staro-2	12	4_Staro-2_Tanz_2.3	Staro-2	11
2_Tanz-1_Bur_1.1	Tanz-1	11	1_Sus-1_Col_1.1	Sus-1	8	4_Sus-1_Cvi_1.1	Sus-1	1	1_Sus-1_Tanz_2.1	Sus-1	7
1_Tanz-2_Bur_1.1	Tanz-2	10	1_Tanz-1_Col_2.3	Tanz-1	9	2_Tanz-1_Cvi_1.1	Tanz-1	10	1_Tanz-1_Tanz_1.1	Tanz-1	11
2_Taz-0_Bur_1.1	Taz-0	8	1_Tanz-2_Col_1.1	Tanz-2	10	2_Tanz-2_Cvi_2.1	Tanz-2	9	4_Tanz-2_Tanz_1.1	Tanz-2	12
2_Toufl-1_Bur_1.1	Toufl-1	11	2_Taz-0_Col_1.1	Taz-0	8	2_Taz-0_Cvi_1.1	Taz-0	11	2_Taz-0_Tanz_2.1	Taz-0	12
1_Ws-4_Bur_*	Ws-4	11	2_Toufl-1_Col_3.1	Toufl-1	8	2_Toufl-1_Cvi_1.1	Toufl-1	10	2_Toufl-1_Tanz_3.1	Toufl-1	10
2_Yeg-1_Bur_1.1	Yeg-1	9	1_Ws-4_Col_*	Ws-4	10	1_Ws-4_Cvi_2.1	Ws-4	12	3_Ws-4_Tanz_1.1	Ws-4	10
3_Zin-9_Bur_1.1	Zin-9	11	2_Yeg-1_Col_1.1	Yeg-1	7	2_Yeg-1_Cvi_1.1	Yeg-1	11	2_Yeg-1_Tanz_1.1	Yeg-1	11
			1_Zin-9_Col_1.3	Zin-9	10	2_Zin-9_Cvi_1.1	Zin-9	10	2_Zin-9_Tanz_2.1	Zin-9	12

Appendix Table 1. *Genotypes and sample sizes after outlier removal used in the data analysis for the species-wide representative cybrid panel of A. thaliana grown under field-like conditions.*

Appendix figure 1: *Photosynthetic active radiation (PAR) recorded in the tunnel for the duration of the experiment.*

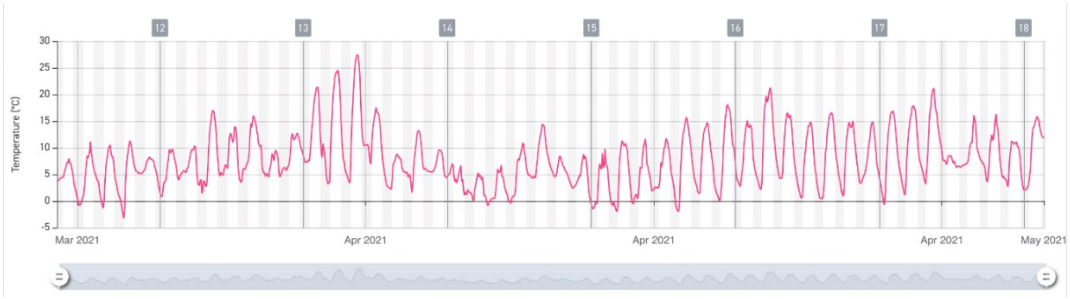

Appendix Figure 2: *Temperature in the tunnel for the duration of the experiment.*

Appendix Figure 3: *Volumetric water content in growing substrate recorded in the tunnel for the duration of the experiment.*

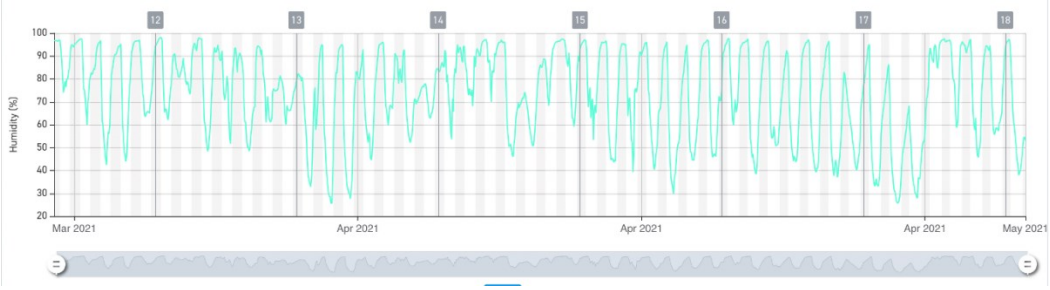

Appendix Figure 4: *Ambient humidity recorded in the tunnel for the duration of the experiment.*

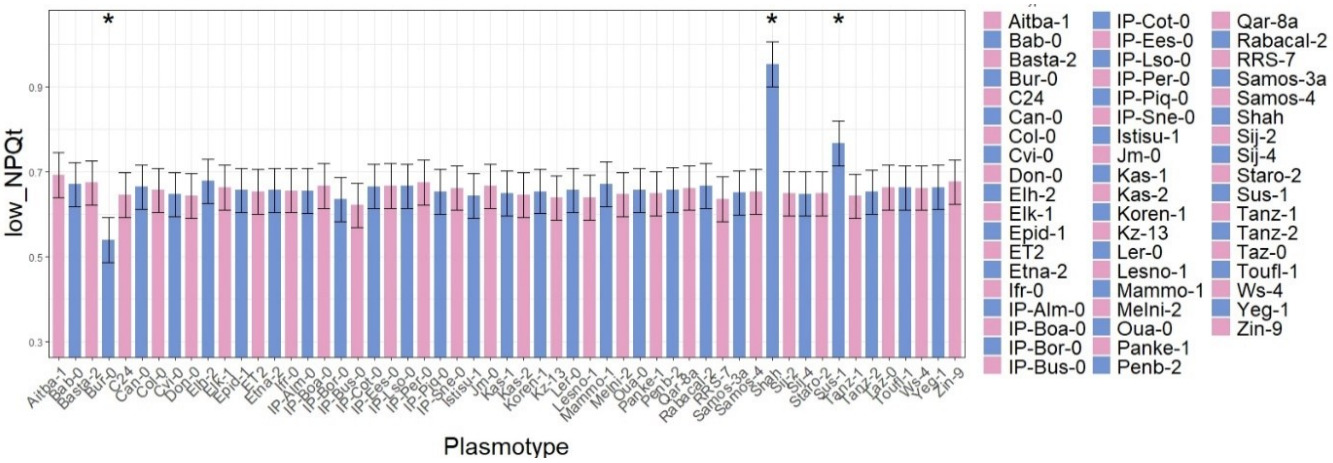

Appendix Figure 5*: Additive effect of the plasmotype on non-photochemical quenching (NPQt) measured at low light after a high light pulse in the Plant Screen System™. Asterisk shows significant differences. Multiple comparisons were made using Benjamini & Hochberg test (α=0.05).*

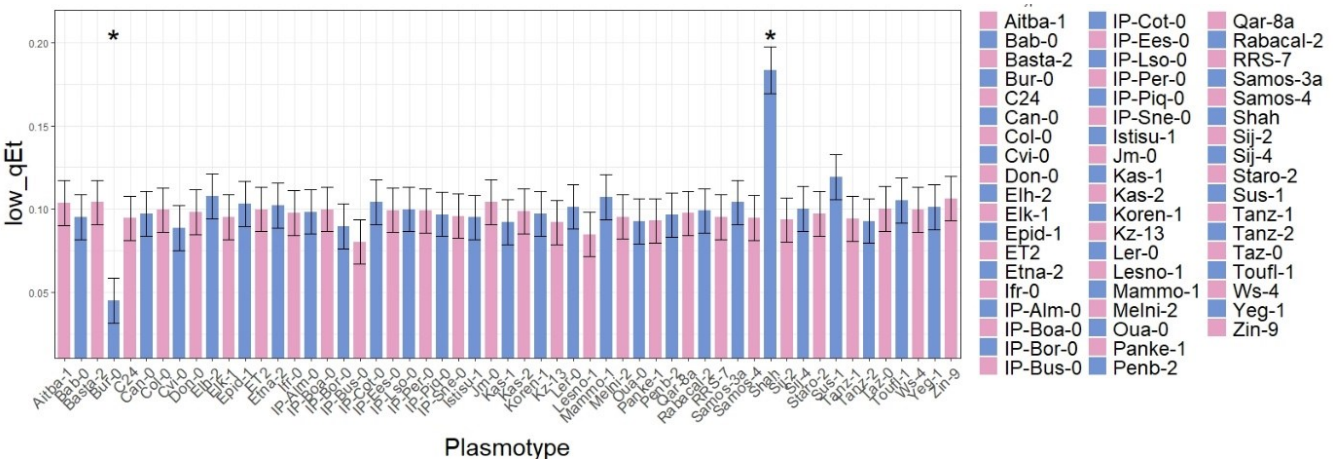

Appendix Figure 6*: Additive effects of the plasmotype on the fast element of NPQ, qE (low_qEt) measured at low light after a high light pulse in the Plant Screen System™. Asterisks show significant differences. Multiple comparisons were made using Benjamini & Hochberg test (α=0.05).*

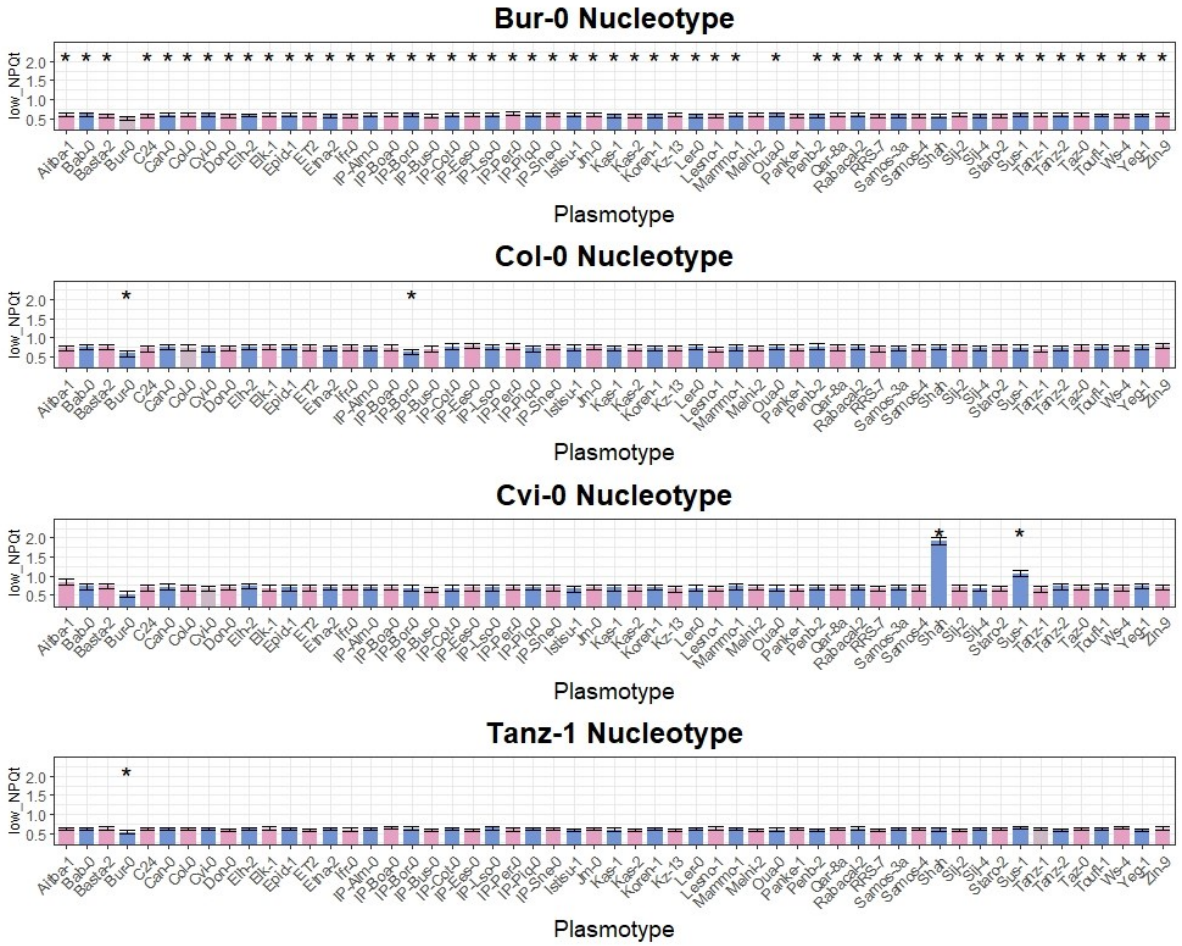

Appendix Figure 7*: Effect of Nucleotype-plasmotype combinations on non-photochemical quenching (Low_NPQt) measured at low light after a high light pulse in the Plant Screen System™. Asterisks show significant differences (α=0.05) as compared to the native plasmotype. Native plasmotypes are shown in brown. Multiple comparisons were made using Benjamini & Hochberg test (α=0.05).*

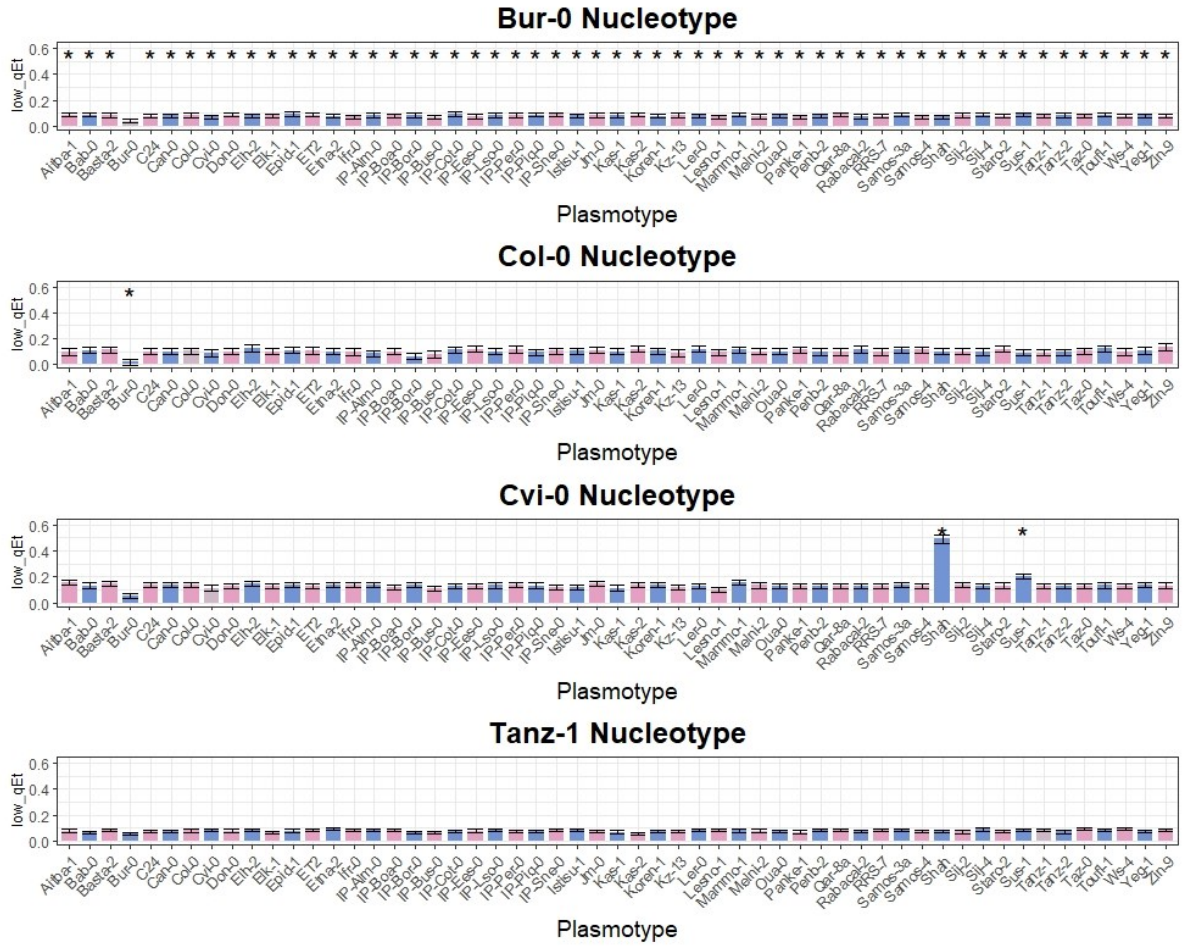

Appendix Figure 8: *Effect of Nucleotype-plasmotype combinations on the fast element of NPQ, qE (low_qEt) measured at low light after a high light pulse in the Plant Screen System™. Asterisks show significant differences (α=0.05) as compared to the native plasmotype. Native plasmotypes are shown in brown. Multiple comparisons were made using Benjamini & Hochberg test (α=0.05).*

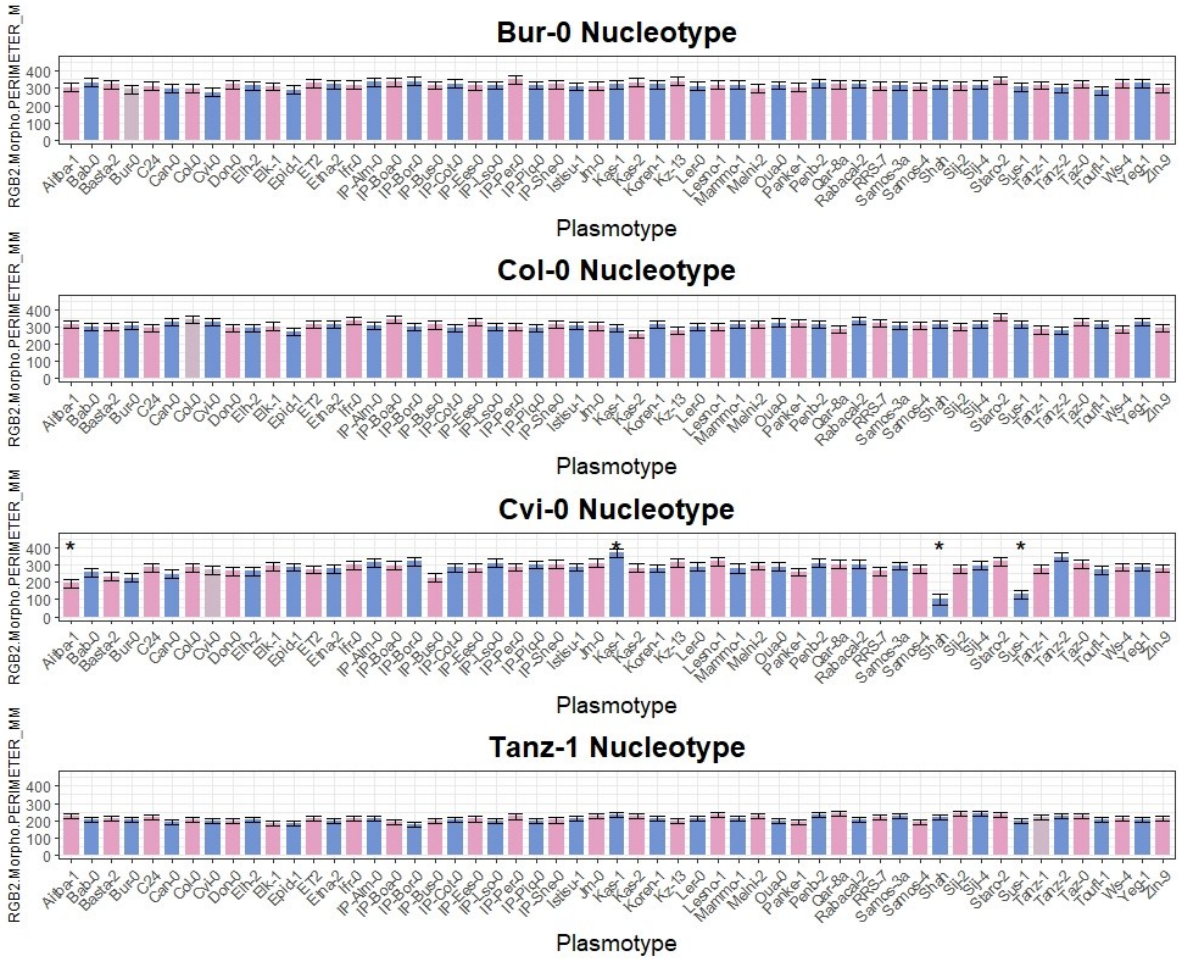

Appendix Figure 9: *Effect of Nucleotype-plasmotype combinations on Leaf Area (mm) recorded in the Plant Screen System™. Asterisks show significant differences as compared to the native plasmotype. Native plasmotypes are shown in brown. Multiple comparisons were made using Benjamini & Hochberg test (α=0.05).*

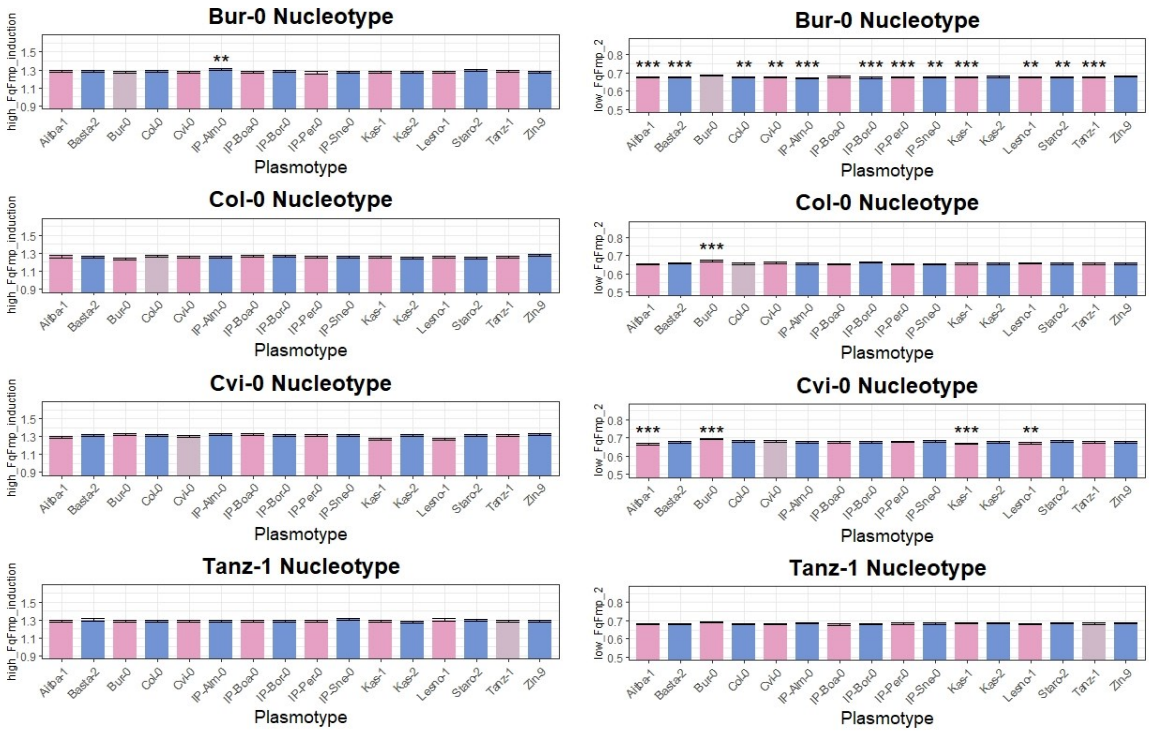

Appendix figure 10: *Left Effect of Nucleotype-plasmotype combinations on Leaf Area (mm) recorded in the Plant Screen System™). Right: Effects on "low FqFmp_2" parameter reflecting the recovery of φ PSII after exposure to high light pulse in the Plant Screen System™. Asterisks show significant differences as compared to the native plasmotype. Native plasmotypes are shown in brown. Multiple comparisons were made using Benjamini & Hochberg test (α=0.05).*

Experiment 2: Genetic cause behind Bur-0 additive effect in the recovery of φPSII.

***MATK* and *NDHG* Primers**	
Oligo name	Oligo sequence 5' ⟶ 3'
Pt_3108_A1	GAAGGTGACCAAGTTCATGCTAGGACATTTTAATTATGTGTTAGATGTACTAA
Pt_3108_A2	GAAGGTCGGAGTCAACGGATTGGACATTTTAATTATGTGTTAGATGTACTAC
Pt_3108_C1	AGGGTTTGAACCAAGATTTCTAGATGGAT
Pt_118888_A1	GAAGGTGACCAAGTTCATGCTAATAATATAATGGATTTGCCTGGACCAAT
Pt_118888_A2	GAAGGTCGGAGTCAACGGATTAATAATATAATGGATTTGCCTGGACCAAA
Pt_118888_C1	GACCGGATCCCAGAAAAACTAAAAGAAAA

Appendix table 2: *KASP™ Primers used to confirm the MATK and NDHG alleles present in accession ID471.*

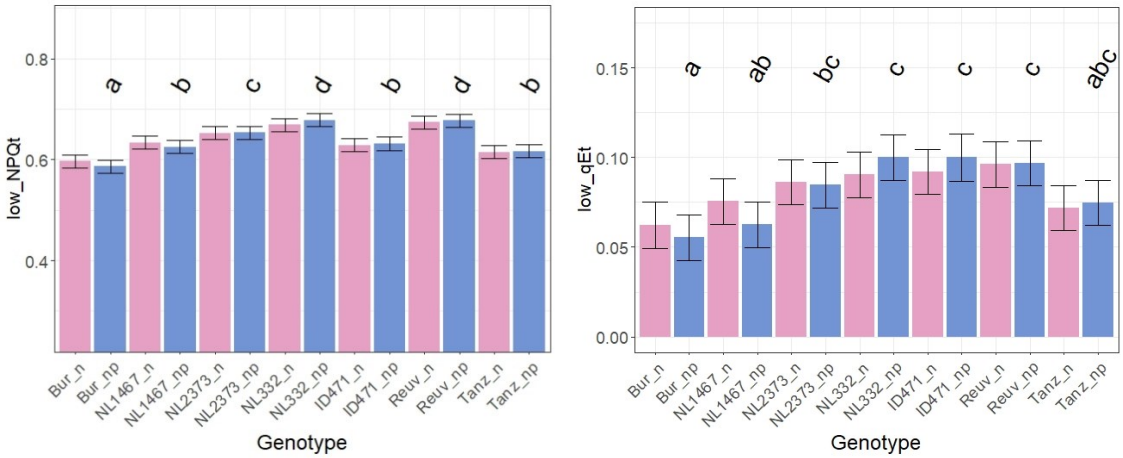

Appendix Figure 11**:** *Effects on "low_NPQ" and "low_qEt" in groups with 50% Nucleotype or 50% Nucleotype + Plasmotype used to map the genetic origin of Bur-0 recovery of ΦPSII. Pink bars represent the average phenotype for groups of crosses with 50% Nucleotype. Blue bars represent the average phenotype of the group with 50% Nucleotype + Plasmotype. Asterisks show significant differences (α=0.05). Multiple comparisons were made using the Tukey test for the group with 50% Nucleotype + Plasmotype.*

Experiment 3.1: ***Impact of the Bur-0 plasmotype additive effects on shoot biomass under growth chamber conditions with fluctuating light treatments.***

Constant	
Genotype	**non_na_count**
Bur_Bur	15
Bur_Col	20
C24_Bur	19
C24_Col	20
Col_Bur	18
Col_Col	19
Ler_Bur	20
Ler_Col	21
ndhM	21
ndhO	20

DEPI	
Genotype	**non_na_count**
Bur_Bur	12
Bur_Col	22
C24_Bur	19
C24_Col	21
Col_Bur	19
Col_Col	20
Ler_Bur	21
Ler_Col	20
ndhM	21
ndhO	22

Maize	
Genotype	**non_na_count**
Bur_Bur	10
Bur_Col	19
C24_Bur	21
C24_Col	19
Col_Bur	20
Col_Col	20
Ler_Bur	21
Ler_Col	20
ndhM	19
ndhO	24

Appendix Table 3: *Sample sizes after outlier removal used for data analysis.*

Cybrids under constant light					
Phenotype	**Nucleotype**	**Plasmotype**	**Nucleotype-Plasmotype**	**Basin**	**Residual**
Dry_Weight	0,434	0,000	0,018	0,001	0,547
low_FqFmp_2	0,317	0,273	0,043	0,000	0,367
low_NPQt	0,164	0,240	0,035	0,155	0,407
low_qEt	0,263	0,139	0,024	0,222	0,352
Cybrids under moderate light fluctuation (DEPI)					
Phenotype	**Nucleotype**	**Plasmotype**	**Nucleotype-Plasmotype**	**Basin**	**Residual**
Dry_Weight	0,352	0,000	0,093	0,125	0,430
low_FqFmp_2	0,242	0,391	0,025	0,047	0,294
low_NPQt	0,020	0,286	0,011	0,486	0,197
low_qEt	0,000	0,430	0,034	0,096	0,440
Cybrids under high light fluctuation (Maize)					
Phenotype	**Nucleotype**	**Plasmotype**	**Nucleotype-Plasmotype**	**Basin**	**Residual**
Dry_Weight	0,490	0,087	0,036	0,018	0,369
low_FqFmp_2	0,245	0,201	0,047	0,191	0,316
low_NPQt	0,089	0,026	0,032	0,601	0,252
low_qEt	0,097	0,021	0,026	0,244	0,613
Cybrids under field-like conditions					
Phenotype	**Nucleotype**	**Plasmotype**	**Nucleotype-Plasmotype**	**Tray**	**Residual**
Dry_Weight	0,517	0,001	0,008	0,099	0,375
low_FqFmp_2	0,311	0,176	0,011	0,030	0,473
low_NPQt	0,251	0,109	0,004	0,001	0,636
low_qEt	0,135	0,242	0,020	0,033	0,571

Appendix Table 4: *Variance components for selected phenotypes of cybrids in all biomass experiments.*

Constant light: Col-0 ,Col-*ndhm*, Col-*ndho*			
Phenotype	**Genotype**	**Basin**	**Residual**
Dry_Weight	0,201	0,045	0,755
low_FqFmp_2	0,515	0,030	0,455
low_NPQt	0,774	0,116	0,109
low_qEt	0,776	0,078	0,146
Moderate light fluctuation: Col-0 ,Col-*ndhm*, Col-*ndho*			
Phenotype	**Genotype**	**Basin**	**Residual**
Dry_Weight	0,092	0,553	0,355
low_FqFmp_2	0,562	0,000	0,438
low_NPQt	0,742	0,131	0,126
low_qEt	0,780	0,000	0,220
High light fluctuation: Col-0 ,Col-*ndhm*, Col-*ndho*			
Phenotype	**Genotype**	**Basin**	**Residual**
Dry_Weight	0,784	0,000	0,216
low_FqFmp_2	0,737	0,116	0,147
low_NPQt	0,085	0,562	0,353
low_qEt	0,053	0,087	0,860

Appendix Table 5: *Variance components for selected phenotypes of Col^{Col} vs. Col-ndhm & Col-ndho in the growth chamber biomass experiments.*

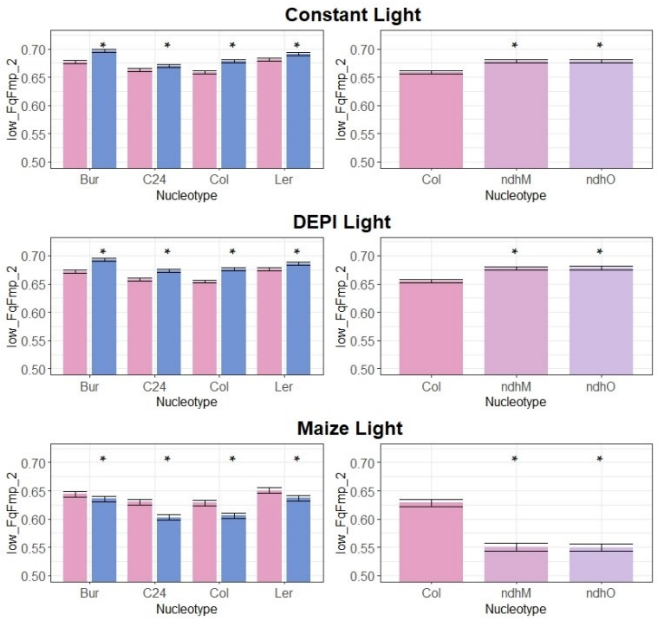

Appendix Figure 12: *Effects on "low FqFmp_2" parameter reflecting the recovery of φ PSII after exposure to a high light pulse in the Plant Screen System™. Left: Interaction effects of different Nucleotype-Plasmotype combinations. Right: Col^{Col} vs. Col-ndhm & Col-ndho. Asterisks show significant differences. Multiple comparisons were made using Benjamini & Hochberg test (α=0.05).*

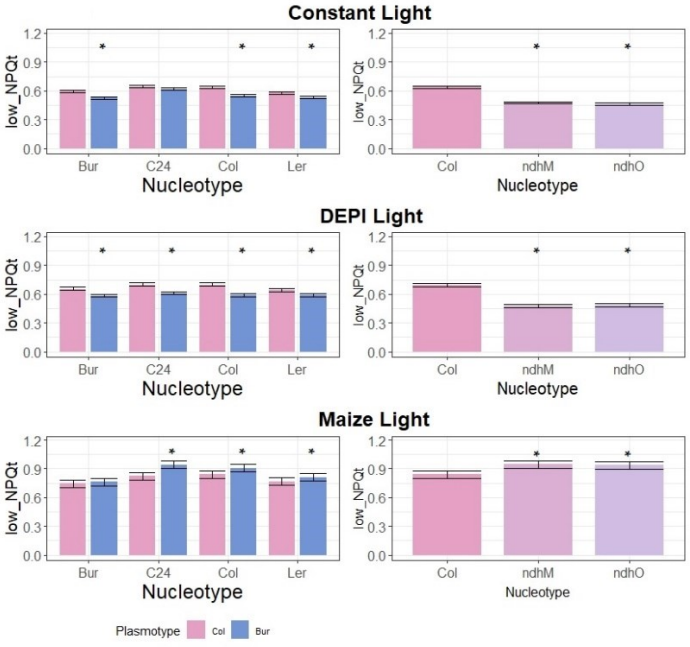

Appendix Figure 13: *Effects on "low NPQt" parameter reflecting NPQ after exposure to a high light pulse in the Plant Screen System™. Left: Interaction effects of different Nucleotype-Plasmotype combinations. Right: Col^{Col} vs. Col-ndhm & Col-ndho. Asterisks show significant differences. Multiple comparisons were made using Benjamini & Hochberg test (α=0.05).*

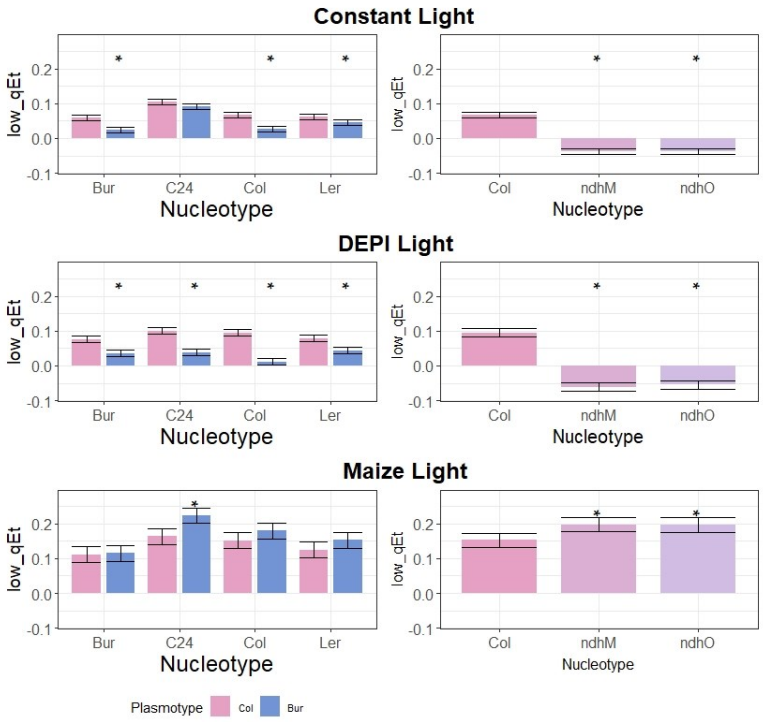

Appendix Figure 14*: Effects on "low qEt" parameter reflecting qE after exposure to a high light pulse in the Plant Screen System™. Left: Interaction effects of different Nucleotype-Plasmotype combinations. Right: Col^{Col} vs. Col-ndhm & Col-ndho. Asterisks show significant differences. Multiple comparisons were made using Benjamini & Hochberg test (α=0.05).*

3.2. Impact of the Bur-0 plasmotype additive effects on shoot biomass under field-like conditions.

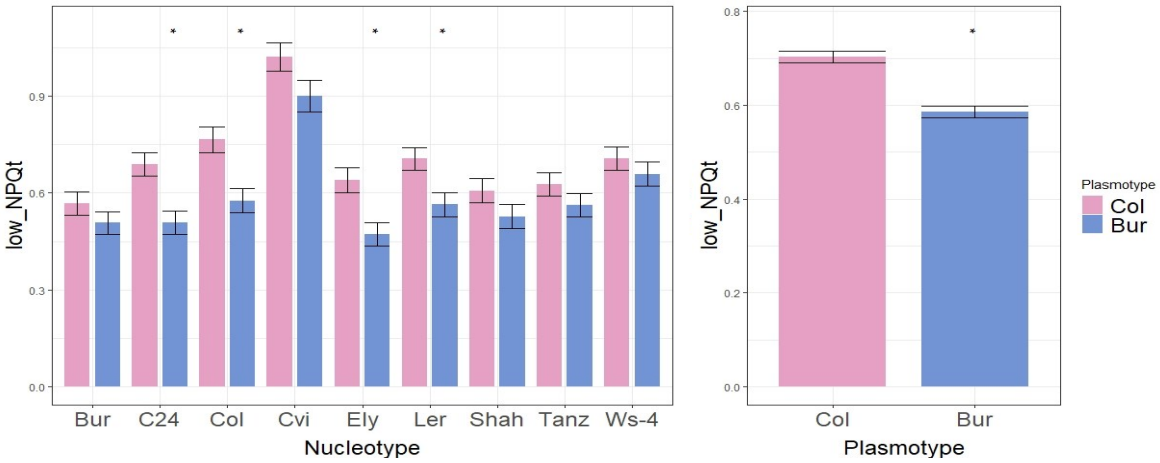

Appendix Figure 15*: Effects on "low NPQt" parameter reflecting NPQ after exposure to a high light pulse in the Plant Screen System™. Left: Interaction effects of different Nucleotype-Plasmotype combinations. Right: Additive plasmotype effects. Asterisks show significant differences. Multiple comparisons were made using Benjamini & Hochberg test (α=0.05).*

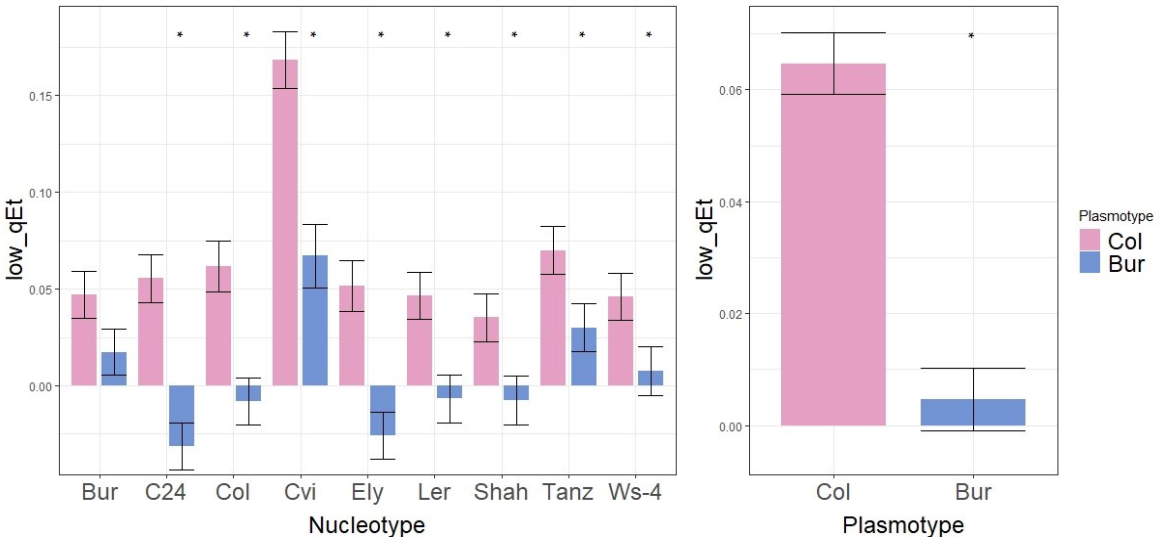

Appendix Figure 16: *Effects on "low qEt" parameter reflecting qE after exposure to a high light pulse in the Plant Screen System™. Left: Interaction effects of different Nucleotype-Plasmotype combinations. Right: Additive plasmotype effects. Asterisks show significant differences. Multiple comparisons were made using Benjamini & Hochberg test (α=0.05).*

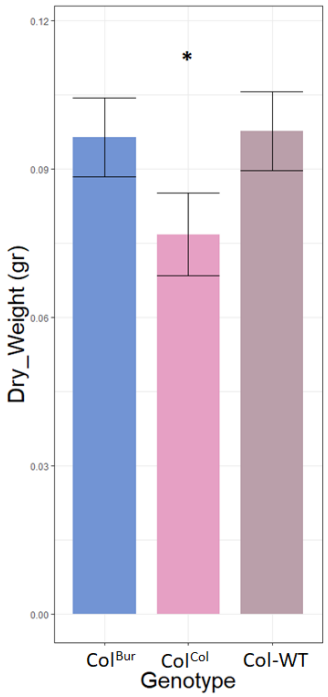

Appendix Figure 17: *Shoot biomass of Col-0l cybrids vs. Col-0 wild-types under field-like conditions grown in spring 2021 at Unifarm, WUR. Asterisks show significant differences. Multiple comparisons were made using Benjamini & Hochberg test (α=0.05).*